



UNIVERSITY OF  
**LIVERPOOL**

SCHOOL OF ENGINEERING

The University *of* Liverpool

**Energy Absorbing Characteristics of Hybrid Composite Pipe  
Systems**

Thesis submitted in accordance with the requirements of the

University *of* Liverpool for the degree of

Master *of* Philosophy

By

**Yaoping Liao**

October 2015

## **ACKNOWLEDGEMENTS**

The author would like to express his appreciation to those who have made contributions throughout the duration of this work.

First of all I would like to express my gratitude for my supervisor, Dr Zhongwei Guan for his invaluable support and guidance throughout this project, for his precious advice and for the time he dedicated to read this dissertation.

I would like to thank Dr Robert S Birch and Mr Stephen Pennington for the guidance and help in this research.

Particular thanks go to Dr Jin Zhou who shared his knowledge in FEM Analysis. I would also like to thank the colleagues with whom I shared the office during the two years I spent in the Brodie Tower of the University of Liverpool.

Finally, special thanks must go to my family and to all of my friends for sharing with me the good and the bad moments I have been through during these two years I have lived in Liverpool.

## **LIST OF PUBLICATIONS**

1. J. Zhou, Z.W. Guan, W.J. Cantwell, Y. Liao, The energy-absorbing behaviour of foam cores reinforced with composite rods, *Composite Structure*, 2014; (116): 346-356.
2. M.Y.M. Zuhri, Y. Liao and Z.W. Guan, The Energy-Absorbing Properties of Bamboo based Structures, *Construction & Building Materials*, 2015 (Submitted).

## **ABSTRACT**

The aim of this research is to investigate the structural response of carbon fibre reinforced plastic (CFRP) tubes and their hybrid systems subjected to quasi-static and dynamic loading conditions. The work also includes the investigation of the mechanical properties and energy-absorbing characteristics of other novel composite structures for the potential use in aerospace and a wide range of engineering applications.

Firstly, a series of experimental tests have been carried out to obtain the mechanical properties of all constituent materials and structural behaviour of the composite structures, which are used to validate numerical models. The material tests undertaken include (1) quasi-static and dynamic crushing of individual CFRP tubes and the related hybrid systems (2) compression of PU foams. The corresponding failure modes are obtained. In addition, specific energy absorption of the individual tubes and the hybrid systems investigated is evaluated.

Then, finite element (FE) models are developed using the commercial code ABAQUS/Explicit to simulate the structural response of CFRP tubes, the related hybrid systems and syntactic foam core based sandwich beams. The agreement between the numerical predictions and experimental results is very good across the range of the structures and configurations investigated. The FE models have produced accurate predictions of the static and dynamic load-displacement responses, the specific energy absorption and failure characteristics recorded for CFRP tube structures. The modelling has been further undertaken on the low velocity impact response of the sandwich beams, with reasonably good correlation to the corresponding experimental results.

The dynamic characteristics of the fibre reinforced composite pipe structures through a series experimental tests and numerical predictions investigated in this project can be used in assisting the design of lightweight composite structures for energy-absorbing applications.

# CONTENTS

ACKNOWLEDGEMENTS .....	i
LIST OF PUBLICATIONS .....	ii
ABSTRACT.....	iii
CONTENTS.....	iv
CHAPTER 1 INTRODUCTION .....	1
1.1 Background of the project .....	2
1.2 CFRP materials in relation to the scopes of the project .....	2
1.3 Related applications .....	3
1.3.1 Commercial airplane.....	4
1.3.2 Military aircraft.....	5
1.3.3 Transportation.....	6
1.3.4 Other applications.....	7
1.4 Aim and objectives of the thesis .....	7
1.5 The thesis outline .....	8
CHAPTER 2 LITERATURE REVIEW .....	10
2.1 Introduction .....	10
2.2 Overview of sandwich structures .....	11
2.2.1 Background and development .....	11
2.2.2 Experimental studies on sandwich structures .....	14
2.2.3 Modelling work on sandwich structures.....	15
2.3 Overview of high energy-absorbing tube structures .....	16
2.3.1 Experimental tests on tube structures .....	18
2.3.2 FE modelling on tube structures .....	23
2.4 Conclusions .....	25
CHAPTER 3 EXPERIMENTAL WORK, RESULTS AND DISCUSSION.....	27
3.1 Introduction .....	27
3.2 Types of CFRP tubes.....	28
3.3 Sample preparation and testing .....	28
3.3.1 Cutting tubes.....	28
3.3.2 Making chamfers .....	31
3.3.3 Manufacturing hybrid tube systems .....	32
3.3.4 Quasi-static compression tests.....	35

3.3.5	Dynamic tests .....	36
3.4	Experimental results of compression tests .....	39
3.4.1	Individual CFRP tubes.....	39
3.4.2	Cubic foams .....	41
3.4.3	Hybrid systems .....	42
3.5	Experimental results of dynamic tests.....	51
3.5.1	Individual CFRP tubes.....	51
3.5.2	Hybrid systems .....	57
3.5.3	Cubic foams .....	70
3.6	Summary .....	71
CHAPTER 4 FINITE ELEMENT MODELLING AND RESULTS .....		72
4.1	Introduction .....	72
4.2	Constitutive models and failure criteria .....	73
4.2.1	Modified 3D Hashin's damage criteria .....	73
4.2.2	Modelling of CFRP tubes .....	75
4.2.3	Modelling of GFRP skins .....	75
4.2.4	Modelling of the foam .....	76
4.2.5	Modelling of cohesive layer .....	78
4.3	Individual models for various structures.....	79
4.3.1	Mesh generation of the composite tubes and the hybrid systems.....	79
4.3.2	Mesh generation of the sandwich beam .....	80
4.4	Mesh sensitivity.....	82
4.5	Output of modelling results.....	83
4.6	Simulation results and discussion .....	83
4.6.1	Simulation of CFRP tubes and hybrid systems .....	83
4.6.2	Simulation of sandwich beams .....	89
4.7	Summary .....	92
CHAPTER 5 THEORETICAL WORK.....		93
5.1	Introduction .....	93
5.2	Carbon/Glass fibre rod embedded in PVC foam cores .....	94
5.2.1	The derivation of equations .....	94
5.2.2	The comparison between the experiment results and calculations.....	96
5.3	Bamboo pipes .....	99

5.3.1	Failure mode 1 .....	99
5.3.2	Failure mode 2 .....	101
5.3.3	Results and Discussion .....	103
5.4	Summary .....	105
CHAPTER 6 CONCLUSIONS AND RECOMMENDATIONS FOR FUTURE WORK ...		106
6.1	General summary .....	106
6.1.1	Composite tubes .....	106
6.1.2	Sandwich beams .....	107
6.2	Recommendations for future work.....	107
REFERENCES .....		109

## **CHAPTER 1 INTRODUCTION**

This chapter gives an overview of carbon fibre reinforced plastic (CFRP) materials, including the background of the CFRP materials and the CFRP tubes, the applications, the aim and objectives of this project, as well as the outline of this thesis.

## **1.1 Background of the project**

Composite materials have been investigated by researchers over the last few decades due to their high ratios of strength and energy absorption to weight. Composite, as a material type, is different from any other traditional engineering materials. In addition, it is the fact that composites can, and should be, tailored to an application means that it is far from straightforward to design and manufacture. Though composites have become synonymous with performance, it is the superior strength-to-weight ratio and parts-consolidation capability that is able to offer dramatic reductions in weight. This ultimately enables performance benefits to particular systems which have a special request in weight. In this case, compared with the traditional material, it allows reducing the weight significantly when designing the structures with composite materials. The previous research work [1-4] has demonstrated the increasing development and applications of the productions consisted of high-performance composite materials manufactured by strong and stiff fibres used in commercial and military aircraft as well as other aerospace applications.

Due to the climate control issue, there is a need to develop lightweight composite structures to replace some existing metallic ones in transportation sector. Here, carbon fibre reinforced plastic (CFRP) is widely used in aerospace and automotive industry, which is adopted to be used in the hybrid CFRP tube systems developed in the current project.

## **1.2 CFRP materials in relation to the scopes of the project**

Composite materials have drawn a great attention for the last a few decades on applying them to high performance structures which need be lightweight and strong to resist huge loads. However, they are mainly used in aircraft structures until the discovery of the carbon fibre at the Royal Aircraft Establishment at Farnborough, UK, in 1961. In the later 1960's, this new composite material started to be applied in both the civil products and military equipment. With the increasing experience of using them, the significant improvement of the fibres and matrix achieved, which results in CFRP composites. Especially, the CFRP tubes are the potential structures used as light-weight components with high energy absorption in the plane and vehicles as the traditional support structures are aluminium alloy or metal rod/cylinder which is much heavier than the hybrid CFRP tube structures

proposed in the current project. The sketch of cross-section of plane is shown in Fig. 1.1., where the metallic support structure can be replaced by the proposed CFRP tube systems.

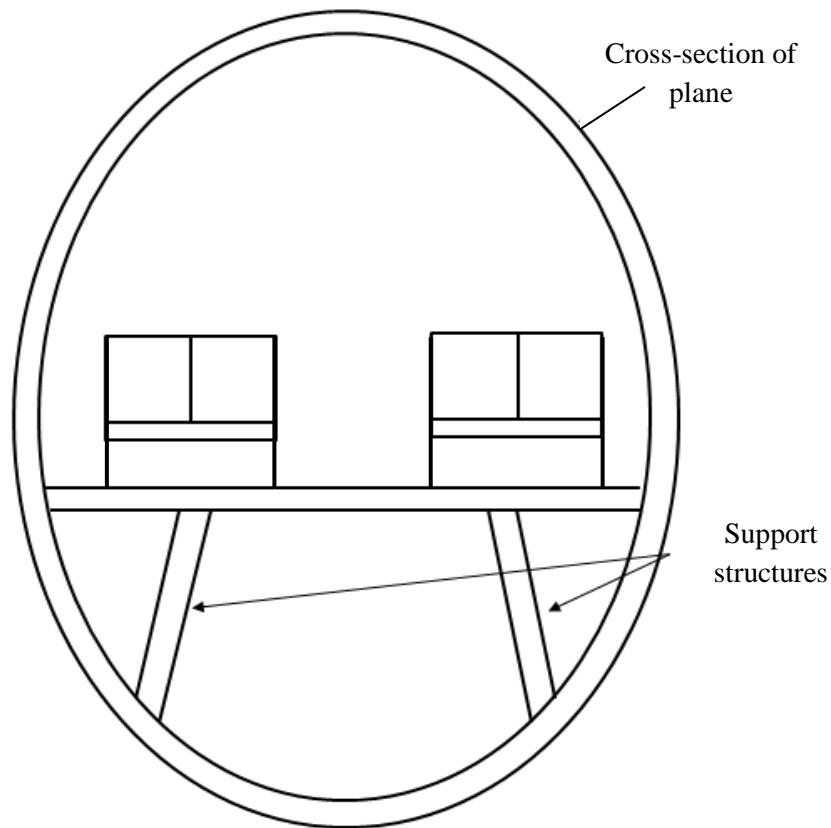


Fig. 1.1 Sketch of cross-section of plane

### 1.3 Related applications

Fibre reinforced plastic/polymer composites are employed in a wide range of applications such as aerospace, automobile and transportation, etc. Hull [5] has briefly introduced some typical fields in which FRP has been used more generally in Table 1-1.

Table 1-1 Some applications of polymer composites [5].

Industrial sector	Examples
Aerospace	Wings, fuselage, radomes, antennae, tail-planes, helicopter blades, landing gears, seats, floors, interior panels, fuel tanks, rocket motor cases, nose cones, launch tubes
Automobile	Body panels, cabs, spoilers, consoles, instrument panels, lamp-housings, bumpers, leaf springs, drive shafts, gears, bearings
Boats	Hulls, decks, masts, engine shrouds, interior panels
Chemical	Pipes, tanks, pressure vessels, hoppers, valves, pumps, impellers
Domestic	Interior and exterior panels, chairs, tables, baths, shower units, ladders
Electrical	Panels, housings, switchgear, insulators, connectors
Leisure	Motor homes, caravans, trailers, golf clubs, racquets, projective

### 1.3.1 Commercial airplane

In the beginning of the flights, the wood were largely used as the structures of the aircraft, as a natural composite, which could be easily obtained and manufactured in the type of wire and fabric. In the 1930s, aluminium and their alloys took over the wood and became the major material in the aircraft industries since then. Currently, however, the civil airplanes have focused on using the fibrous composites to replace the secondary structures, in which the CFRP tubes can be used as the

In recent years, advanced composites have been increasingly used in Boeing Company's products such as the Boeing 767, 777 and 787 etc. In comparison with previous products, for example, the composite materials have been used in Boeing 787, shown in Fig. 1.2 are 50% by weight of the total materials.

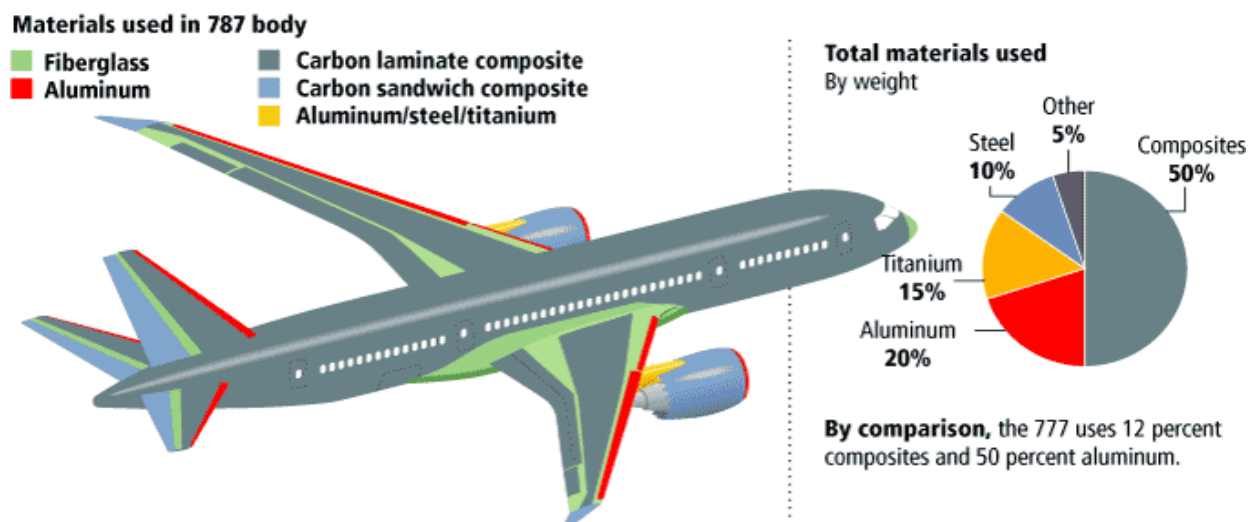


Fig. 1.2 The ratio of materials used in Boeing 787 [6]

On the other hand, the Airbus Company studied the possibility and excellent advantages of fibre reinforced composites which has been used in their products, such as A320, A380 and A350, as well. The A350, for instance, is an aircraft which has employed 52% of composites by weight of the total materials like the Boeing 787. The ratio of materials used in A350 is shown in Fig. 1.3.

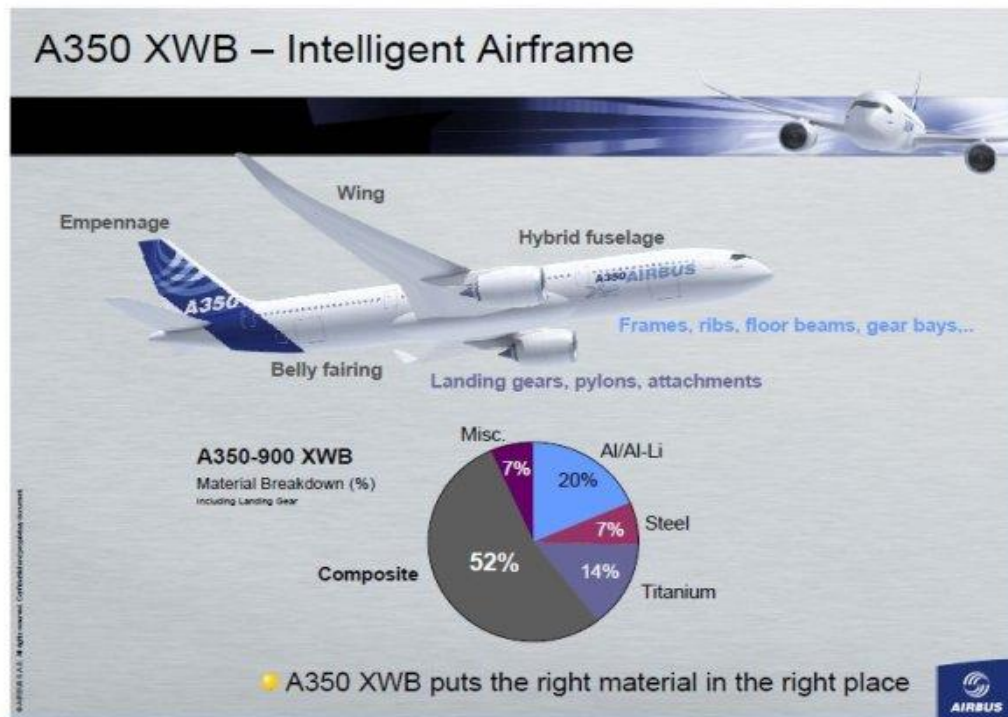


Fig. 1.3 The ratio of materials used in A350 [7]

It is believed that the advanced composite material will be increasingly used in the airplane, with the reasons listed as follows:

- More electrical than metals
- Lighter and stronger
- Fatigue free
- Significant energy-saving
- Environmentally friendly

### 1.3.2 Military aircraft

Apart from the applications in commercial aircraft, composite materials can be used in the military aircraft massively as well. Phil and Costas [8] introduced the history of the composite materials used in the military aircraft particularly. In the 1980s, the composites have been employed in Bell helicopters as they can reduce 20 % in weight compared with the metallic airframes. Furthermore, composites have been extensively applied on the new military aircraft, for example, the JFC, EFA in Fig. 1.4.



Fig. 1.4 The Typhoon jet fighter, Eurofighter [8]

### 1.3.3 Transportation

Composite, as a material type, is more varied than any traditional engineering material. Composites can be, and should be, tailored to an application, which means that it is far from straightforward to design and manufacture. The new composite materials have provided the promise of innovative applications in transportation. Apart from the applications in aerospace engineering, the composite materials have been also extensively used in the field of transportation such as the automobile, the high-speed train and the marine etc. As shown in Fig. 1.5, there are some typical examples of the extensive applications of composites.

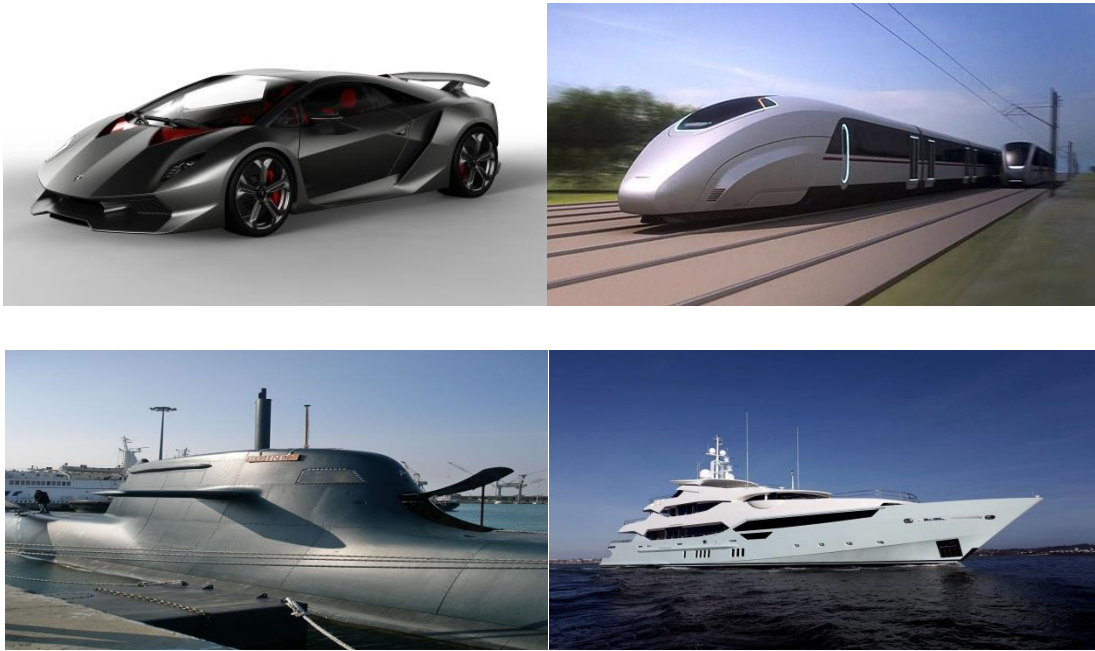


Fig. 1.5 Examples of composites used in transportation

### 1.3.4 Other applications

In terms of sporting goods, the increasing use of composites is a tendency as illustrated by Spence [9] that, in the world, the sport and recreation applications are the third largest market of advanced composites and this trend of increasing request of composites is expected to continue into 21<sup>st</sup> century.

The products of sports equipment based on composites are listed as follows:

- Fishing rod
- Bicycle
- Hockey stick
- Racket
- Golf shaft
- Softball bat

### 1.4 Aim and objectives of the thesis

Currently, the increasing demand of light-weight and environmentally friendly materials with high-energy-absorbing characteristics used in airplane and automotive course researchers to investigated

the novel structures made of CFRP, such as individual CFRP tubes, CFRP tubes with various cross-sections and hybrid CFRP tube systems. As traditional materials, aluminium alloy and metal are relatively heavy and have lower energy absorption compared with CFRP.

This thesis is combined with experimental and numerical studies with the aim to investigate both the quasi-static and dynamic performance of composite tube structures for their potential applications in aerospace, automotive and marine industry. Individual CFRP tubes and a wide range of the hybrid systems are studied.

The energy-absorbing characteristics of individual carbon fibre reinforced plastic tubes and hybrid systems have been investigated for the possible use in lightweight impact-resistance structures. The rate-sensitivity of those structures has also been evaluated. Both the peak load and energy-absorbing capacity of the hybrid systems subjected to dynamic loading are higher than those in quasi-static loading condition. The hybrid system filled with low density foam reinforced by small CFRP tubes is the best one in energy-absorption and impact resistance among all the five hybrid system tube.

## **1.5 The thesis outline**

This thesis is concentrating on the study of the energy-absorption characteristics of hybrid CFRP tube systems subjected to both quasi-static compression and dynamic impact. There are six chapters.

Chapter one gives an introduction of fibre reinforced composite materials, including the history and development, the definition and basic classification, applications and the overview of composite materials, the CFRP composites and applications of fibre reinforced materials.

Chapter two covers the literature review related to the composites, which contains the overview of the energy absorption behaviour of CFRP pipes under crash, sandwich structures and natural composite materials, for example, bamboo.

Chapter three describes the techniques of manufacturing the CFRP tube systems and experimental procedures to test the samples subjected to the both quasi-static compression and low velocity impact.

It also presents the results obtained from the experiments on the CFRP pipes and gives detailed discussion in relation to the experimental data.

Chapter four focuses on the finite element modelling. Firstly, the CFRP pipes with multiply lay-ups subjected to quasi-static compression and drop-weight impact are modelled with the 3D Hashin's damage criteria using the subroutine VUMAT. On the other hand, the sandwich beams based on glass fibre faces and syntactic foam core under impact and three-point bending load are investigated. Finally, the results obtained from the simulation are validated against the experimental data.

Chapter five presents the theoretical calculations of two structures. At first, the peak load and the corresponding displacement of PVC foams reinforced by CFRP/GFRP rods under quasi-static compression load are calculated. Furthermore, the yield strength and the related strain of bamboo tubes subjected to compression load are computed. Subsequently, calculations based on the theoretical work are validated by the experimental data.

Chapter six draws the conclusions of this project programme and gives the recommendations for the future work.

## **CHAPTER 2 LITERATURE REVIEW**

### **2.1 Introduction**

This chapter presents an overview of literature review of the studies on composite structures, including sandwich structures and composite tubes such as carbon fibre, glass fibre and natural fibre tubes. Firstly, the background and development of both the composite sandwich structures and tubes are reviewed. Subsequently, the experimental studies and simulation work are reviewed on sandwich structures as well as composite tubes.

## **2.2 Overview of sandwich structures**

In recent decades, composite sandwich structures are increasingly used as light-weight structures in a wide range of industries due to their specific mechanical properties. A sandwich structure is made up of two thin skins and a low density core. One of the main functions of the thin face sheet is to resist the damage caused by a hard projectile such as runway debris and hail [10, 11]. Furthermore, the performance of sandwich structures following crush depend on the properties of the skin, core materials and bond between skin and core.

### **2.2.1 Background and development**

Sandwich structures consisting two skins and a low density foam core material have been studied extensively. The history and development of sandwich structure have been reviewed by Ramadan et al [22]. The initial application of sandwich structure can be dated to the WORLD WAR II, when plywood based sandwich structure being used in a mosquito night bomber in England. Meanwhile, sandwich structure based on two thin plastic faces and a foam core material has been studied in other countries such as USA and Germany etc. For example, Anerson and Madenci [13] carried out the experimental study on the in-plane compressive behaviour of sandwich panels in 1944.

As a material used in a wide range, the Polyvinyl Chloride (PVC) foam has a long history and the development [14]. In the early stage, the Great Britain and Germany were the first two countries, when the PVC was studied in 1912. However, it became marketable applications until the beginning of 1930s. Around twenty years later, in 1950s, more companies in the world started to produce the PVC, with the volume being increased dramatically. PVC, currently, is still the material which ranks in the top three of plastics most used in a wide range of industrial applications around the world.

#### **2.2.1.1 Skins of sandwich structures**

The face skins employed for sandwich structures request a high strength to resist the in-plane tensile and compressive stresses and prevent the fracture of face sheet or perforated by loading such as

projectile impact. In the later 20<sup>th</sup> century, researches [15-21] were increasingly focusing on the investigation and manufacture of novel sandwich skins and cores materials, shown as follows:

- PVC, Liner, PET,PEI,PU, PMI [15]
- Glass fabrics, carbon fabrics, carbon/Kevlar hybrid fabrics, Kevlar fabrics with vinyl ester resin [16]
- Glass fibre/ polyester [17]
- Woven carbon/ epoxy [18]
- A bidirectional carbon/epoxy [19]
- Woven carbon fibre/epoxy laminates [20]
- A woven glass/phenolic resin [21]

The composite skins, such as carbon, glass and aramid fibre reinforced composites, were studied and used. Furthermore, metallic materials, such steel and aluminium sheet, are employed in the structures to resist the high-speed impact and even a hybrid skin face made of novel FML-reinforced skin.

### **2.2.1.2 Core types of sandwich structures**

The cores used in sandwich structures are of significant importance to carry the steady compressive loadings to resist impact to prevent the face skins to be a buckling mode of fracture. By reviewing the literatures studied by researchers before, the energy-absorbing capacity of sandwich structures is determined by the properties of cores. The classification of cores is based on the materials or structures. Firstly, the cores can be classified based on the types of materials, as shown in Table 2-1.

Table 2-1 Categories of cores for sandwich structures

Core types	Core material categories
PVC foam	PVC, Liner, PET, PEI, PU, PMI [14]
Metal foam	Open-cell, closed-cell, aluminium, titanium and tantalum [22]
Honeycomb	Hexagonal, square, triangular [23]
Natural fibre	Wood, Balsa, bamboo [24]
fold	Paper fold, wood fold [25]
Truss	Pyramidal, tetrahedral, 3D kagome [26]
Textile	Square textile, diamond collinear and diamond textile [27]

On the other hand, Fig. 2.1 presents the classification summarised by Zhu et al [28] of the core types used in sandwich structures.

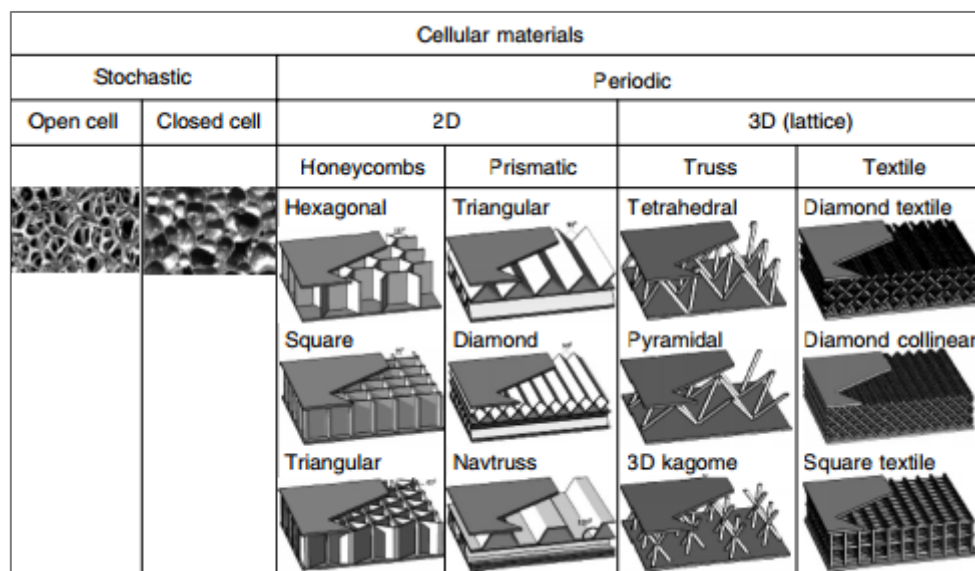


Fig.2.1 Classification of core types used in sandwich structures [28]

Apart from the core types shown in the Table 2-1, a large number of other core structures have been investigated and employed for the applications in aircraft requesting the high quality in energy

absorption. A range of triangular corrugation structures made of glass or carbon fibre reinforced plastic and aluminium alloy under low velocity compression loading were investigated by Rejab and Cantwell [29], in which the researchers studied the effects such as unit cells, the thickness of the cell walls and the width that would influence the mechanical response and energy absorption of sandwich structures.

The energy-absorbing capacity of polymer foams reinforced by carbon fibre tubes subjected to both quasi-static compression and blast loadings was investigated by Alia et al. [30]. In the research, the researchers studied the foam density and arrangement of tubes affecting the crush behaviour of these sandwich structures with light-weight cores and the capacity of energy absorption of carbon tube reinforced the polymer honeycombs, aluminium honeycombs and metal foams have been presented as well. Furthermore, the selective laser melting (SLM) lattices based on body-centred cubic core subjected to compressive loading were tested to study the yield strength and energy absorption was investigated by Smith et al [31]. The results suggest that the reduction of the unit aspect ratio could improve both the yield strength and energy-absorbing capacity.

### **2.2.2 Experimental studies on sandwich structures**

Extensive experimental studies have been conducted on sandwich structures subjected to both static and dynamic load in order to investigate the mechanical properties such as tension, compression and bending strength of sandwich structure. The sandwich structures based on different types of foam such as PVC, PET and PU subjected to low velocity impact were tested by Hassan and Cantwell [15]. It compares the compression strength of sandwich structure with various cores. The RPU core material with different skins, such as carbon fabrics, Kevlar fabrics and carbon/Kevlar hybrid fabrics under low velocity impact was investigated by Xia and Wu [16]. Furthermore, Lendze et al [17], Schubel et al [19, 20] focused on the sandwich structures with closed cell PVC core and glass fibre/polyester and woven glass fabric/epoxy laminates subjected to impact loading with low velocity. Apart from the foam cores above, sandwich structures with aluminium honey core and unidirectional glass fibre face sheets under different impact energy were studied [32, 33].

Foams, as one of the most used core materials for sandwich structures, have various types, such as PVC, PET, PMI, PS, PEI, PU, which can be employed in sandwich structures due to their light-weight characteristics and excellent mechanical properties. In early stage, foam was extensively used in the structures of aircraft. In recently, the sandwich structure based on foam cores with reinforcements were studied [34-36]. The summary of sandwich structure based on foam with reinforcement performed much better than the plain foams and the energy-absorbing capacity has improved significantly was concluded. A series of tests including quasi-static compression and dynamic impact have been carried out on crosslink PVC, linear PVC and sandwich structures based on PET foam core and thin glass fibre reinforced plastic skins by Hassan and Cantwell [37]. During the tests, the compression properties were compared between the quasi-static and dynamic tests and subsequently, the energy-absorbing capacity was summarised. The purpose of undertaking both the quasi-static and dynamic tests was to evaluate the effects of the strain-rate.

Apart from the tests on the sandwich structures based on foam cores, Villanueva and Cantwell [38] investigated the mechanical behaviour of novel sandwich structure with FML-reinforced skin and aluminium foam core subjected to the impact load from a gas gun. In addition, the sandwich structures with varying novel cores including honeycombs, prismatic and lattice were investigated and summarised by Zhu et al. [39]. Honeycomb is widely used as a light-weight sandwiched core. A large number of researches were carried out to investigate the sandwich structures based on honeycomb cores. The tests on sandwich structures based on honeycomb core and woven glass fibre reinforced plastic were conducted by Mines et al [40], so did the sandwich structures composed of aluminium honeycomb cores and glass/phenolic by Nettles and Hodge [41].

### **2.2.3 Modelling work on sandwich structures**

Apart from the experimental method to study the response of sandwich structures subjected to crush, a number of researchers attempted to use the finite element modelling to simulate the behaviour of sandwich structures under both the quasi-static and dynamic impact. A model used the refined formulation of a composite sandwich panel was developed to investigate the impact response of the

sandwich plate by Lee et al [42] and a good agreement between the predicted and observed impact behaviour was obtained. Moreover, a model was introduced to simulate the dynamic response of sandwich beams composed of two face sheets and soft cores by Yang and Qiao [43] in which the effect of mass of projectile, depth of core, initial velocity and core stiffness were investigated. It suggested that the change of core depth would cause the significant influence on the impact behaviour of sandwich beam. In addition, a finite element model of sandwich plate based on a Nomex honeycomb was developed to analyse the impact damage under bending load by Palazotto et al [44]. The comparison between low velocity impact and quasi-static data showed that the behaviours of the sandwich panels subjected to impact could be predicted. The finite element model of graded foam-based sandwich panel under perforation failure was developed by Zhou et al. [45]. Here, the FE modelling predicted the impact load-displacement trace and a good agreement were obtained between the predicted and observed data. The value of energy absorbed by the structure during the perforation was predicted accurately as well.

Furthermore, extensive models were developed to study the perforation response of sandwich structures subjected to impact loading by some researchers. A model using the finite element analysis technique was developed to investigate the residual flexural strength after impact and hydrostatic cyclic loading of sandwich beam based on glass skins syntactic foam core by Pavlopoulou [46]. In addition, a model used to predict the response of low-velocity impact of sandwich panel based on glass epoxy skin and aluminium honeycomb core was developed by Lin and Hoo [47]. Moreover, the model of a sandwich panel based on carbon fibre/epoxy skin and aluminium honeycomb core under impact perforation was developed by Buitrago et al. [48]. These researchers summarised that the sandwich panel with 2 mm thick composite skins would absorb the most perforation energy and only 10-20% impact energy would be absorbed by the core.

### **2.3 Overview of high energy-absorbing tube structures**

A number of researchers have studied the response of metal and composite tubes subjected to static and dynamic loadings to investigate the energy-absorbing capacity. Metal tubes with thin-walled structure have been widely used in civil and military applications due to their high energy absorption.

Especially, aluminium alloys have attracted a great attention due to their low weight, low cost and ease manufacture. The aluminium alloys are classified based on the fabrication process, chemical composition and heat treatment. As the aluminium alloys with different designation have varying mechanical properties, the associated designation of aluminium alloy was established by Mazzolani [49] in Table 2-2 as follows:

Table 2-2 Classification of aluminium alloy [49]

Series designation	Major alloying elements
1XXX	Aluminium (99.00% pure), can be worked hardened
2XXX	Copper
3XXX	Silicon, with additions of copper, magnesium
4XXX	Silicon or silumin
5XXX	Magnesium
6XXX	Magnesium and silicon. Easy to machine, are weldable unused series of numbers
7XXX	Zinc, hardened to the highest strengths
8XXX	Tin, other elements

Currently, with the increasing request of high energy absorption and dynamic resistance when accidents happen to avoid loss of life and damage, more research work was conducted to study the mechanical properties of composite tubes. The composite tubes reinforced by carbon or glass fibre are increasingly used in a wide range of engineering structures with high-performance in energy absorption currently. The main reason why these lightweight materials being widely used is their significant energy-absorbing capacity subjected to certain well-defined loading conditions. Farley and Jones [50] investigated that the failure mechanisms such as fibre fracture, matrix cracking, debonding and delamination which contributes to the significant energy absorption when testing the composite

tubes following compressive loading. The crushing process is shown in Fig. 2.2 [51]. The impressive energy-absorbing characteristic of composite tubes has attracted great interests from researchers and engineers.

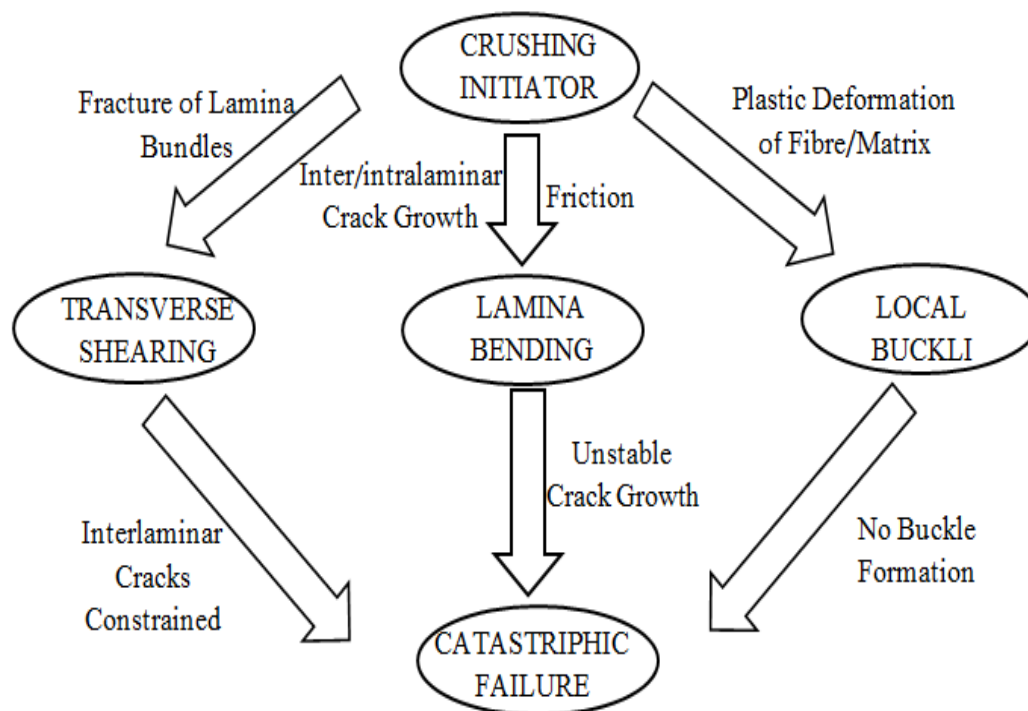


Fig. 2.2 Crushing process of continuous fibre-reinforced composite tubes [51]

### 2.3.1 Experimental tests on tube structures

#### 2.3.1.1 Metal tubes

A large number of researchers have conducted the experimental study in order to investigate the mechanical response and energy-absorbing capacity of the metal tubes. Fan et al. [52] investigated the dynamic lateral crushing of individual metallic tubes and associated hybrid systems. Besides, investigations on the response of lateral crushing of empty tubes were extensively conducted by many researchers [53-58]. All of the investigations presented that the crushing of these tubes involving plastic bending, which may be used as ideally plastic hinges in order to model the lateral collapse of tubes. As the strain localization around the plastic hinges, it may not be more efficient for energy absorption in this condition. Thus, in order to further improve the performance of energy absorption, a hybrid tube system filled with metal foam might be an alternative structure. Previous researches on

the quasi-static behaviour identified this enhancement in the crush strength and energy-absorbing capability [59]. However, the reports on the response of hybrid tube systems under dynamic lateral compressive loading are very limited in the public domain. Furthermore, metallic foams are strain-rate sensitive [60-61] with a higher plateau stress and a higher energy dissipation capacity under impact or blast loadings compared with the quasi-static loading case.

Moreover, the benefit of thin-walled structures is clear, due to their lightweight, low cost and easy to production. A number of researchers have investigated the tube structures with circular, square, triangular, polygonal, and conical sections individually or in combination with polymeric and metallic foam subjected to both the quasi-static and dynamic axial impact. The cylinders introduced as energy absorber subjected to axial loading were investigated by Alexander [62] for the first time. Furthermore, the thin-walled tubes was studied as a mechanism for energy absorption and both the experimental as well as theoretical studies on square/circular tubes following dynamic and quasi-static loadings were conducted by Abramowicz and Wierzbicki [63, 64], Abramowicz and Jones [65, 66], and Andrewsetal [67]. Square tubes made of mild steel were tested by Abramowicz and Jones [65, 66], suggesting that both symmetric and asymmetric happened during the crush. The super folding element (SFE) theory used to predict the mean crushing load of multi-comer sections based on the deformation folds of bending on the square and polygonal cross-section was introduced by Abramowicz and Wierzbicki [63, 64]. The SFE theory was optimised and employed to predict the results which were closer to the experimental results Wierzbicki [63]. The aluminium alloy tubes with square-section subjected to both the static and dynamic loadings were carried out by Langseth and Hopperstad [68]. The experimental results were summarised that the value of the mean crushing force in static test is greater than that in the dynamic mode and the folds were similar for both the circular and square section. In terms of load-displacement trace, the force started to rise to peak load rapidly and then showed oscillations under axial compressive loading. Both the experimental and theoretical studies were conducted to the octagonal sections of tubes made of aluminium alloy to investigate their mechanical behaviours by Mamalis et al. [69]. Moreover, Zhang [70] tested the steel polygons with various cross-section types such as rhomboid, square and octagonal. Alavi and Parsapour [71] investigated the mechanical behaviour of multi-cell square tubes with equal or unequal cells subject to

impact. The tests on optimized multi-cell square tubes with the same sized cells were carried out by Hou et al. [72], showing that the SEA increased with the increasing number of cells. Both the hexagonal and square tubes with multi-cell sections were investigated by Zhang and Zhang [73], summarising that the good agreement between the experimental data and the simulation results. Using both the experimentally and numerically methods, Alavi and Parsapour [74] carried out the investigations on the thin-walled tubes made from thin aluminium sheets (foil) with two types of multi-cell triangular, square, hexagonal and octagonal sections, concluding that the octagonal tubes with multi-cells absorbed the largest energy among all sections, as shown in Fig. 2.3.

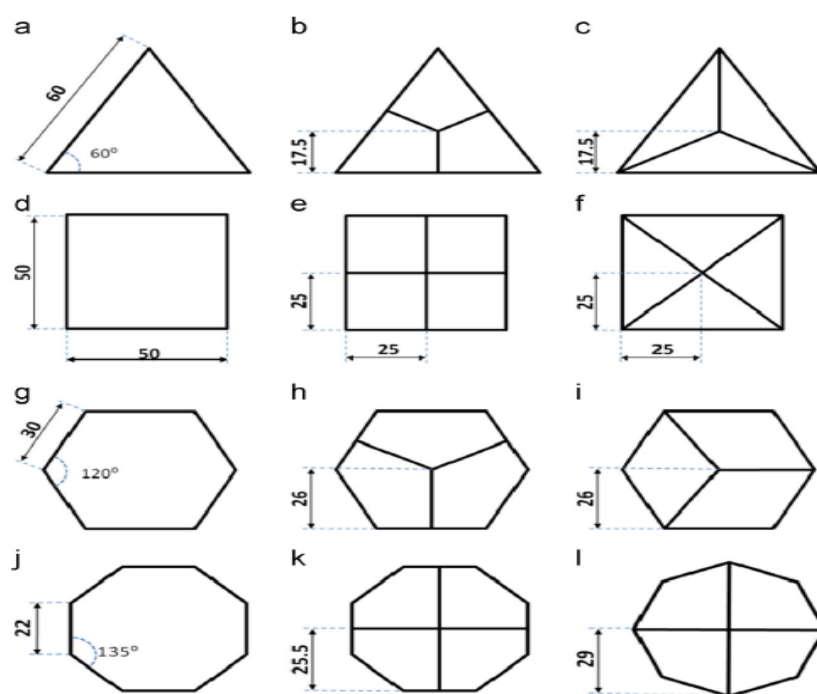


Fig. 2.3 Section geometry and dimensions of specimens made of aluminium alloy [74]

### 2.3.1.2 Composite tubes

On the other hand, as a high energy-absorbing structure, fibre reinforced plastic (FRP) cylinders or tubes are now being used in the applications of transportation [75-80]. As the geometry of a certain structure is one of the parameters affecting energy-absorption capacities of composite materials, a number of investigations on those parameters were carried out and published. For example, Palaniveluetal [81] investigated the composite tubes made from glass-fibre reinforced polyester with different geometry, as shown in Fig. 2.4. From the experimental data, the author summarised that the

tubes with circular cross-section (CD) exhibited the highest value for the specific energy absorption (SEA), while the lowest was recorded for the tubes with hexagonal cross section (HXD). In terms of mean crushing force, the highest value was recorded for the tubes with square cross-section (SD) and conical cross-section (CX), while the lowest was the HXD one.

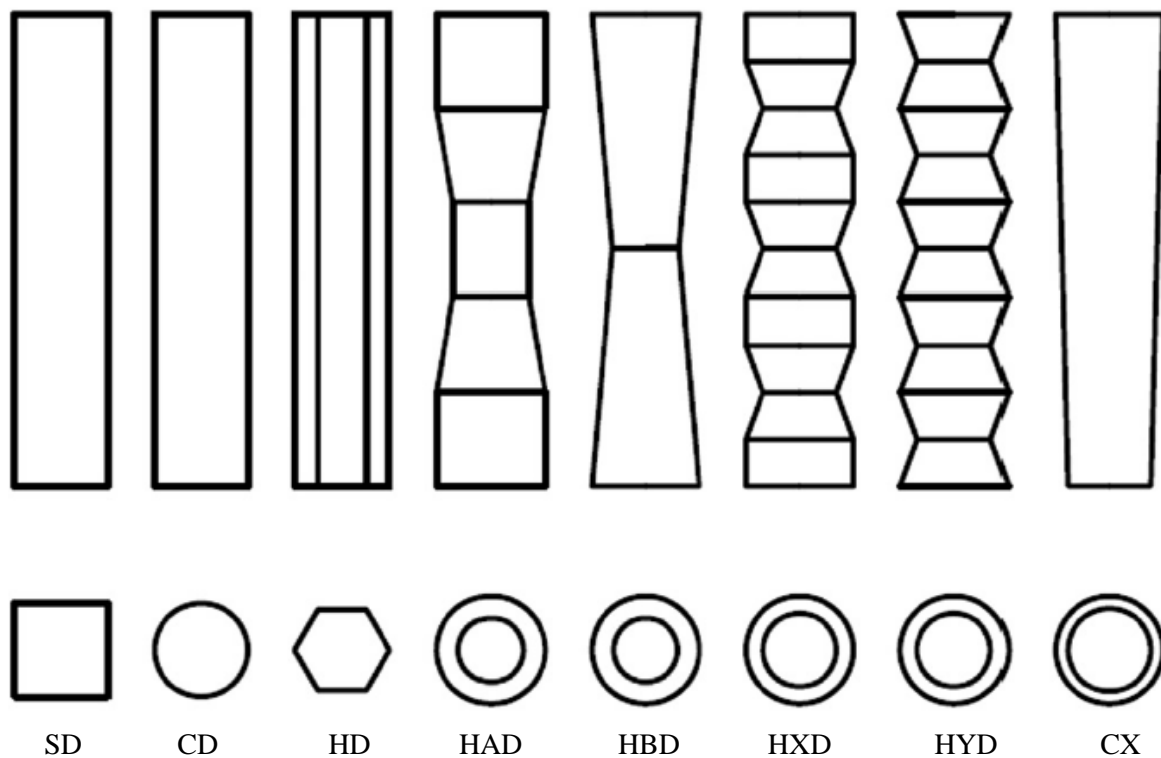


Fig. 2.4 Different geometry of the composite tubes [81]

Furthermore, the influence of corrugated angle of circular tubes made from glass and carbon fibre reinforced epoxy composites on the energy-absorbing capacity under crush was investigated by Elgalai et al. [82]. The results were summarised that the introduction of corrugation in a uniform manner could improve the energy-absorbing capacity of composite tubes significantly and the composite tubes with a corrugation angle of  $40^{\circ}$  exhibited the highest value of specific energy-absorbing capability. Three types of tubes with circular, radial-corrugated composite and a combination of both circular and radial-corrugated tubes were investigated by Abdewi et al. [83, 84]. All specimens used in the test was made from woven roving-glass/epoxy with the same values of layers and then the experimental results were summarised that both of the energy absorption and

stability of tubes with radial-corrugated were better than the other two types when subjected to both the axial and lateral quasi-static loading.

Apart from the variables affecting the energy-absorbing capacity on composite tubes reported above, a number of researchers have investigated the energy absorption ability of composite tubes made of various materials, such as carbon, glass and natural fibre reinforced composite tubes. The carbon fibre reinforced tubes subjected to static compression tests were studied and compared with the tube reinforced foam structure by Cantwell et al [85]. The energy absorbing capacity of carbon fibre reinforced tube with various D/t ratios from approximately 8 to 33 was summarised, which suggested that the D/t ratio with very low value could contribute to a great improvement on energy absorption in tubular structures. Besides, Ramakrishna and Hull [86] studied the energy-absorbing capacity of composite tubes reinforced by knitted carbon fibre fabric and used the specific energy absorption (SEA) capacity measured in kJ/kg to evaluate the energy-absorbing ability of composite tube. It summarised that the SEA of composite tubes increased with the enhancement of fibre content. Ramakrishna et al [87] investigated the carbon fibre, with fibre orientations of  $0^{\circ}$ ,  $\pm 5^{\circ}$ ,  $\pm 10^{\circ}$ ,  $\pm 15^{\circ}$ ,  $\pm 20^{\circ}$ ,  $\pm 25^{\circ}$ , reinforced composite tubes with different matrix such as polyetheretherketone (PEEK), polyetherimide (PEI), polyimide (PI) and polyarylsulfone (PAS). The results suggested that the specific energy absorption capacity was dependent on the fibre orientation. Various types of fibre-reinforced composite tubes such as carbon fibre-epoxy unidirectional laminated tubes, woven glass cloth-epoxy tubes, filament-wound angle-ply glass fibre-polyester tubes and plane random chopped glass fibre-polyester tubes were investigated and the parameters affecting the crushing behaviour and energy-absorbing capacity were summarised [88]. In addition, natural fibre reinforced bamboo tube and its reinforced cross-linked PVC foam structures were tested by Umer et al. [89] and the alternatives were investigated to enhance the SEA of the bamboo tubes.

Moreover, a number of researchers have investigated the SEA characteristics of composite tubes and its related structures. According to the published literatures, the values of SEA of extensively used composite structures, for example, carbon fibre rods and tubes vary from 13-90 kJ/kg. Jacob [90] investigated experimentally on pultruded glass fibre/epoxy tubes and the corresponding SEA was

found to be 20 kJ/kg. Furthermore, extra carbon fibre-based systems were investigated as well, with the value of SEA being more than 100 kJ/kg [91]. Apart from the factors (matrix phase, fibre type and fibre orientation) which could affect the energy-absorbing capacity of composite tube significantly, the geometry of the composite tube could influence the value of SEA as well. The influence of geometry of composite tubes on their energy-absorbing response subjected to both static and dynamic loadings was investigated by Thornton and Edwards [93]. Further study on the energy absorption capacity of composite tubes based on circular, square and rectangular cross-sections were summarised by Thornton [93]. It was suggested that the circular tube is the most effective one to absorb energy compared with the other two cross-section shapes. The tests were conducted on carbon and Kevlar fibre reinforced circular tubes with different orientations multiplies. It was found that the D/t (diameter to thickness) ratio was of great importance in energy absorption capacity [104]. The same results were summarised by Alia et al. [95], illustrating that the energy-absorbing capacity increased by more than 50% with the D/t ratio decreased from 42 to 6.

Apart from the tests on individual composite tubes above, further studies on the tube reinforced foam structures were investigated by other researchers as well. The influence of strain-rate on the energy-absorbing capacity was studied on the composite tube reinforced foam structures by Zhou et al. [96] as well as by Schmusser and Wickliffe [97]. It was suggested that the SEA values of composite tube reinforced foam structures were lower following static compressive loading than those values subjected to dynamic rates of loading. The comparison of values of SEA between the quasi-static and dynamic experimental results were summarised [97], which suggested that the values of energy absorption decreased by over 30% when carbon, glass and Kevlar tubes subjected to static loading.

### **2.3.2 FE modelling on tube structures**

Compared with the experimental approaches, the FE modelling, if it is validated, is a more economical method to study the crushing behaviour of composite tubes and its reinforced foam structures to obtain the energy-absorbing characteristics, as the experimental tests are always costly and time-consuming. Prior to the test, the corresponding models can be employed to predict the

behaviour of composite rods, tubes and their reinforced foam structures in different boundary and loading conditions. A model using LS-DYNA was developed to analyse the failure mode and energy-absorbing behaviour of braided composite tube subjected to axial compression by McGregor et al. [98]. Here, the model of two-ply and four-ply square tubes used as front rail structural components of vehicles was developed to predict the energy-absorbing capacity when crush happened. It is a challenge task to develop a model to predict the both energy-absorbing capability and the failure mode of fibre reinforced plastic tube under both the static and dynamic loading. There are few publications on simulating the crushing of composite tubes and the failure mode. A micromechanical model was developed by using in the ABAQUS/Implicit with a user-defined subroutine to simulate the crush process of composite tube with plug-initiated triaxially braided and the failure mode [99]. Also, a model used ABAQUS/Explicit was developed to simulate the dynamic behaviour of composite tube under crushing load by Flesher [100]. Another model using LS-DYNA was developed to predict the SEA values of composite tube without damage initiation (chamfer), which were 30-40% lower than the experimental results [101].

Although the difference between the predicted and observed failure modes still exists, more researchers were trying to optimise the models to obtain reasonable results in terms of energy-absorbing capacity and failure modes, respectively. A finite element model was developed to simulate the axial crush of CFRP square tubes following both the static and dynamic crushing by Mamalis et al. [102]. A layer used to model the resin layer was turned into debris during crushing and the deletion criterion of failure elements was introduced. A model was developed to simulate the splaying mode of glass-polyester tubes under axial loading by using the LS-DYNA to obtain the typical load-displacement traces and predict a delamination, damage initiation and propagation during the splaying failure of the glass/polyester circular tube by Silcock et al. [103] and Pinho et al. [104].

Apart from the simulations on composite tubes, the behaviour of tubes made of aluminium alloy with circular, square, triangular and tapered sections was analysed by Alavi and Hamedani [105] using FE modelling and validated against the experimental tests. The specimen was fabricated by argon welding of aluminium and the influence of the weld line on the modelling results was ignored. Zhang

and Zhang [70] investigated steel polygons with rhomboid, square, and octagonal sections using numerical simulations and the results of modelling were validated against experimental data. The specimens were welded at the middle of the opposite sides symmetrically to mitigate the effects of the weld. The effect of weld line was ignored in simulations due to the slight influence of the weld line on the results. Moreover, numerical investigations on the characteristics of multi-cell square tubes were carried out by Alavi and Parsapour [106], in which the modified formula used to predict the mean crushing load for unequal sized cell sections was presented as well. Then the simulation results were validated by the experimental data. Zhang and Zhang [107] carried out both the numerically and analytically investigations on the influence of element angle in multi-cell tubes. The energy-absorbing capacity of multi-cell square tubes with irregularly-formed cells was investigated using both the analytically and numerically methods by Najafi and Rais-Rohani [108]. Tang et al. [109] studied the mechanical response of circular tubes with multi-cell sections using finite element method and presented that the capacity of energy-absorbing for circular tubes is greater than that of square tubes.

The models developed so far on the composite materials under crush were usually using the failure criteria with 2D elements, such as plane stress and shell elements. However, the existing failure criteria in the commercial packages such as LS-DYNA and ABAQUS is not accurate enough to predict both the reasonable SEA values and failure modes for composite tubes as the rate-dependent through composite thickness is not taken into account. Therefore, a model using 3D solid elements with associated failure criteria need to be developed to simulate the composite materials.

## **2.4 Conclusions**

This chapter has reviewed studies on the high energy absorption tubes under both lateral and axial crushing load as well as sandwich structures under both the static and dynamic compressive loadings. Firstly, the overview on sandwich structures including the history and development, experimental work and numerical simulations has been introduced. The types of skins and classification of cores based on materials and structures have been discussed. Furthermore, the finite element modelling of steel and aluminium alloy subjected to quasi-static and dynamic crush loadings has been reviewed and extensive researches on the simulation of composite tubes has been introduced as well. Subsequently,

both the experimental and numerical studies on the composite tubes have been reviewed, including the investigations on the influence of the geometry, D/t ratio, corrugation angle and fibres types on the energy-absorbing capacity and peak crushing load. Summarising from previous research work, the CFRP tubes with novel structure have not been investigated before. As the increasing demand of energy conservation and emission reduction, the light-weight composite materials, especially the CFRP materials with high energy absorption will be extensively used in the future.

## **CHAPTER 3 EXPERIMENTAL WORK, RESULTS AND DISCUSSION**

### **3.1 Introduction**

This chapter presents the procedures to prepare for samples and undertake experimental work. Firstly, carbon fibre tubes with different diameter were cut to make hybrid pipe systems with and without foam filling. Then, the quasi-static uniaxial compression tests were conducted on the individual CFRP tubes with various outer diameters, followed by testing the systems with various combinations. According to the data obtained from the quasi-static tests, the mass and height of the drop weight used in the impact tests were estimated. Then the dynamic tests were subsequently conducted. Experimental data were recorded, processed and presented. The detailed discussion was given to evaluate the response of individual tubes and the related hybrid systems.

## 3.2 Types of CFRP tubes

Carbon fibre tube can be used to replace or substitute aluminium or steel tubes in a wide range of applications due to their superior mechanical properties, such as high strength to weight ratio, high stiffness to weight ratio and high energy absorption. All of the CFRP tubes were purchased from EASYCOMPOSITES Company [110] and there were two types of CFRP tubes utilized in this research programme:

- Roll wrapped
- Pultruded

These roll wrapped tubes with layers placed in [90,0,90,0,90] pattern are manufactured predominantly using high modulus (T700) unidirectional prepreg carbon fibre oriented to provide the maximum strength in the longitudinal direction, but the use of prepreg reinforcement oriented at 90° also ensures that the tube has a good crush-strength, which is ideal for energy absorbing applications. The use of unidirectional fibres and maximum strength in the longitudinal way means that the tube is not strong across its diameter as it is longitudinal direction, so should be used in such a way as to avoid unnecessary crushing forces across the tube.

The pultruded tubes are the most commonly used type of carbon fibre tube. Pultrusion is a method of manufacturing continuous lengths of fibre reinforced section by pulling continuous strands of carbon fibre through resin and a former before curing the resin all in one process. Pultruded tubes feature 100% longitudinal fibre orientation which gives them excellent strength along their length, but does make them vulnerable to crushing forces.

## 3.3 Sample preparation and testing

### 3.3.1 Cutting tubes

The carbon fibre reinforced epoxy tubes investigated in this study were based on a range of circular T700 carbon fibre reinforced epoxy cylinders purchased from the supplier with dimensions of 1000 and 2000 (in mm). As the individual tubes tested in this project programme are 20 (in mm) in length, the longer tubes were cut into shorter ones with the length of 20mm. In order to obtain the flat end

surfaces, the Dremel with diamond saws and the matched mould were used to connect the Dremel and lathe, shown in Fig. 3.1.



Fig. 3.1 The Dremel, saws and matched mould used to cut tubes

The Dremel and the matched mould, as shown above, were assembled in the lathe in Fig. 3.2 and Fig. 3.3.



Fig. 3.2 The overview of Dremel, saw and matched mould assembled in lathe



Fig. 3.3 The top view of Dremel, saws and matched mould assembled in lathe

There are three OD (outer diameter) sizes of CFRP tubes tested i.e. 8, 34 and 54.4 mm. In the hybrid tube systems, the individual CFRP tubes mentioned above were employed. Fig. 3.4 shows the images of individual CFRP tubes, and the details of those CFRP pipes are summarized in the Table 3-1.



CFRP1 (8 mm)



CFRP2 (34.8 mm)



CFRP3 (54 mm)

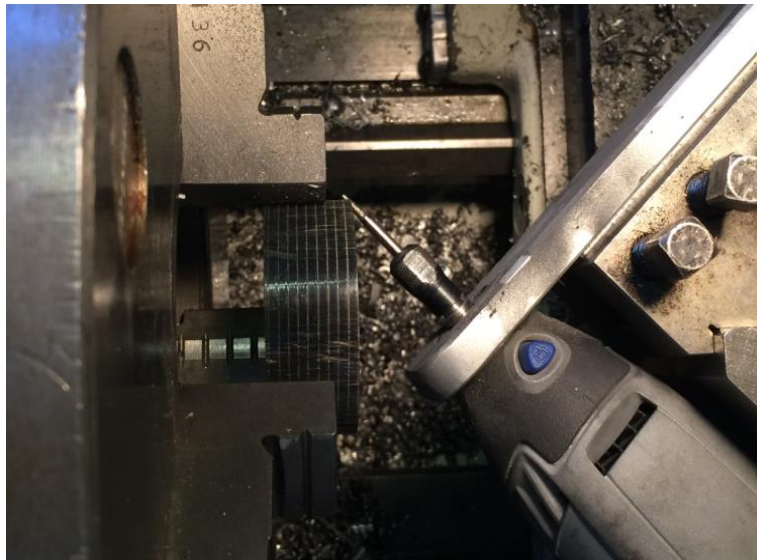
Fig. 3.4 Images of individual CFRP pipes with outer diameter 8, 34.8 and 54 mm.

Table 3-1 Summary of the geometrical characteristics of the 20 mm length CFRP tubes

Test ID	Outer diameter Do (mm)	Inner diameter D (mm)	Thickness, t (mm)	D/t	Mass (g)	Fibre weight fraction
CFRP1	8	6	1	6	0.7	0.58
CFRP2	34.8	32	1.4	22.9	4.4	0.64
CFRP3	54	50.8	1.6	31.8	9.6	0.60

### 3.3.2 Making chamfers

According to the previous research [111], the use of crush initiators as a collapse trigger mechanism encourages suitable progressive crushing of the specimens. Then the 45° chamfer was introduced at one end of the tube shown in Fig. 3.5(b). The tools used to make chamfers were based on the previous Dremel with the tread pins (Fig. 3.1). The image of Dremel with thread pin is assembled in the lathe, as shown in Fig. 3.5(a).



(a) Equipment to make chamfer



(b) CFRP tube with 45° chamfer

Fig. 3.5 Overview of Dremel, pin and matched mould assembled in lathe and a tube with a chamfer

### 3.3.3 Manufacturing hybrid tube systems

Apart from the individual CFRP tubes, the hybrid systems were manufactured as well. Hybrid tube systems used in this project are consisting of tubes in different dimensions with and without filling foam. The exterior pipe chosen from the tubes in Table 3-1 is CFRP3 and the CFRP2 for the interior one. There are five types of hybrid systems. Hybrid system 1 was based on the small tubes (CFRP1) without any foam filling, which were placed in the gap between the two larger tubes (CFRP2 and CFRP3). On the other hand, the second types of the hybrid systems 2 and 3 were made up of CFRP2 and CFRP3 tubes with foams with two densities filled the gap between them. The HS4 and HS5 were based on the HS1 with the two foams filled. Fig. 3.6 shows the images of hybrid systems.



Hybrid system 1  
(HS1)

Hybrid systems 2 and 3 (foams with two densities)  
(HS2, HS3)

Hybrid systems 4 and 5  
(HS4, HS5)

Fig. 3.6 Images of hybrid systems

For manufacturing the HS1, a compass was employed to help to locate the position of the small tubes.

The adhesive used to bond them together is shown in Fig. 3.7.



Fig. 3.7 The adhesive used to bond the tubes

The adhesive used is a kind of PU adhesion consisting of two components. The part A is m-Phenylenebls (Methylamine), while part B is made up of Diphenylmethane 4.

The foams used in HS2 and HS3 were obtained from two mixed resin, with two densities of 57 and 198 kg/m<sup>3</sup>. Specifically, in order to obtain the lower density foam, there were two parts of the Polyurethanes being mixed to obtain the foam. The procedure to fill the foam is shown in Fig. 3.8.

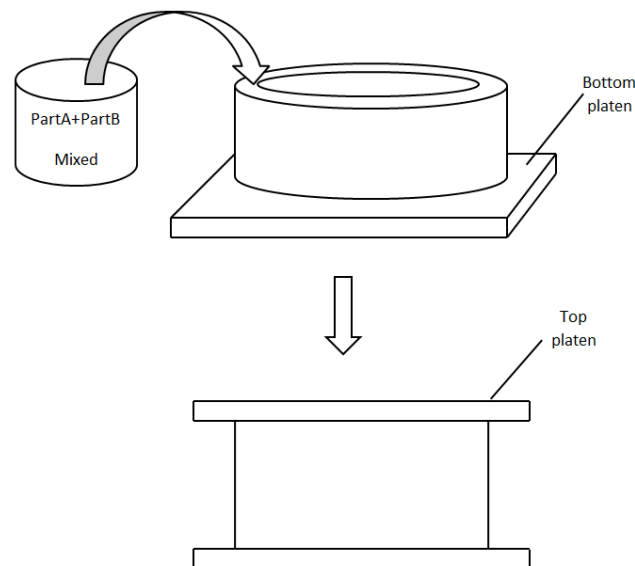


Fig. 3.8 Sketch of the procedures to fill the foam for hybrid systems 2 and 3

The first step is to mix the two parts by volume which is determined by the volume of the gap between two tubes and then pour the mixed liquid into the gap gradually after the two types of Polyurethanes are well mixed. A rigid platen was put on the top in order to ensure the complete

expansion of the Polyurethanes mixed. The Polyurethanes used to make the foam with a density of 57 kg/m<sup>3</sup> are shown in Fig. 3.9.



Fig. 3.9 The Polyurethanes used to make low density foam

On the other hand, the Polyurethanes used to make the foam and the microspheres are employed to reduce the density of the foam are shown in Fig. 3.10.



Fig. 3.10 The Polyurethanes (left) and glass bubbles microspheres (right)

Table 3-2 presents the constituent components of five hybrid tube systems.

Table 3-2 Summary of hybrid systems

ID	HS1	HS2	HS3	HS4	HS5
Component parts	CFRP1	CFRP2	CFRP2	CFRP1	CFRP1
	CFRP2	CFRP3	CFRP3	CFRP2	CFRP2
	CFRP3	Foam1	Foam2	CFRP3	CFRP3
	-	-	-	Foam1	Foam2
	-	-	-	-	-

Apart from the specimens described above, two cubic foams with densities 57 and 198 kg/m<sup>3</sup> were manufactured as well and the corresponding quasi-static compression tests were carried out in order to obtain the mechanical properties of the foams to be used in the simulation work. The details of the cubic foams are summarized in Table 3-3.

Table 3-3 Summary of the foams used in this programme

Specimen images		
Foam ID	Foam1	Foam2
Density (kg/m <sup>3</sup> )	57	198
Cubic Foam dimension (mm*mm*mm)	20*20*20	20*20*20

### 3.3.4 Quasi-static compression tests

Quasi-static compression tests on the individual CFRP tubes and hybrid tube systems were undertaken using the Instron 4505 universal testing machine, which is shown in Fig. 3.11. The samples were placed between two stainless steel platens and then subjected to loading at a crosshead displacement rate of 1mm/min. The load-displacement traces were recorded to obtain the compressive response and energy absorption characteristics of the CFRP tube and the related hybrid systems. Three repeated tests were undertaken on each types of the sample.

In addition, the two types of cubic foams were tested subject to quasi-static compression loading using the same machine. The load-displacement traces were recorded to obtain the corresponding material properties to be used in the crushable foam model.

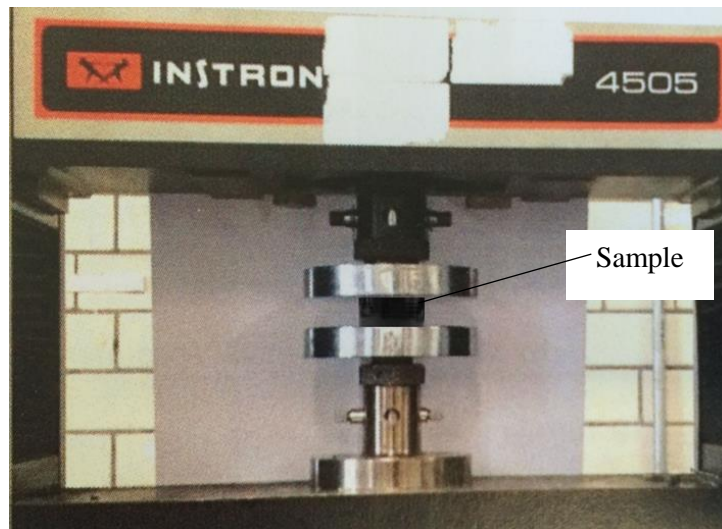


Fig. 3.11 Image of Instron 4505 universal testing machine

### 3.3.5 Dynamic tests

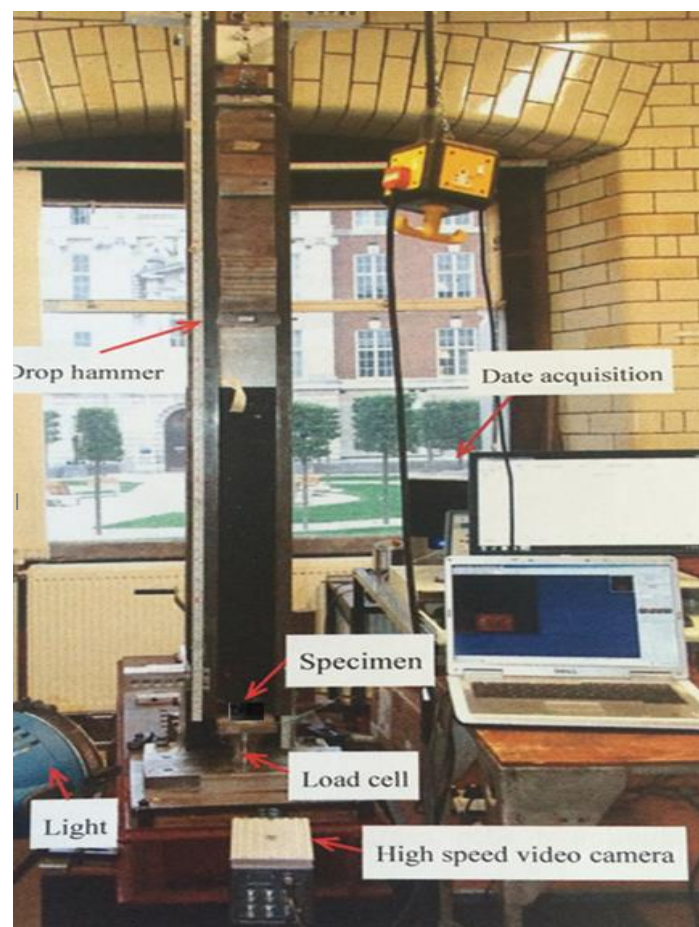
The crush tests were conducted on the individual CFRP tube, hybrid systems and cubic foams using the drop-weight impact towers, as shown in Figs. 3.12(a), (b). The individual CFRP tubes were placed on a bottom rigid platen and the dimension of the support is 100mm placed on a 100 kN load cell shown as in Fig. 3.12(a). On the other hand, the hybrid tube systems were tested using the drop hammer in cooperation with laser Doppler used to record data, as shown in Fig. 3.12(b). The energies absorbed by individual CFRP tubes and hybrid tube systems subjected to quasi-static were calculated by the software Matlab according to the typical load-displacement traces recorded. The energy was then used to estimate the weight and the height of the drop-weight for the impact test, with the similar impact energy. Tables 3-4 and 3-5 present the details of impact mass, height, velocity and energy of drop weight used for specimens for dynamic tests.

Table 3-4 Details of drop hammer used for CFRP tubes in dynamic impact.

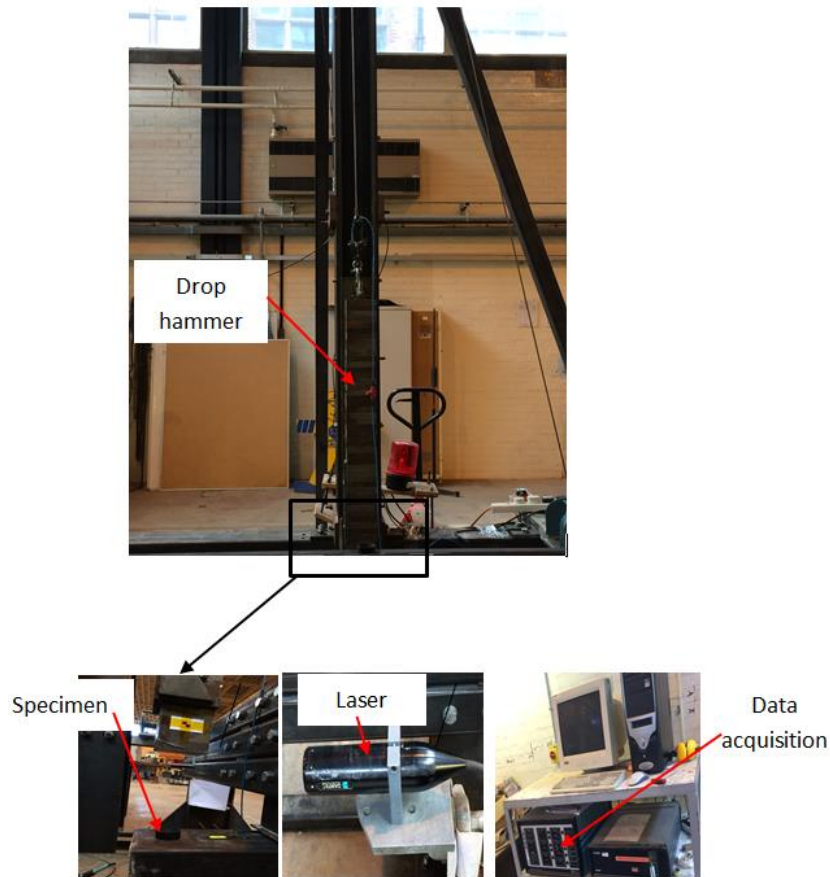
ID	Energy	Mass (kg)	Height (m)	Velocity (m/s)
CFRP1	52.5	7.8	0.67	3.66
CFRP2	218.6	15.0	1.46	5.40
CFRP3	434.6	26.7	1.63	5.71

Table 3-5 Details of drop hammer used for hybrid tube systems in dynamic impact.

ID	Energy	Mass (kg)	Height (m)	Velocity (m/s)
HS1	735.6	107	0.7	3.74
HS2	605.6	107	0.58	3.41
HS3	667.4	107	0.64	3.58
HS4	762.5	107	0.73	3.82
HS5	824.3	107	0.79	3.98



(a) drop-weight impact tower for individual CFRP tubes



(b) drop-weight impact tower for hybrid tube systems

Fig. 3.12 Drop hammer impact tower test rig

Fig. 3.13 presents the sketch of the load-displacement trace of structure under crush. The energy absorption of structure should be the shade area of the load-displacement as shown below.

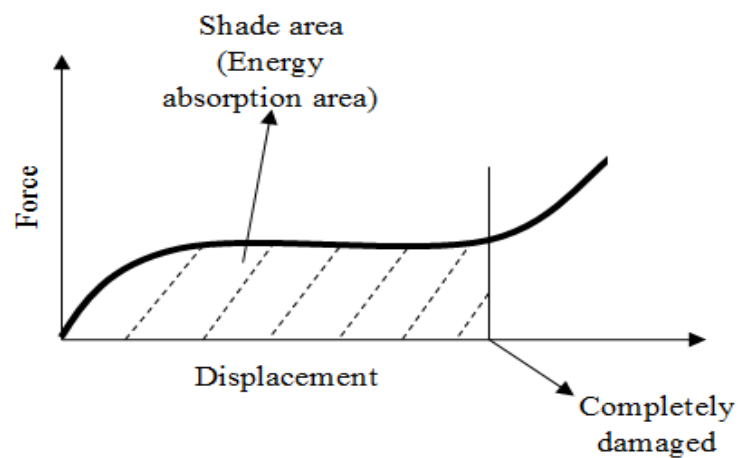


Fig. 3.13 Sketch of load-displacement trace

The equation of SEA is shown as follow:

$$SEA = \frac{E}{m} \quad (3-1)$$

where E is the energy absorption of shade area part, m is the mass.

### 3.4 Experimental results of compression tests

This section presents the experimental results of the quasi-static compression and impact tests on individual CFRP pipes, hybrid systems and cubic foams. The load-displacement traces and failure modes of the specimens are presented and the parameters that affect the energy-absorbing ability are discussed. The results would be further used to evaluate the energy-absorbing behaviour and the compressive response of the CFRP tubes, hybrid systems and foams obtained from the numerical modelling later.

#### 3.4.1 Individual CFRP tubes

Fig. 3.14 presents a comparison of load-displacement traces of CFRP tubes with different diameters. The trace for the tube with an outer diameter of 8 mm is quite different from others. For example, the force of the CFRP1 increases almost linearly up to the peak load and then it stays in a plateau stage to the end. On the other hand, the general trend of the traces for CFRP2 and CFRP3 are similar, but the latter with a much higher load. For instance, for CFRP2, the force is increased sharply to the maximum value when the displacement is about 1.2 mm and then it decreases to a plateau line. The peak load of carbon fibre tubes increases significantly with the outer diameter from 8mm to 54mm (D/T ratio varies from 6 to 31.8).

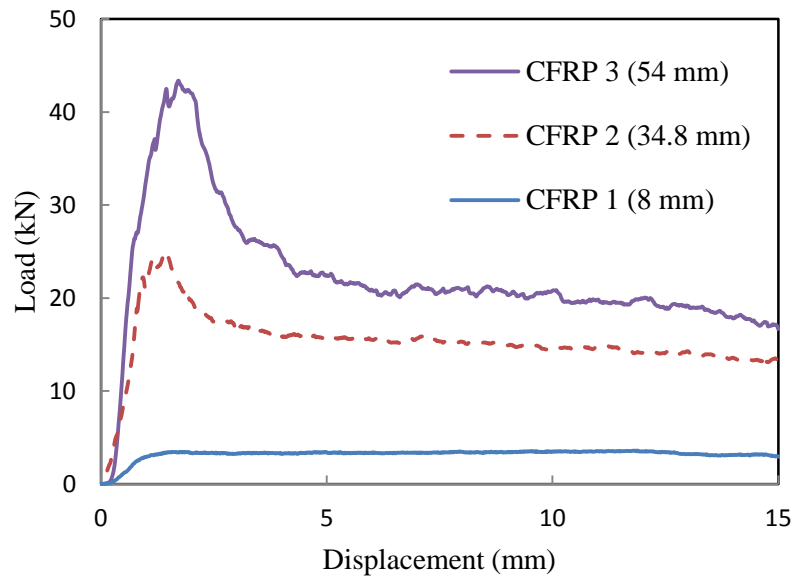


Fig. 3.14 Load-displacement traces of CFRP tubes with different outer diameters (8, 34.8 and 54 mm) subject to quasi-static compression loading

Fig. 3.15 shows the progressive failure of the carbon fibre tubes subjected to quasi-static compressive loading. As can be seen from the images, it is clear that the carbon fibre tube under compression induces the upper part of the cylinder splaying outwards. The fractured debris and dust illustrate that the tubes have absorbed a large amount of energy during crush. Compared with the image failed carbon tubes, it can be found that the CFRP1, as a pultruded type, was crushed to the dust completely, while the relatively large debris were for the roll wrapped tubes.

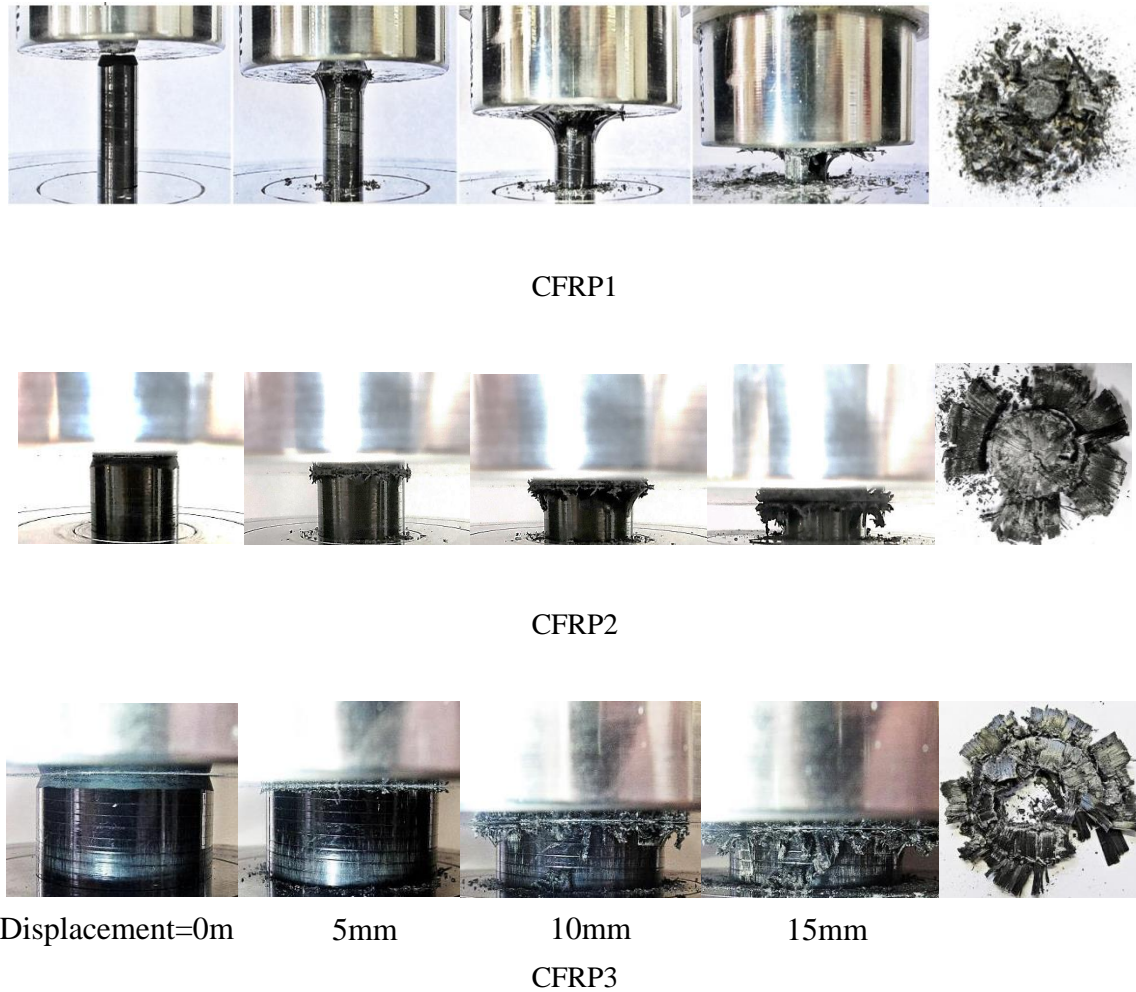


Fig. 3.15 Images of the crushing process in carbon fibre reinforced epoxy cylinders with outer diameters of 8 mm, 34.8 mm and 54 mm ( $D/t$  values of 6, 22.9 and 31.8)

### 3.4.2 Cubic foams

Fig. 3.16 shows the stress-strain curves for the two cubic foams with different density. The yield stress for the Foam2 is nearly 5.5 MPa about 6 times more than the value of Foam1 which is about 0.9 MPa. Both of the two traces display a similar trend. The stress of both foams increases rapidly in a linear manner to the maximum with the corresponding strain of 0.05 before decreases a little, then moves up again due to the hardening of the foam under compression.

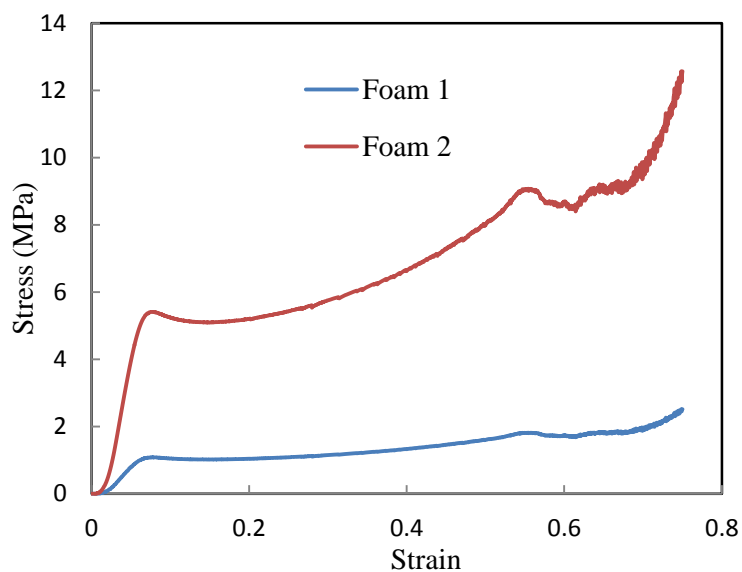


Fig. 3.16 Stress-strain curve of casting foams subjected to quasi-static loading.

### 3.4.3 Hybrid systems

Fig. 3.17 shows the comparison of load-displacement traces for hybrid systems subjected to quasi-static loading. Compared with the HS1, the HS4 and HS5 were filled with foams of two densities between the outer and inner tubes. The entire traces exhibit a similar trend, characterising as a rapid increase of the load, followed by a gradual drop of it. Here, the peak load for HS1 also HS5 is the largest, while that for HS2 is the lowest. After the peak point, the load for all hybrid systems decreases steadily until the end. On the other hand, the curves of HS4 and HS5 display a more similar trend, except for HS4 keeping a down trend until the end, whilst the force on HS5 is more or less in a plateau stage at the later stage.

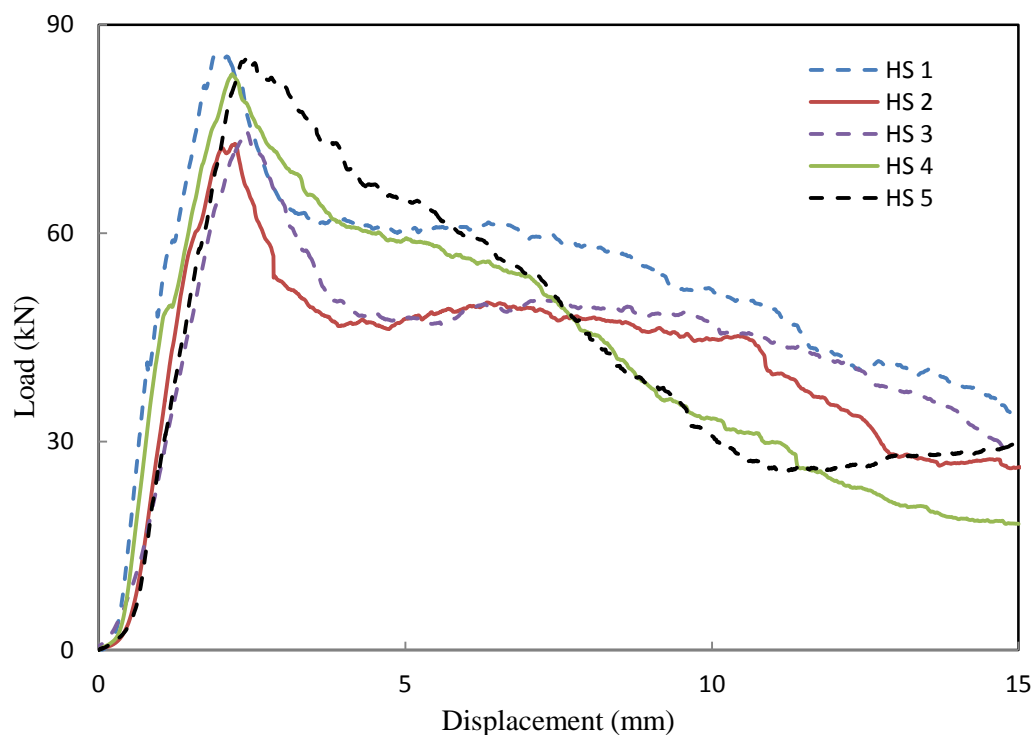
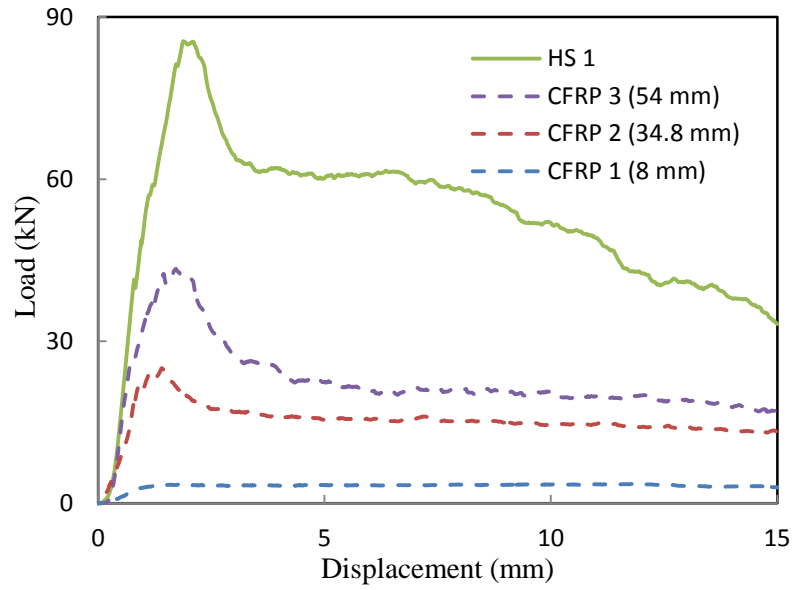
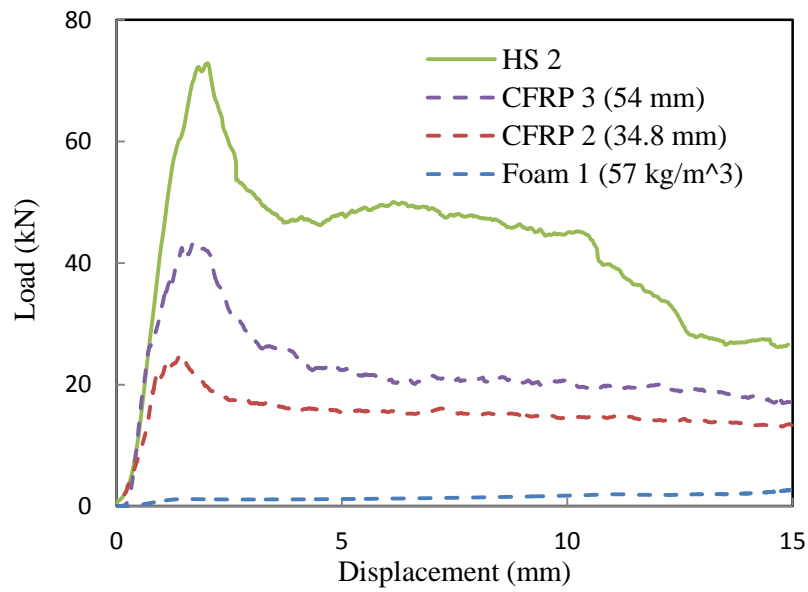


Fig. 3.17 Comparison of the typical load-displacement traces for hybrid systems subjected to quasi-static loading.

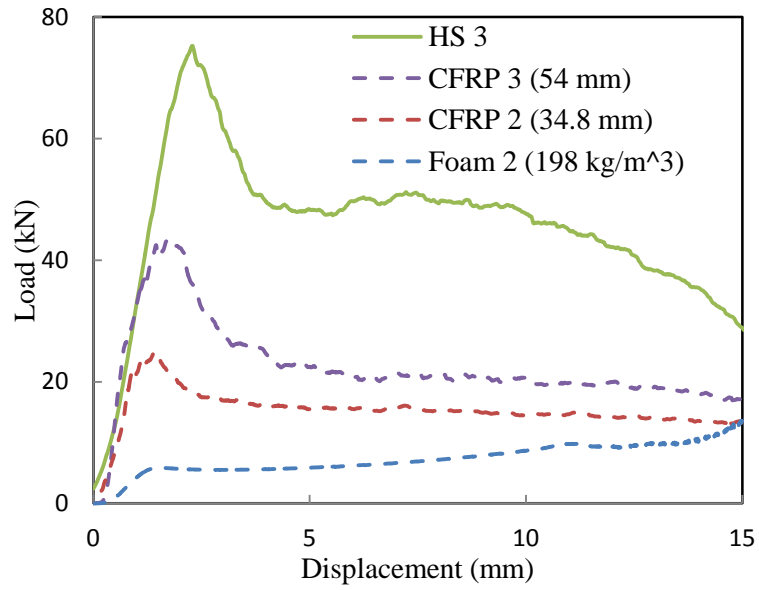
Figs. 3.18(a), (b), (c), (d) and (e) show the comparison of load-displacement traces between the hybrid systems and the corresponding constituent components subjected to quasi-static compression. The curves of hybrid systems exhibit the similar trends. Fig. 3.18(a), for instance, shows the value of force increasing quickly to the maximum load and then dropping to a plateau line to the end for all individual components. On contrast, the force of HS1 increases to the peak load rapidly and then decreases to the end gradually. In Fig. 3.18(b), similar to the curves for constituent components, the force for HS2 rises to the maximum value quickly and it drops to a relatively plateau stage until the displacement of 10 mm followed by a slow drop to the end. The load-displacement trace for HS3 and associated individual components was presented in Fig. 3.18(c). Compared with the force for HS2 and corresponding components, the force for the Foam2 ( $198 \text{ kg/m}^3$ ) displays an increasing trend after the displacement of 6 mm rather than a plateau line as the Foam1 ( $57 \text{ kg/m}^3$ ). The load-displacement trace for HS4 and HS5 are shown in Figs. 3.18(d) and (e), respectively.



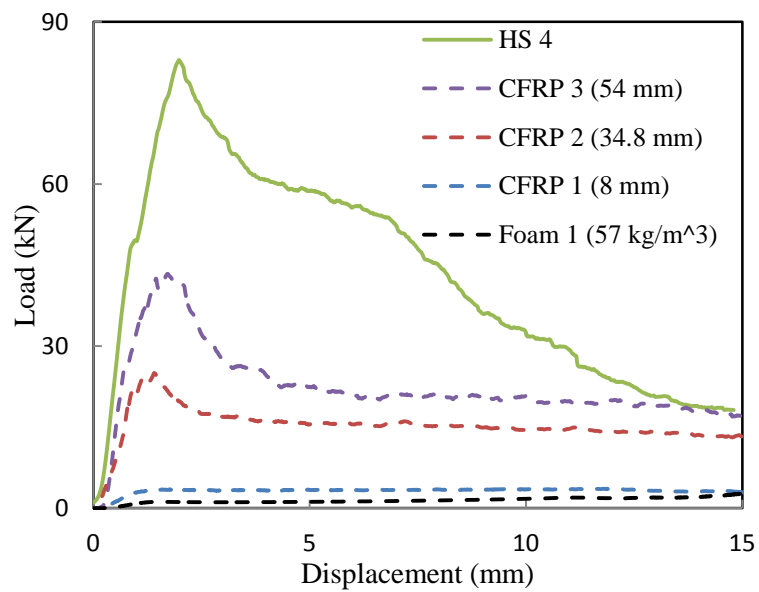
(a) HS1 and associated constituent components



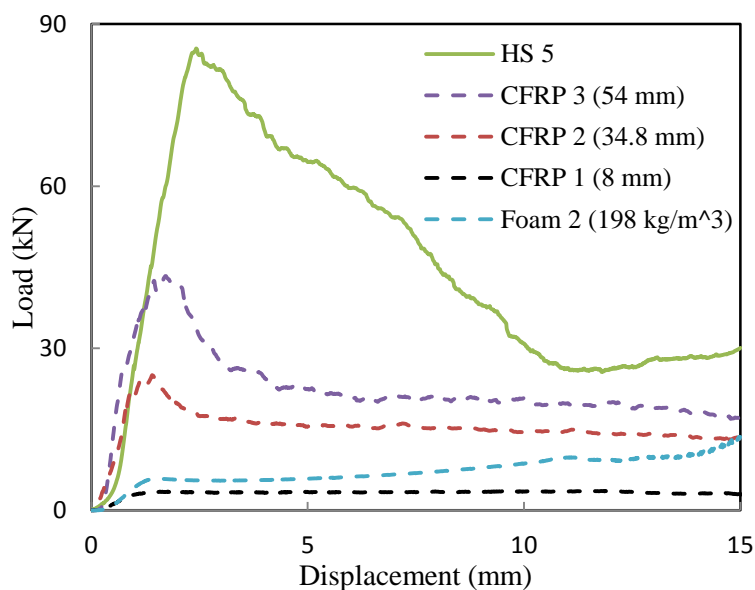
(b) HS2 and associated constituent components



(c) HS3 and associated constituent components



(d) HS4 and associated constituent components



(e) HS5 and associated constituent components

Fig. 3.18 Comparison of typical load-displacement traces for hybrid systems and the corresponding constituent components

Table 3-6 presents the images of failed hybrid systems. The failed samples from both the top and bottom views are shown. It is clear that composite tube CFRP1 in the HS1, HS4 and HS5 was damaged completely. Failure in the HS1, HS2 and HS3 resulted in the formation of long fibre tows having a length to that of the original tube. Fracture in the two larger tubes was associated with the formation of large platelets, formed as a result of the propagation of delamination along the mid-thickness of the cylinder. Moreover, the failure in the HS4 and HS5 was characterised in the formation of small separate parts due to the expansion of the foam hardening.

Table 3-6 Images of failed hybrid systems from both top and bottom views

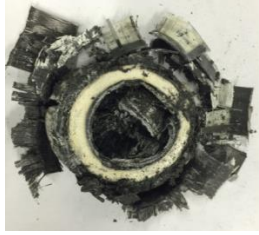
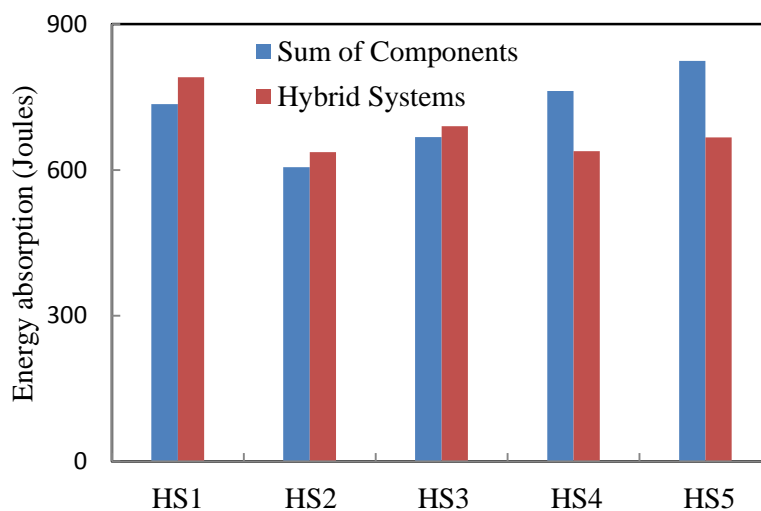
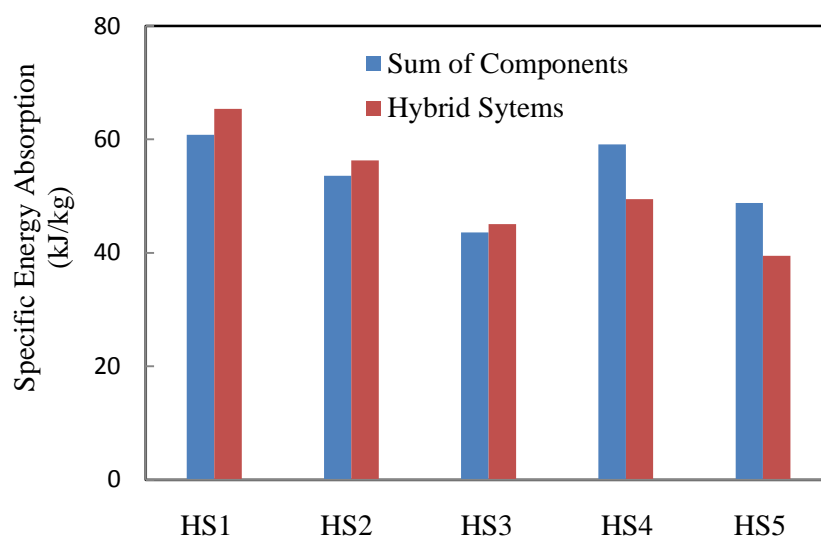
ID	Top view	Bottom view
HS1		
HS2		
HS3		
HS4		
HS5		

Fig. 3.19(a) presents the comparison of energy-absorbing capacity obtained from software Matlab between the hybrid systems and the corresponding individual components. It is clear that the energy absorption for HS1, HS2 and HS3 are higher than the sum of the energy absorption of the individual components. In contrast, the sum of energy absorbed by the individual components is larger than those of the HS4 and HS5. The maximum value of the energy absorption is corresponding to the HS1, while that for HS4 is the lowest. HS1 has the largest enhancement on energy absorption in

comparison with the total energy absorbed by its components. On contrast, the energy-absorbing capacity of HS4 and HS5 is lower than those of the sum of the corresponding individual parts under quasi-static loading. It is suggested that the hybrid tube system without foam filling was damaged more completely than those with foam filling as the hardening of the foam during the compression could accelerate the splaying failure of the outer tube, which leads to an early failure with the relatively lower energy absorption. Fig. 3.19(b) shows the comparison of specific energy absorption (SEA) between hybrid systems and associated individual components subjected to quasi-static compressive loading. The maximum value of SEA is for HS1, while that for HS5 is the lowest. Different from the hybrid systems, the largest one for the sum of constituent components, the associated components in HS1 is highest, whilst the total SEA for the components in HS3 is the minimum one. It is evident that the hybrid tube system without foam filling can exhibit a relatively stable crushing process throughout the whole test, contributing to higher energy absorption.



(a) Energy absorption



(b) Specific energy absorption

Fig. 3.19 Summary of (a) Energy absorption and (b) Specific Energy Absorption of the hybrid systems and associated components subjected to quasi-static compressive loading.

The maximum values of mean crushing load of hybrid systems subjected to quasi-static loading and the sum of corresponding components were summarised in Fig. 3.20. All of the five hybrid systems exhibit a similar trend that the peak load for all hybrid systems is higher than the sum of associated components. The maximum value of the peak load is for HS1 whereas the lowest one is the HS2. In comparison to the hybrid systems and corresponding components, the largest improvement of the maximum mean crushing load is between the HS1 and the sum of its component parts with an enhancement of approximately 8%, while the minimum one is for HS5 (0.6%). In terms of loading resistance, all of the five hybrid systems are better than the sum of individual component separately subjected to quasi-static loading. The reason why values of the peak load for all hybrid systems are higher than the sum of components is that the constituent components in hybrid systems act in an integrated manner. In other words, the components interact with each other, which offers a necessary constraint and enhances the resistance to the compressive load.

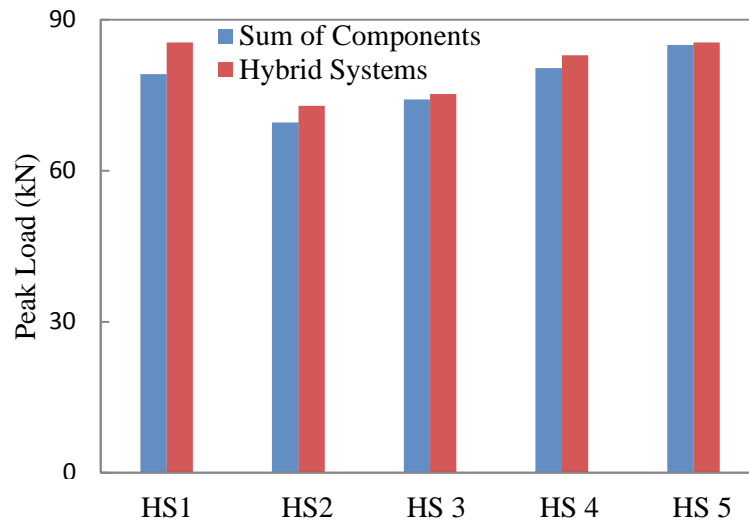


Fig. 3.20 Comparison of the mean crushing load of the hybrid tubes and the sum of associated component parts subjected to quasi-static compressive loading.

Table 3-7 summarises the comparison of energy absorption and mean crushing load between the hybrid systems and the sum of individual components under quasi-static compression test. It is clearly that the value of energy absorption for HS1 is the maximum one (791.2 J) which is about 7.6% more than the sum of energy absorbed by the associated components (735.6 J). The largest crushing force for the HS1 is 85.5 kN, which is 8.3% higher than the sum values of components (79.2 kN) and the lowest one is 72.9 kN for HS2, with about 4.7 % more than those of the summed value for the individual components. The maximum SEA is 65.4 kJ/kg for HS1, while that for HS3 is the lowest one (39.5 kJ/kg). On the other hand, the value of SEA for the sum of components in HS1 (60.8 kJ/kg) is the largest, whilst the lowest is 43.6 kJ/kg for the sum of components in HS3. Overall, the SEA for HS1, HS2 and HS3 is higher than the sum of associated individual components respectively, while for HS4 and HS5 is on the contrary for the reasons mentioned before.

Table 3-7 Summary of the energy absorption, SEA and peak load of hybrid systems and related components subjected to quasi-static loading

Test ID	Mass (kg)	Energy absorption (J)		SEA (kJ/kg)		Peak load (kN)	
		Hybrid system	Sum of Components	Hybrid system	Sum of Components	Hybrid system	Sum of Components
HS1	12.1	791.2	735.6	65.4	60.8	85.5	79.2
HS2	11.3	636.6	605.6	56.3	53.6	72.9	69.6
HS3	15.3	690.3	667.4	45.1	43.6	75.3	74.2
HS4	12.9	638.6	762.5	49.5	59.1	82.9	80.4
HS5	16.9	666.8	824.3	39.5	48.8	85.4	85.0

### 3.5 Experimental results of dynamic tests

Apart from the quasi-static compression tests conducted for both the individual tubes and hybrid systems, dynamic tests were further carried out on the specimens. This part presents the experimental results obtained from impact tests and compares the data between quasi-static and dynamic compressive loading.

#### 3.5.1 Individual CFRP tubes

Fig. 3.21 shows the comparison of load-displacement traces of individual carbon fibre tubes with outer diameters of 8, 34.8 and 54 mm. All three curves exhibit the similar trends as the force rises to the maximum value rapidly and then becomes highly oscillatory. The fluctuated response of the individual CFRP tubes is likely caused by the staged failure of the CFRP laminates and the ring effects in the load cell.

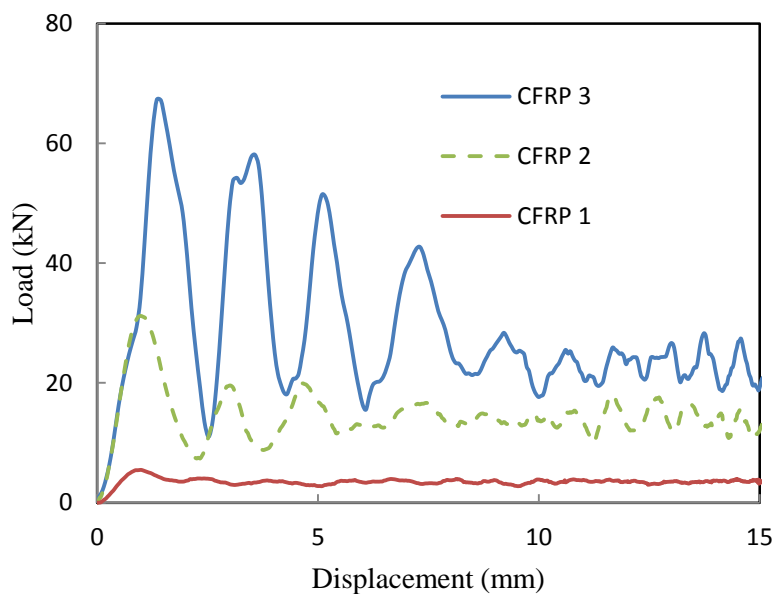
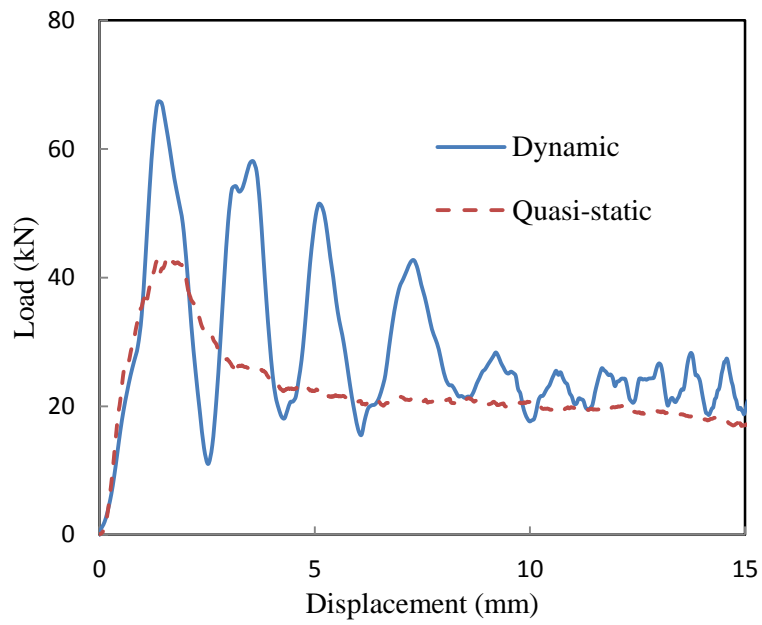
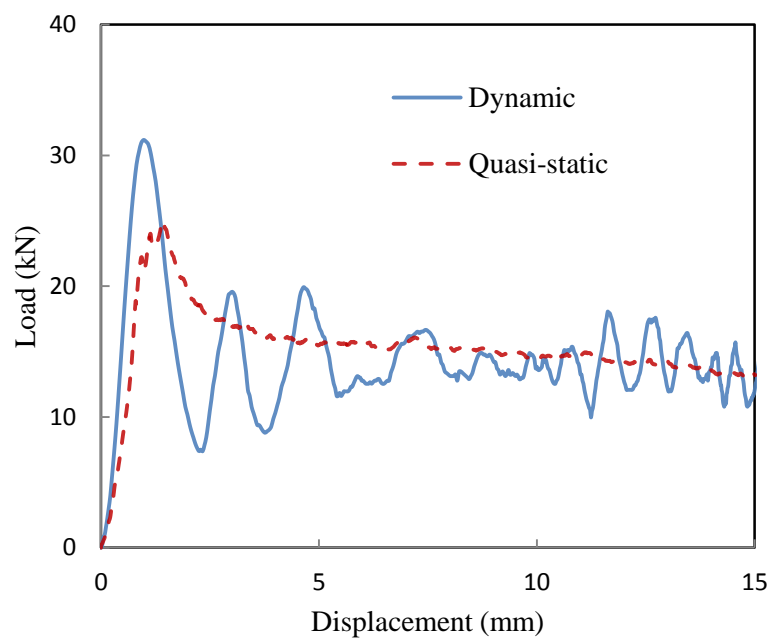


Fig. 3.21 Typical load-displacement traces for CFRP 1, 2 and 3 (OD 8 mm, 34.8 mm and 54 mm) following dynamic compression test

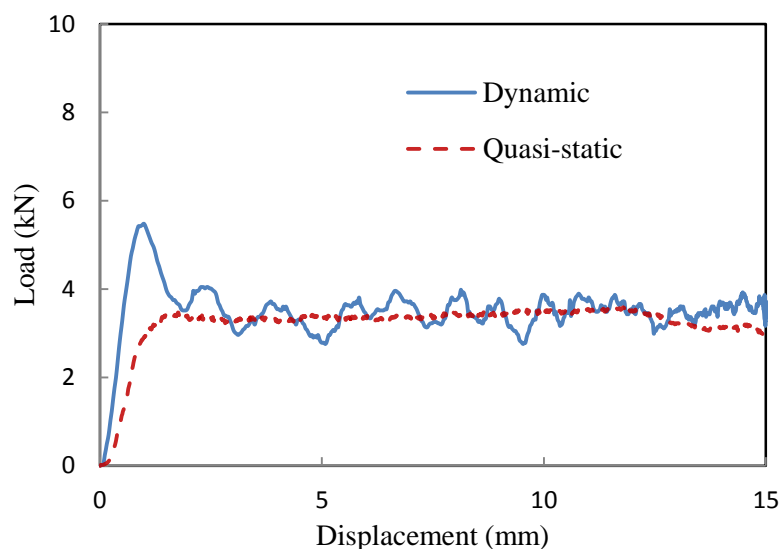
A comparison of load-displacement trace between the quasi-static and dynamic tests for the carbon fibre tube with 54 mm outer diameter is shown in Fig. 3.22(a). Clearly, both of the two curves exhibit the similar trend with the force increasing sharply to the peak load before decreasing and then going through a plateau stage. However, for the quasi-static test, the force goes through a plateau stage smoothly, while the curve for the dynamic one becomes highly oscillatory after the peak point for the reasons mentioned before. The maximum load value for the tube under impact is much higher than that of the tube in quasi-static loading condition. Nevertheless, the values of the plateau load for both the curves are close with each other, especially in the later stage. For the other two tubes (OD 8mm and 34.8 mm), both of the curves perform a similar trend with the previous one (Figs. 3.22(b) and 3.22(c)). The maximum loads for these CFRP tubes in dynamic loading condition are again higher than their quasi-static counterparts.



(a) CFRP3 (OD 54.8 mm)



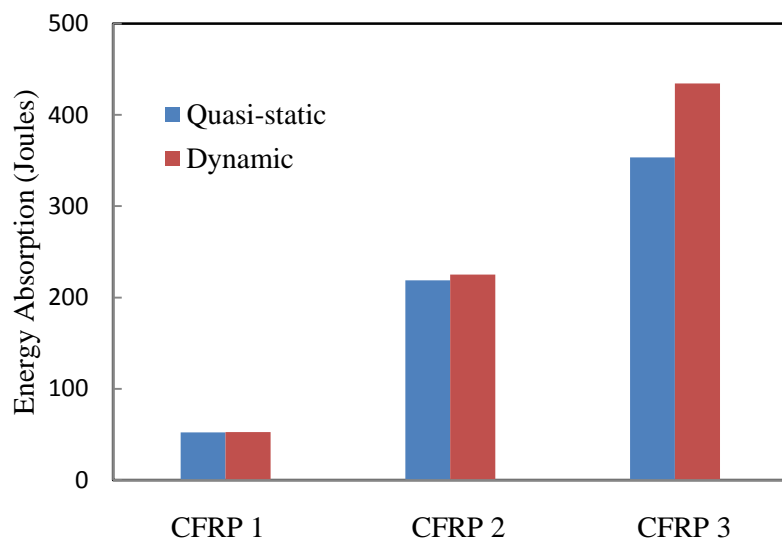
(b) CFRP2 (OD 34.8 mm)



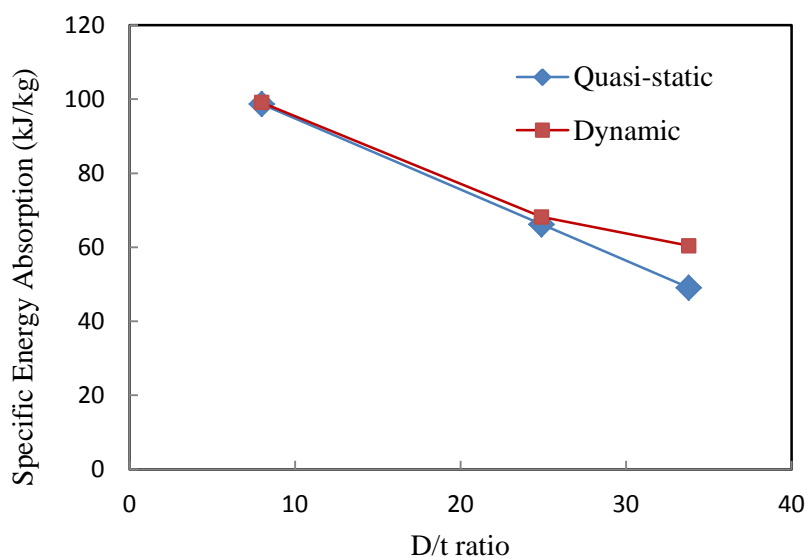
(c) CFRP1 (OD 8 mm)

Fig. 3.22 Comparison of typical load-displacement traces following quasi-static and dynamic tests on (a) CFRP3 (b) CFRP2 and (c) CFRP1.

The comparison of energy absorption of individual CFRP tubes under quasi-static and dynamic loading was presented in Fig. 3.23(a). The energy absorption increases with increasing the diameter of CFRP tubes, for both the loading conditions as expected. The energy absorption values of CFRP1 are more or less equal for those two loading conditions. In comparison with the quasi-static loading, the value of energy absorption of CFRP3 is greater than its dynamic counterpart. Fig. 3.23(b) shows the comparison of specific energy absorption for CFRP1, CFRP2 and CFRP3 with  $D/t$  ratios of 8, 24.9 and 33.8 respectively, for the quasi-static and dynamic loading conditions. It is clear that the SEA values for CFRP1 and CFRP2 under impact compressive load are close to the static values, while the dynamic value for CFRP3 is higher.



(a) Energy absorption



(b) SEA

Fig. 3.23 Summary of (a) Energy absorption and (b) Specific energy absorption for the individual CFRP tubes subjected to quasi-static and dynamic tests.

Fig. 3.24 shows the comparison of mean crushing load of individual CFRP tubes subjected to quasi-static and dynamic compression loading. The maximum mean forces for all of the three sized tubes under dynamic loading are larger than those in quasi-static loading condition and the CFRP3 has the highest enhancement (55 %) among the tubes.

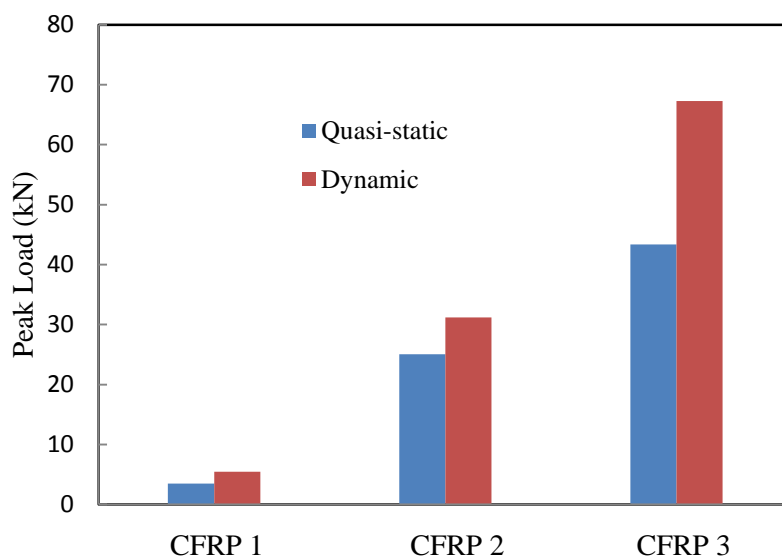


Fig. 3.24 Summary of the mean crushing load of the individual CFRP tubes subjected to quasi-static and dynamic loading.

Table 3-8 presents the comparison of energy absorption, peak load and SEA for individual CFRP tubes subjected to both the quasi-static and dynamic loading. The maximum values of energy absorption is 353.6 J and 434.6 J for CFRP3 (OD 54 mm), while the lowest is for CFRP1 (OD 8 mm) with the energy absorption of 52.3 J and 52.5 J when subjected to quasi-static and dynamic respectively. The energy absorption for CFRP2 (OD 34.8 mm) is 218.6 J following quasi-static loading which is lower than that of the tube subjected to the dynamic compressive loading with the value of 225.1 J. All tubes exhibit an uptrend of the maximum crushing load as the value of mean crushing load for CFRP1, CFRP2 and CFRP3 is 3.5, 25.0 and 43.4 kN respectively when subjected to the quasi-static loading, while the maximum crushing load is 5.5, 31.2 and 67.3 kN when the tubes were tested in the dynamic loading condition. Both of the SEA for tested tubes decreases with the increasing of the D/t ratio under quasi-static and dynamic loadings. The maximum value of SEA is 99.6 kJ/kg for CFRP1 and the minimum one is 49.1 kJ/kg for CFRP3 when tested by the quasi-static compression. During the dynamic test, the largest SEA is 99.9 kJ/kg for CFRP1 and the lowest one is 60.4 kJ/kg for CFRP3, which is about 23% higher than the value in quasi-static loading condition (49.1 KJ/kg).

Table 3-8 Summary of the Energy absorption, Peak load and SEA for individual CFRP tubes subjected to quasi-static and dynamic loading.

Test ID	Mass (g)	Quasi-static			Dynamic		
		Energy absorption (J)	Peak load (kN)	SEA (kJ/kg)	Energy absorption (J)	Peak load (kN)	SEA (kJ/kg)
CFRP1	0.7	52.3	3.5	99.6	52.5	5.5	99.9
CFRP2	4.4	218.6	25.0	66.2	225.1	31.2	71.7
CFRP3	9.6	353.6	43.4	49.1	434.6	67.3	60.4

### 3.5.2 Hybrid systems

The Fig. 3.25 shows the comparison of load-displacement traces for hybrid systems under dynamic compression loading. It is clear that all the five traces exhibit a similar trend as the force rises to the peak load rapidly before it drops and then the curves become oscillating sharply for HS1, HS4 and HS5. However, it fluctuates relatively mildly for HS2 and HS3 as the hybrid tube systems without small CFRP tubes placed between the two larger tubes are of less severe failure than the others during the crush.

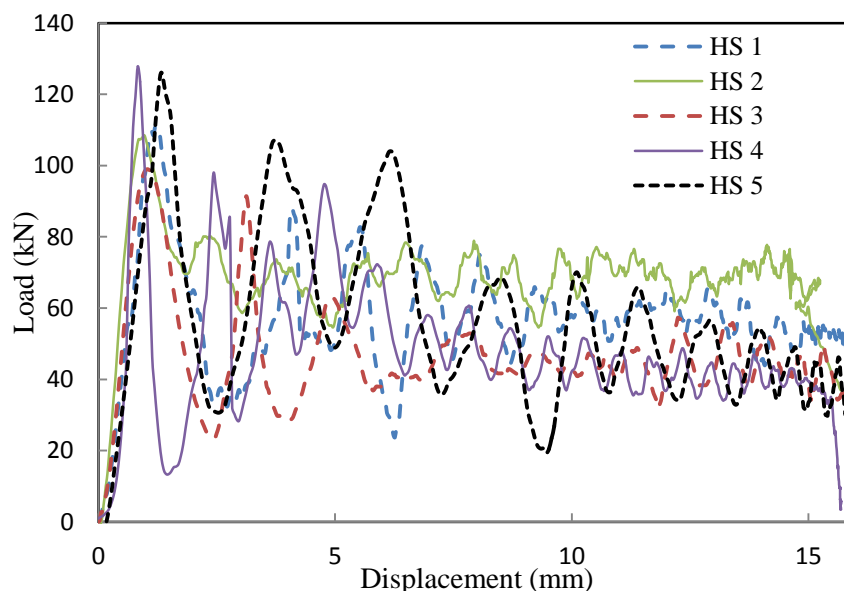
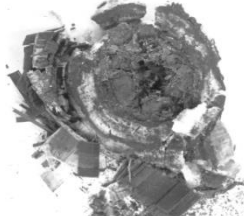


Fig. 3.25 Comparison of typical load-displacement traces following dynamic tests on the hybrid systems

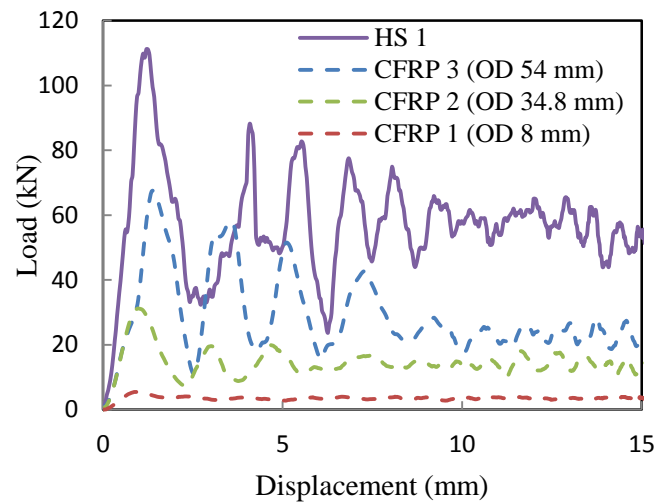
Table 3-9 shows images of the crushed hybrid systems from top view under dynamic compression. It is clear that the failure modes of the hybrid systems in impact test are similar to those subjected to quasi-static crush (Table 3-6).

Table 3-9 Images of failed hybrid systems from top views

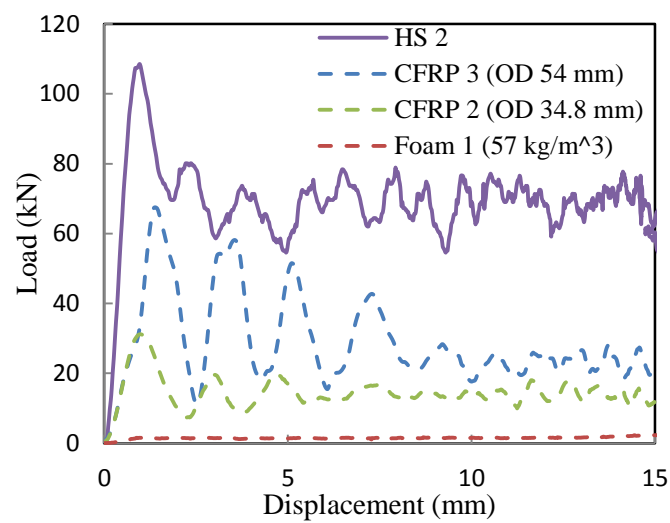
ID	Top view
HS1	
HS2	
HS3	
HS4	
HS5	

The comparison of load-displacement traces of hybrid systems and associated components were analysed in Fig. 3.26. For example, for the HS1 in Fig. 3.26(a), all the four curves exhibit a similar trend, i.e. the force rises to the maximum value rapidly before drop. After the peak point, the line is

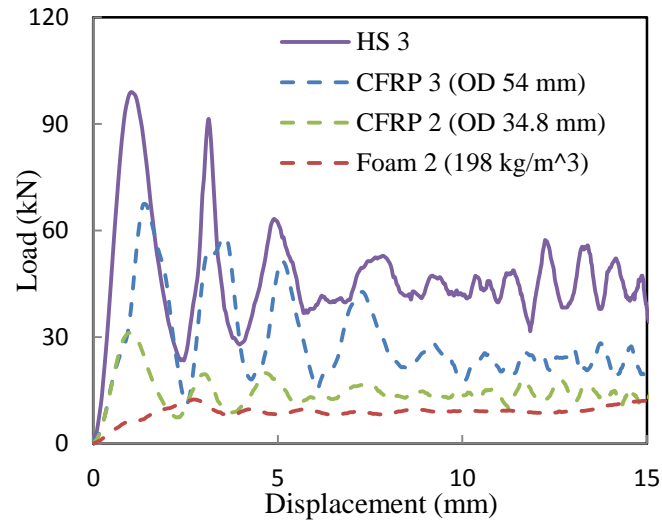
staying oscillating drastically until to the displacement of about 10 mm and then it fluctuates relatively mildly to the end. The similar load-displacement curves for HS2, HS3, HS4 and HS5 are presented in Figs. 3.26(b), (c), (d) and (e) respectively.



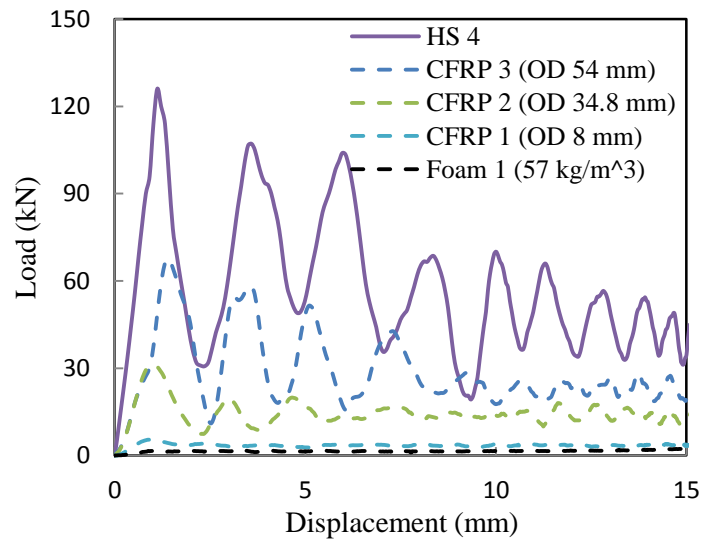
(a) HS1 and associated constituent components



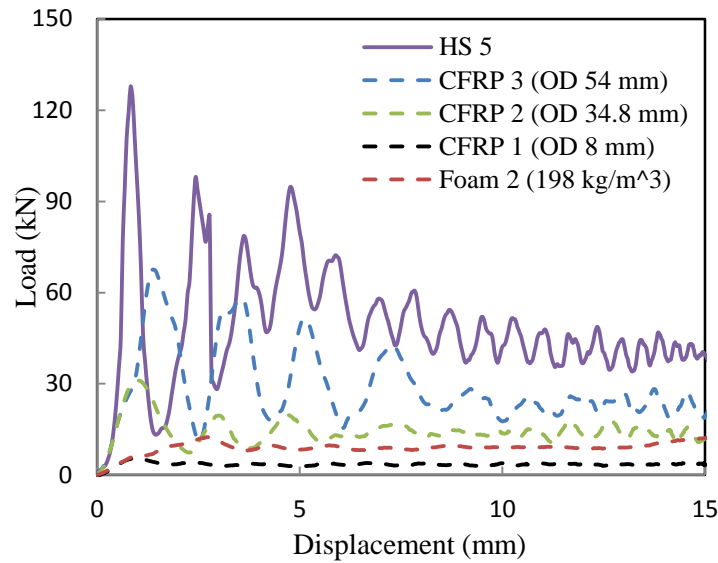
(b) HS2 and associated constituent components



(c) HS3 and associated constituent components



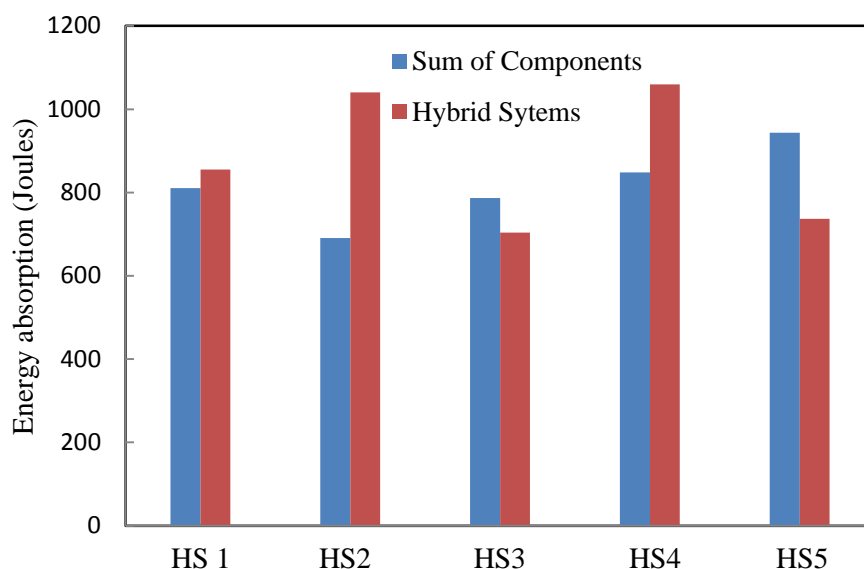
(d) HS4 and associated constituent components



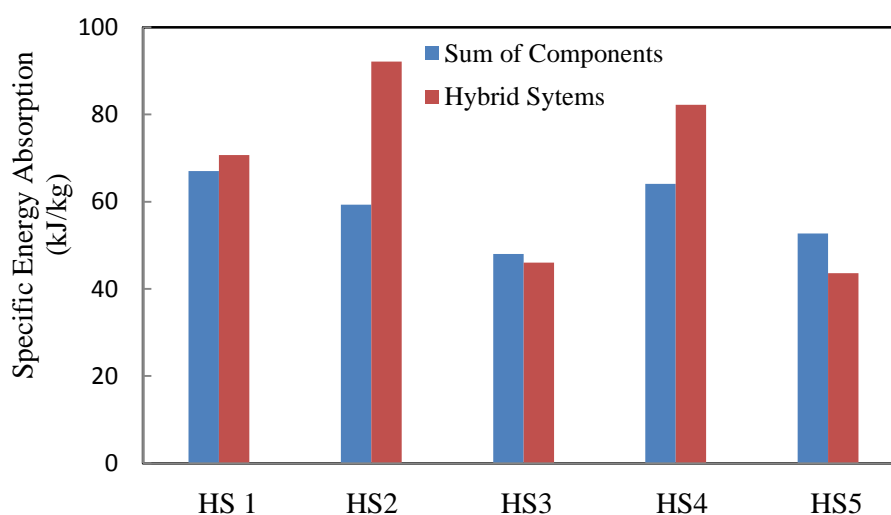
(e) HS5 and associated constituent components

Fig. 3.26 Comparison of load-displacement traces subjected to dynamic impact of hybrid systems (a) HS1 (b) HS2 (c) HS3 (d) HS4 (e) HS5 and corresponding components.

The comparison of energy-absorbing capacity between hybrid systems and the sum of the constituent corresponding components is summarised in Fig. 3.27(a). The energy absorption values for HS1, HS2 and HS4 are higher than the sum of their individual components, while those for HS3 and HS5 are on the contrary. The energy absorption for HS4 is the largest among all hybrid systems, while that for HS3 is the lowest. The possible reason is that the hybrid tube systems filled with the foam with a high density of  $198 \text{ kg/m}^3$  are damaged into relatively large pieces of debris, since the lateral expansion of the foam with a higher density is larger than that of the lower density foam during the impact compression. As the result, the failure of the outer tube is triggered early, which leads to a lower energy absorption. Fig. 3.27(b) presents the comparison of SEA values between hybrid systems and the sum of related constituent components. The SEA for HS2 is the highest, which is approximately the double of that for HS3 which has the lowest SEA. The SEA values for HS1, HS2 and HS4 are larger than the sum of the related components respectively. It is clearly that the hybrid tube systems with the filling of a high density foam are not effective for the structures to absorb energy when subjected to impact due to the reasons mentioned before.



(a) Energy absorption



(b) SEA

Fig. 3.27 Summary of the (a) Energy absorption and (b) Specific Energy Absorption for hybrid systems and sum of corresponding components subjected to dynamic compressive loading.

Fig. 3.28 shows the comparison of mean crushing load between hybrid systems and the sum of associated components following dynamic loading. The peak loads for HS1, HS3 and HS5 are lower than that of the sum of components, while that for HS2 and HS4 is to the contrast. The largest value of crushing force among all the five hybrid systems is for HS5, while HS3 is the minimum one when subjected to the dynamic compression test. Compared with quasi-static tests (Fig. 3.19), the difference

on the peak load between the hybrid system and the sum of the individual constituents is also not significant in the dynamic loading case (Fig. 3.28).

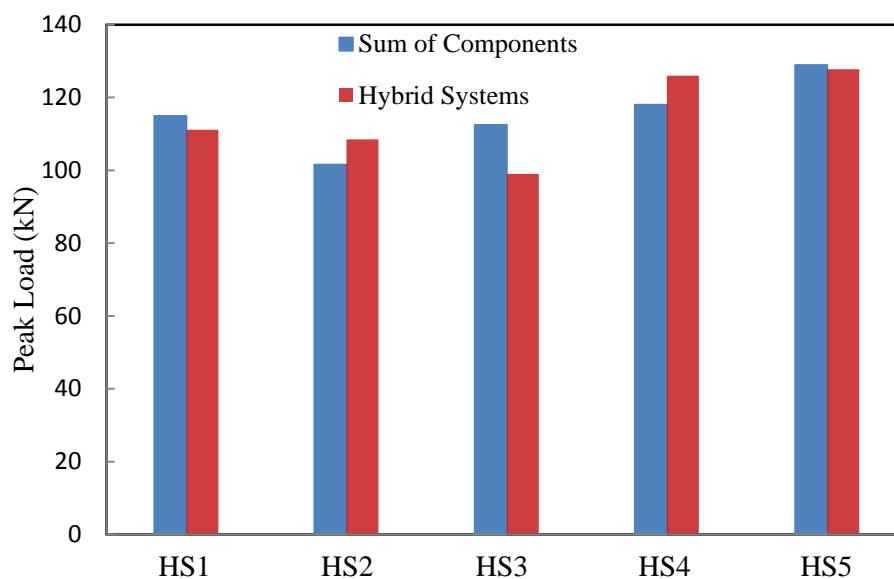


Fig. 3.28 Comparison of the peak load for hybrid systems and the sum of associated components subjected to dynamic compressive loading.

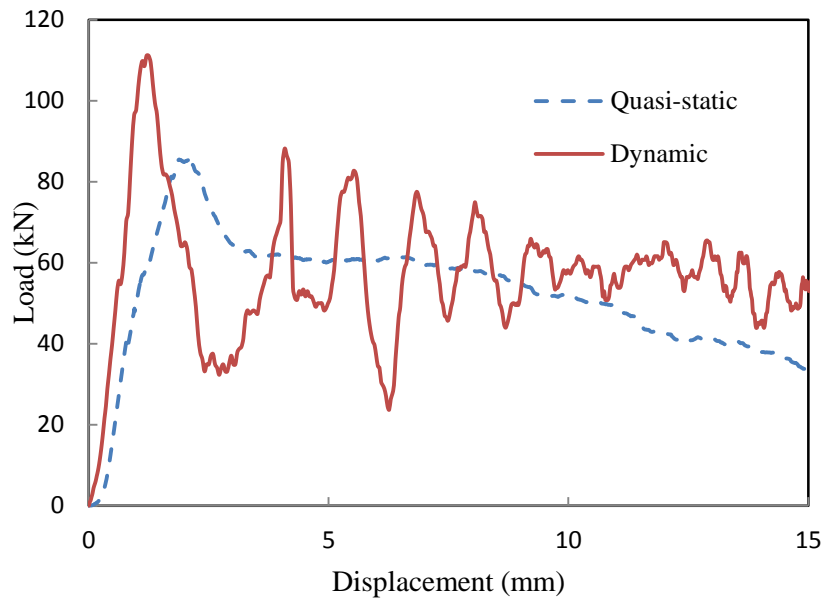
Table 3-10 summarises the details of energy absorption, SEA and peak load between the hybrid systems and the sum of individual components. The maximum energy absorption for hybrid system is HS4 with the value of 1059.7 J and the minimum one is HS3 (703.8 J). The greatest enhancement on energy absorption between hybrid systems and the sum of corresponding individual components is for HS2 (1040.2 J) and the sum of components (669.5 J) with the improvement of approximately 55.4%. The mean crushing load for HS2 (109 kN) and HS4 (126.5 kN) is higher than that of the sum of components in HS2 (101.6 kN) and HS4 (118 kN), while the maximum crushing force for HS1, HS3 and HS5 is lower than that of the summed value of associated components respectively, when subjected to dynamic crush loading. The largest SEA is 92.1 kJ/kg for HS2, while that for the sum of related components is 59.3 kJ/kg. Moreover, the minimum value of SEA is 43.6 kJ/kg for HS5. The reasons behind are likely: 1) the incomplete damage of small tubes for HS1 and HS5; 2) a low density foam filling with relatively low lateral expansion can integrate the inner and outer tubes better for HS2 and support the small tube to be relatively upright from beginning to the end through the whole

compression for HS4; 3) the large expansion of the filled high density foam speeds up the failure of outer tube for HS3 and HS5.

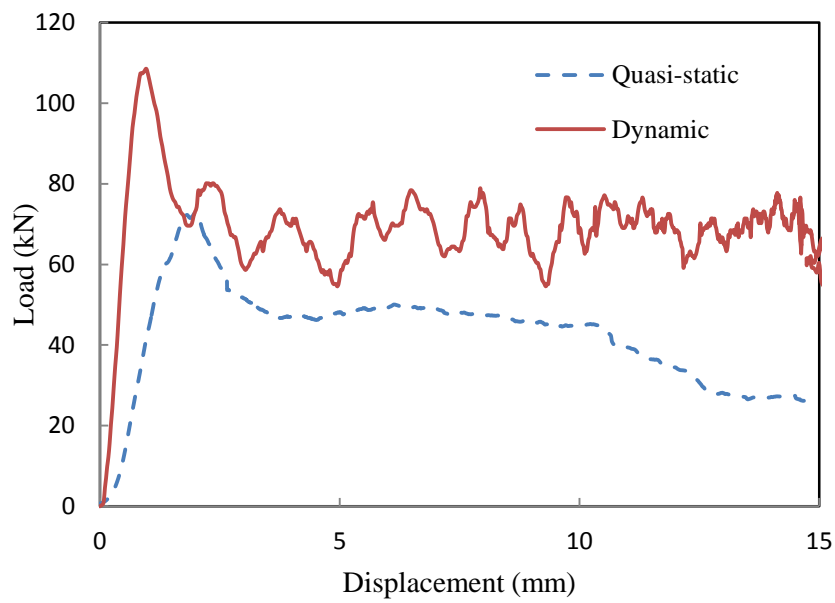
Table 3-10 Summary of the energy absorption, SEA and peak load for hybrid systems and sum of related components subjected to dynamic loading

Test ID	Mass (kg)	Energy absorption (J)		SEA (kJ/kg)		Peak load (kN)	
		Hybrid system	Sum of Components	Hybrid system	Sum of Components	Hybrid system	Sum of Components
HS1	12.1	855.31	810.7	70.7	67	111.0	114.9
HS2	11.3	1040.2	669.5	92.1	59.3	109.0	101.6
HS3	15.3	703.8	733.7	46	48	98.9	112.5
HS4	12.9	1059.7	826.9	82.2	64.1	126.5	118
HS5	16.9	736.9	891.2	43.6	52.7	128.1	128.9

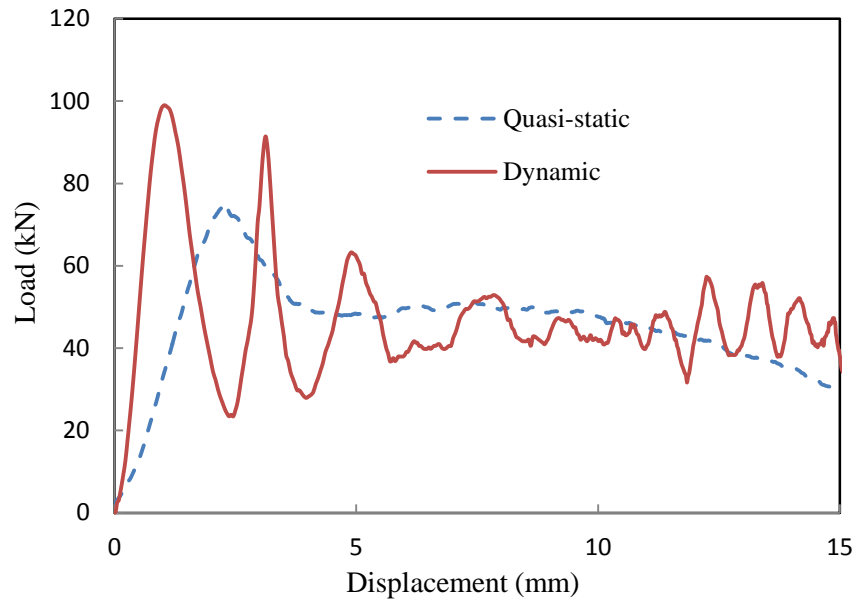
The comparison of load-displacement traces of 5 hybrid systems subjected to both quasi-static and dynamic impact is summarised in Fig. 3.29. All of the five hybrid systems display a similar trend, i.e. the crushing load for hybrid systems under quasi-static compression test is lower than that in dynamic loading condition. It is similar to the CFRP3, in which the peak load related to dynamic loading is much higher than its quasi-static counterpart. The curves for HS1, HS2, HS3, HS4 and HS5 were presented in Figs. 3.29(a), (b), (c), (d) and (e) respectively. It is clear that the force for all hybrid systems increases rapidly to the peak load under both the quasi-static and dynamic compressive loading. After peak point, the curve decreases steadily in quasi-static loading condition, while that for hybrid systems keeps oscillating to the end subjected to dynamic loading.



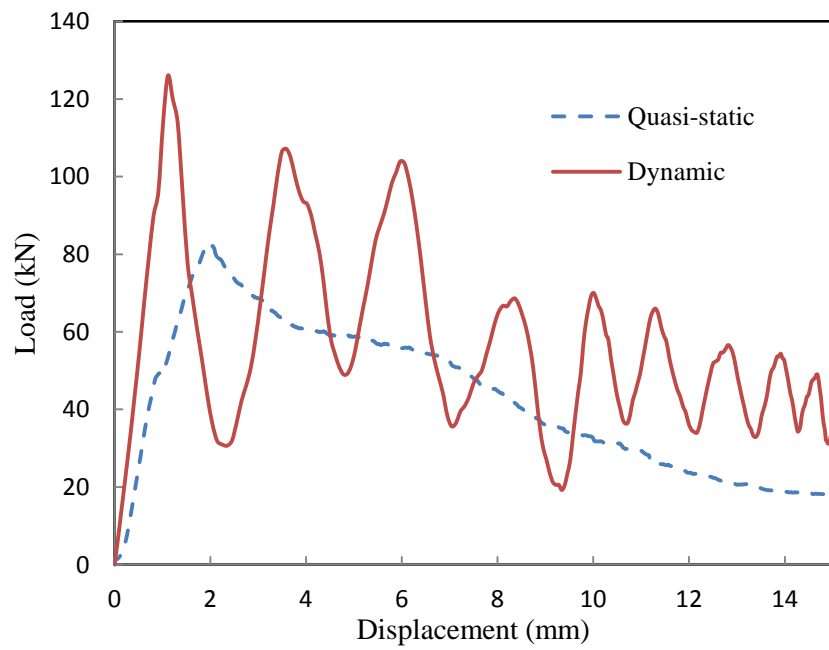
(a) HS1



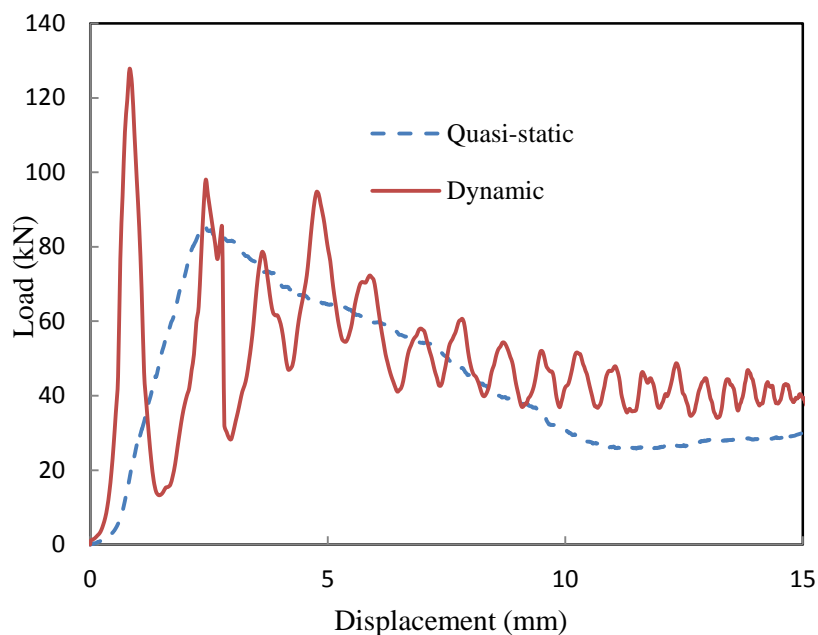
(b) HS2



(c) HS3



(d) HS4



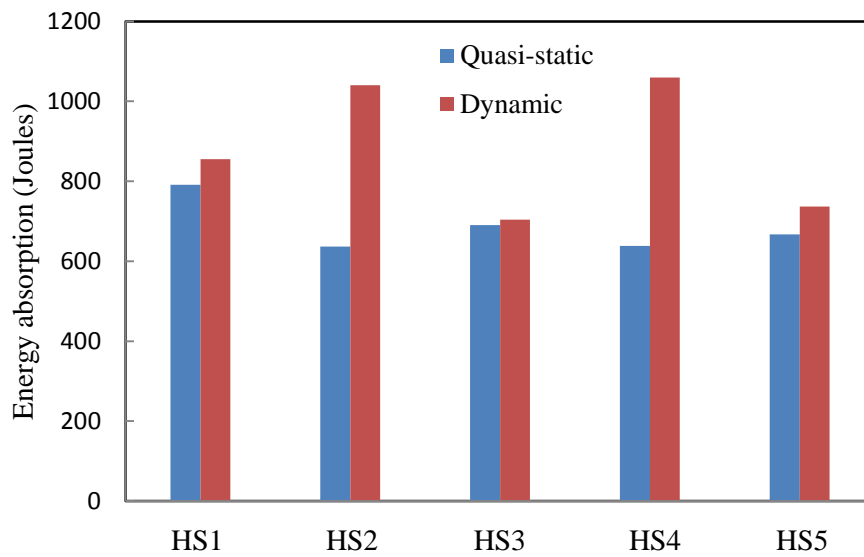
(e) HS5

Fig. 3.29 Comparison of typical load-displacement traces following quasi-static and dynamic tests on

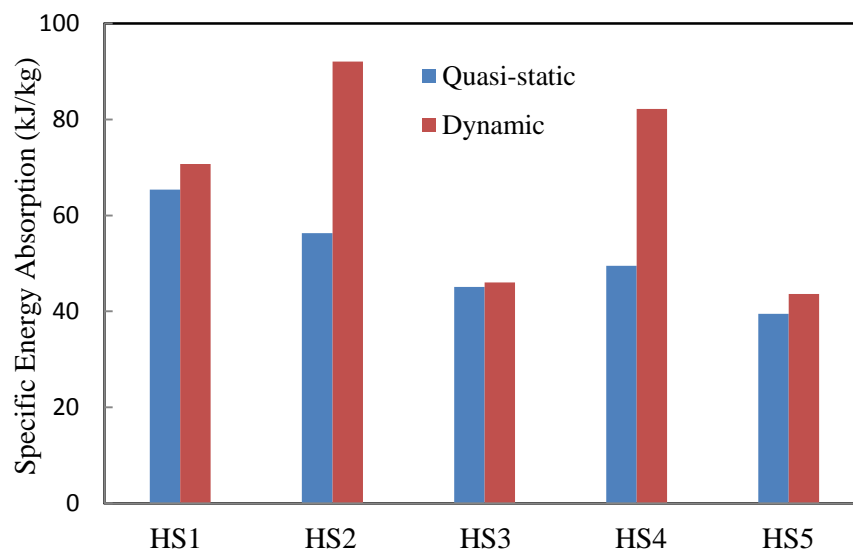
(a) HS1 (b) HS2 (c) HS3 (d) HS4 and (e) HS5

The summary of energy absorption for hybrid systems following the quasi-static and dynamic impact is presented in Fig. 3.30(a). The values for all five hybrid systems in quasi-static loading condition are lower than their dynamic counterparts. The largest energy-absorbing capacity tested in quasi-static compressive loading condition is HS1, while the lowest one is for HS2. On the other hand, the highest one is HS4 when subjected to dynamic loading, while that for HS3 is the lowest. It is clear that the energy absorption for all hybrid systems in dynamic loading condition is higher than that recorded in quasi-static compression tests. Fig. 3.30(b) compares the SEA for hybrid systems between quasi-static and dynamic loading condition. Similar with energy absorption, the SEA values for all hybrid systems subjected to dynamic impact are higher than their corresponding values under quasi-static loading condition. The highest SEA in dynamic compression test is for HS2, while that for HS3 is the lowest. On the other hand, in quasi-static compression test, the largest SEA value is for HS1, whilst that for HS3 is the lowest as well. It is evident that the hybrid tube systems are damaged more completely subjected to dynamic compression than those under quasi-static, especially for HS2 and HS4 with

fillings of low density foam, in which the small tubes are crushed relatively fully with the support of foam.



(a) Energy absorption



(b) SEA

Fig. 3.30 Summary of the energies absorbed by the individual CFRP tubes subjected to quasi-static and dynamic tests.

Fig. 3.31 shows the comparison of mean crushing load for hybrid systems subjected to quasi-static and dynamic compression loading. The peak load for all hybrid systems placed in dynamic loading condition is larger than that subjected to quasi-static compression loading. The maximum value of peak load for hybrid systems subjected to quasi-static compressive loading is for HS1, while that for HS2 is the lowest. Moreover, in dynamic test, the peak load for HS5 is the largest, while the lowest one is for HS3.

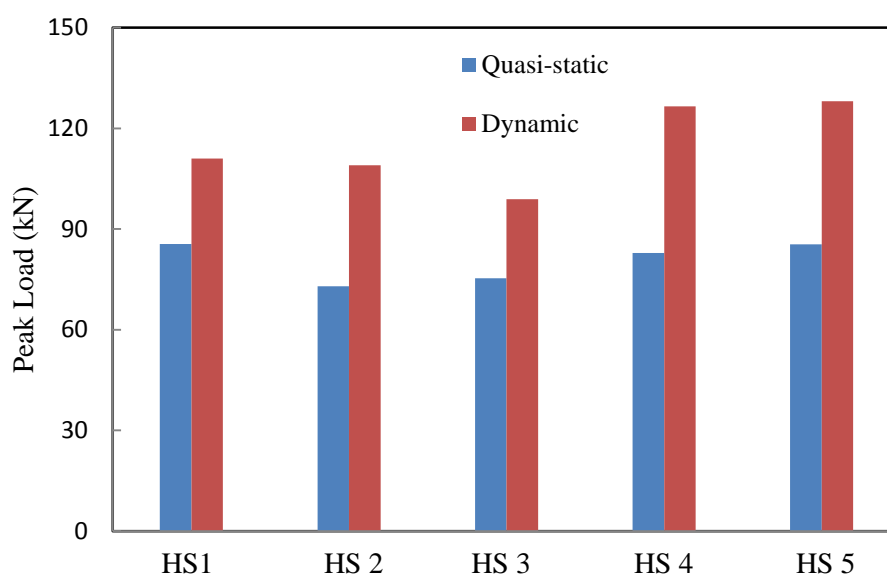


Fig. 3.31 Comparison of the peak load for hybrid systems subjected to quasi-static and dynamic loading.

Table 3-11 presents the comparison of energy absorption, SEA and peak load for hybrid systems subjected to both the quasi-static and dynamic loading. All of the energy absorption, SEA and peak load for hybrid systems subjected to quasi-static compressive loading are lower than the values in dynamic loading condition. Especially, the values of peak load for all hybrid systems in dynamic loading condition are greater than their quasi-static counterparts. The maximum energy absorption is 1059.7 J for HS4 in dynamic loading condition, which is 66 % more than its quasi-static counterpart (638.6 J), while the lowest one is 703.8 J for HS3 with 2 % enhancement in quasi-static compression (690.3 J). Similar with the energy absorption, the values of SEA for all hybrid systems subjected to dynamic loading are higher than their quasi-static counterparts for the reasons mentioned before. In

dynamic loading condition, the largest is 92.1 kJ/kg with improvement of 64 % in comparison with quasi-static loading condition (56.3 kJ/kg) for HS2, while the lowest one is 43.6 kJ/kg for HS5. The values of peak load for all hybrid systems under impact are great higher than their quasi-static counterparts, in which the maximum one is 128.1 kN for HS5, while the minimum value is 98.9 kN for HS3 subjected to dynamic loading. It is suggested that the hybrid tube systems perform similarly to the individual tubes with the same outer diameter as CFRP3 (OD 54mm), while larger thickness. As illustrated in section 2.3.1.2, all the energy absorption, SEA and peak load of CFRP tubes under impact are higher than their quasi-static counterparts.

Table 3-11 Summary of the energy absorption, SEA and peak load for hybrid systems subjected to quasi-static and dynamic loading.

Test ID	Mass (kg)	Energy absorption (J)		SEA (kJ/kg)		Peak load (kN)	
		Quasi-static	Dynamic	Quasi-static	Dynamic	Quasi-static	Dynamic
HS1	12.1	791.2	855.31	65.4	70.7	85.5	111.0
HS2	11.3	636.6	1040.2	56.3	92.1	72.9	109.0
HS3	15.3	690.3	703.8	45.1	46	75.3	98.9
HS4	12.9	638.6	1059.7	49.5	82.2	82.9	126.5
HS5	16.9	666.8	736.9	39.5	43.6	85.4	128.1

### 3.5.3 Cubic foams

The comparison of stress-strain curves for cubic foams with two densities subjected to the quasi-static and dynamic crushing loading is shown in the Fig. 3.32. The maximum stress for Foam1 (57 kg/m<sup>3</sup>) and Foam2 (198 kg/m<sup>3</sup>) subjected to dynamic crush is larger than that in the quasi-static loading condition, where the peak value for Foam2 in dynamic loading condition is nearly doubled of that under quasi-static test, showing a strong rate sensitivity.

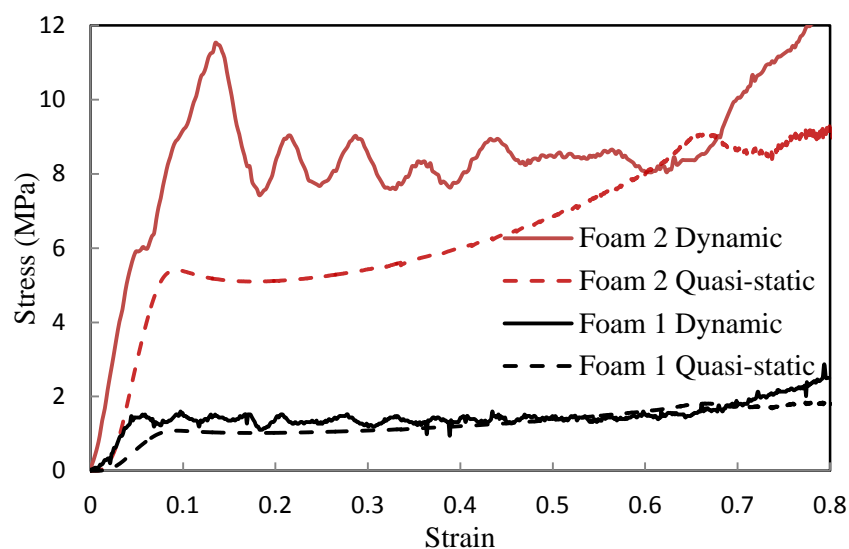


Fig. 3.32 Comparison of stress-strain curve for cubic foams subjected to quasi-static and dynamic test

### 3.6 Summary

Initially, the carbon fibre reinforced plastic tubes, cubic foams and hybrid systems have been manufactures. Subsequently, experimental work on the individual CFRP tubes and hybrid systems under both the quasi-static and dynamic compressive tests has been conducted and the load-displacement traces have been recorded and processed.

The experimental results have been compared and summarised. Initially, the SEA decreases with the increasing  $D/t$  ratio for individual carbon fibre reinforced plastic tubes. In the quasi-static test, the hybrid systems with foam reinforcement have a significant enhancement on energy absorption in comparison with the sum values of the associated components. Whereas, in the dynamic loading condition, the hybrid systems with a low density foam sandwich tube have a greater improvement in both the energy absorption and mean crushing load, when compared with the sum of the individual values of corresponding individual parts. All the hybrid systems perform better in dynamic loading condition than in the quasi-static loading condition, in terms of both the energy absorption and crush resistance.

## **CHAPTER 4 FINITE ELEMENT MODELLING AND RESULTS**

### **4.1 Introduction**

This chapter presents the finite modelling analysis technique to predict the mechanical response of various composite structures studied. The finite element models of hybrid CFRP tube systems and sandwich beams based on glass fibre reinforced plastic skins and syntactic foam core are developed by employing a commercial finite element analysis (FEA) package, ABAQUS/Explicit. In this chapter, the constitutive models and associated failure criteria are detailed. Subsequently, the FE models developed are validated against the experimental results.

## 4.2 Constitutive models and failure criteria

Numerical simulations were firstly developed to model the mechanical behaviour of the sandwich structures which consist of woven glass fibre/epoxy resin skin and syntactic foam core subjected to quasi-static three-point bending and low velocity impact loading. On the other hand, the finite element models of composite CFRP tubes were then developed. Here, ABAQUS/Explicit [112], together with user-defined subroutines, is used to carry out finite element modelling.

### 4.2.1 Modified 3D Hashin's damage criteria

The modified Hashin's 3D failure criteria introduced by Hashin [113] and Vo et al. [114] are used to simulate woven glass–fibre/epoxy resin composite layer and carbon fibre reinforced plastic tubes, which are given as follows:

Fibre tension: ( $\sigma_{11} \geq 0$ )

$$\text{If } \left(\frac{\sigma_{11}}{X_{1t}}\right)^2 + \left(\frac{\sigma_{12}}{S_{1r}}\right)^2 + \left(\frac{\sigma_{13}}{S_{13}}\right)^2 = 1, \text{ then } d_{ft} = 1 \quad (4-1)$$

Fibre compression: ( $\sigma_{11} \leq 0$ )

$$\text{If } \frac{|\sigma_{11}|}{X_{1c}} = 1, d_{fc} = 1, \text{ then } d_{fc} = 1 \quad (4-2)$$

Matrix tension: ( $\sigma_{22} + \sigma_{33} \geq 0$ )

$$\text{If } \frac{(\sigma_{22} + \sigma_{33})^2}{X_{2t}^2} + \frac{\sigma_{23}^2 - \sigma_{22}\sigma_{33}}{X_{23}^2} + \frac{\sigma_{12}^2 + \sigma_{13}^2}{X_{32}^2} = 1 \text{ then } d_{mt} = 1 \quad (4-3)$$

Matrix compression: ( $\sigma_{22} + \sigma_{33} \leq 0$ ):

$$\text{If } \left[ \left( \frac{X_{2c}}{2S_{23}} \right)^2 - 1 \right] \frac{(\sigma_{22} + \sigma_{33})}{X_{2c}^2} + \frac{(\sigma_{22} + \sigma_{33})^2}{4S_{23}^2} + \frac{\sigma_{23}^2 - \sigma_{22}\sigma_{33}}{X_{23}^2} + \frac{\sigma_{12}^2 + \sigma_{13}^2}{X_{12}^2} = 1 \text{ then } d_{mc} = 1 \quad (4-4)$$

where  $X_{1t}$ ,  $X_{1c}$ ,  $X_{2t}$ ,  $X_{2c}$ ,  $S_{12}$ ,  $S_{13}$  and  $S_{23}$  are the various strength components [124] in which  $X_{1t}$ , and  $X_{1c}$  are tensile and compression strengths along fibre direction,  $X_{2t}$  and  $X_{2c}$  are tensile and compression strengths perpendicular to the fibre direction,  $S_{12}$ ,  $S_{13}$  and  $S_{23}$  are shear strengths in 1-2, 2-3 and 1-3 planes respectively,  $d_{ft}$ ,  $d_{fc}$ ,  $d_{mt}$  and  $d_{mc}$  are the damage variables corresponding to the four failure modes. The mechanical behaviour of the composite after damage initiation is given in the following equation:

$$\sigma = C(d) \cdot \varepsilon \quad (4-5)$$

$$\begin{bmatrix} \sigma_{11} \\ \sigma_{22} \\ \sigma_{33} \\ \sigma_{12} \\ \sigma_{23} \\ \sigma_{13} \end{bmatrix} = \begin{bmatrix} C_{11} & C_{12} & C_{13} & & & \\ C_{21} & C_{22} & C_{23} & & & \\ C_{31} & C_{32} & C_{33} & & & \\ & & & C_{44} & & \\ & & & & C_{55} & \\ & & & & & C_{66} \end{bmatrix} \begin{bmatrix} \varepsilon_{11} \\ \varepsilon_{22} \\ \varepsilon_{33} \\ \varepsilon_{12} \\ \varepsilon_{23} \\ \varepsilon_{13} \end{bmatrix} \quad (4-6)$$

where the damaged matrix with the non-zero phrases in equation above can be written as follows:

$$\begin{aligned} C_{11} &= (1 - d_f)E_1(1 - v_{23}v_{32}) \Gamma \\ C_{22} &= (1 - d_f)(1 - d_m)E_2(1 - v_{13}v_{31}) \Gamma \\ C_{33} &= (1 - d_f)(1 - d_m)E_3(1 - v_{12}v_{21}) \Gamma \\ C_{12} &= (1 - d_f)(1 - d_m)E_1(v_{21} - v_{31}v_{23}) \Gamma \\ C_{23} &= (1 - d_f)(1 - d_m)E_2(v_{32} - v_{12}v_{31}) \Gamma \\ C_{31} &= (1 - d_f)(1 - d_m)E_3(v_{31} - v_{21}v_{32}) \Gamma \\ C_{44} &= (1 - d_f)(1 - S_{mt}d_{mt})E_1(1 - S_{mc}d_{mc}) G_{12} \\ C_{55} &= (1 - d_f)(1 - S_{mt}d_{mt})E_1(1 - S_{mc}d_{mc}) G_{23} \\ C_{66} &= (1 - d_f)(1 - S_{mt}d_{mt})E_1(1 - S_{mc}d_{mc}) G_{13} \end{aligned} \quad (4-7)$$

Here, the global fibre and matrix damage variables as well as the constant  $\Gamma$  are also can be written as:

$$\begin{aligned} d_f &= 1 - (1 - d_{ft})(1 - d_{fc}) \\ d_m &= 1 - (1 - d_{mt})(1 - d_{mc}) \\ \Gamma &= 1/(1 - v_{12}v_{21} - v_{23}v_{32} - v_{13}v_{31} - 2v_{21}v_{32}v_{13}) \end{aligned} \quad (4-8)$$

Also,  $E_i$  is the Young's modulus in  $i$  direction,  $G_{ij}$  is the shear modulus in  $i$ - $j$  plane while  $v_{ij}$  is the Poisson's ratio for transverse strain in the  $j$  direction. The phrases  $S_{mt}$  and  $S_{mc}$  are defined as the factors to control the reduction in shear stiffness caused by tensile and compressive failure in the matrix, which are given as  $S_{mt}=0.9$  and  $S_{mc}=0.5$  in ABAQUS [112].

#### 4.2.2.1 Strain-rate effect on material strengths

The effect of strain-rate on the properties of a composite material are analysed by using strain-rate dependent functions. The logarithmic functions to explain the influence of strain-rate on the strength and modulus of a composite material by Yen [115] as follows:

$$\{S_{RT}\} = \{S_0\} \left( 1 + C_1 \ln \frac{\dot{\varepsilon}}{\dot{\varepsilon}_0} \right) \quad (4-9)$$

$$\{E_{RT}\} = \{E_0\} \left(1 + C_2 \ln \frac{\dot{\bar{\epsilon}}}{\dot{\bar{\epsilon}}_0}\right)$$

where:

$$\begin{aligned} \{\dot{\bar{\epsilon}}\} &= \{|\dot{\epsilon}_1| \quad |\dot{\epsilon}_2| \quad |\dot{\epsilon}_1| |\dot{\epsilon}_2| \quad |\dot{\epsilon}_{12}| \quad |\dot{\epsilon}_{13}| \quad |\dot{\epsilon}_{23}|\}^T \\ \{S_{RT}\} &= \{X_{1t} X_{2t} \quad X_{1c} \quad X_{2c} \quad S_{12} \quad S_{13} \quad S_{23}\}^T \\ \{E_{RT}\} &= \{E_1 \quad E_2 \quad E_3 \quad G_{12} \quad G_{13} \quad G_{23}\}^T \end{aligned} \quad (4-10)$$

where the subscript 0 corresponds to the static value,  $\dot{\bar{\epsilon}}_0 = 1s^{-1}$  is the reference strain-rate, in which  $\dot{\bar{\epsilon}}$  is the effective strain-rate, and  $C_1 = 0.02$  and  $C_2 = 0$  are the strain-rate constants respectively [112].

### 4.2.2 Modelling of CFRP tubes

The composite tube, with different mechanical properties in longitudinal, hoop and through-thickness directions, is an anisotropic material. The mechanical properties and damage initiation of CFRP tubes used in this project are listed in Tables 4-1 and 4-2 as follows:

Table 4-1 Summary of elasticity properties and damage initiation data of CFRP tubes

$E_1$ (GPa)	$E_2$ (GPa)	$E_3$ (GPa)	$G_{12}$ (GPa)	$G_{13}$ (GPa)	$G_{23}$ (GPa)	$\nu_{12}$	$\nu_{13}$	$\nu_{23}$	$\rho$ (kg/m <sup>3</sup> )
70	70	10	8.6	8.6	8.6	0.1	0.14	0.14	1600

Table 4-2 Damage initiation data for the CFRP tube

$X_{1T}$ (MPa)	$X_{1C}$ (MPa)	$X_{2T}$ (MPa)	$X_{2C}$ (MPa)	$S_{12}$ (MPa)	$S_{13}$ (MPa)	$S_{23}$ (MPa)
600	570	600	570	280	280	280

### 4.2.3 Modelling of GFRP skins

The woven glass fibre/epoxy resin composite panel is manufactured by placing the fibre in  $[0^0/90^0]$  pattern. Therefore, the material behaviours in these two directions should be similar. Therefore, the GFRP layers have been modelled as an orthotropic material which means that the longitudinal and transverse moduli of elasticity in plane were assumed to be the same. Nevertheless, the thickness of the layer being used is varied from 1 to 3mm [115], which is quite large for 2D shell structure, thus it is not accurate to ignore the material response in the direction through-the-thickness. Hence, the 2D

Hashin's failure criteria are not suitable for this simulation. The modified 3D Hashin's failure criteria in section 4.2.2 were used to simulate overall response of a composite layer accurately in a rectangular coordinate system (x, y, z) rather than the cylinder coordinate system (r,  $\theta$ , z). The mechanical properties and damage initiation of GFRP skins investigated in the sandwich beam have been shown in Tables 4-3 and 4-4.

Table 4-3 Summary of elasticity properties and damage initiation data of GFRP skins

$E_1$ (GPa)	$E_2$ (GPa)	$E_3$ (GPa)	$G_{12}$ (GPa)	$G_{13}$ (GPa)	$G_{23}$ (GPa)	$\nu_{12}$	$\nu_{13}$	$\nu_{23}$	$\rho$ (kg/m <sup>3</sup> )
38	38	8.5	3.5	3.5	3.5	0.1	0.3	0.3	1870

Table 4-4 Damage initiation data for the GFRP skins

$X^T$ (MPa)	$X^C$ (MPa)	$Y^T$ (MPa)	$Y^C$ (MPa)	$S^T$ (MPa)	$S^C$ (MPa)	$G_{ft} = G_{mt}$ (J/m <sup>2</sup> )	$G_{fc} = G_{mc}$ (J/m <sup>2</sup> )
480	4332	480	432	480	480	110000	120000

#### 4.2.4 Modelling of the foam

The crushable foam model with hardening behaviour obtained from compression test was employed to model the syntactic foam used as core in sandwich beams under three-point bending and impact loading. In terms of damage evolution, the syntactic foam was modelled with a ductile damage criterion in conjunction with a shear damage criterion [112]. The model assumes that the equivalent plastic strain at the onset of damage is a function of stress triaxiality and strain rate. The shear damage initiation criterion is a model for predicting the onset of damage due to shear band localization. The model assumes that the equivalent plastic strain at the onset of damage is a function of the shear stress ratio and strain rate. The fracture strains related to the initiation of both the ductile and shear damage are specified by Arezoo et al. [117] and more information corresponding to the ductile and shear damage are included in [118].

Deshpande and Fleck [119] investigated the phenomenological yield surface for both open and closed-cell foam materials, which is;

$$\phi = \frac{1}{[1+(\alpha/3)^2]} [q^2 + \alpha^2 \sigma_m^2] - \sigma_y^2 \leq 0 \quad (4-11)$$

where  $\sigma_y$  is the uniaxial yield strength of the foam in tension or compression,  $q$  is the Von Mises stress, and  $\sigma_m$  is the mean stress. The parameter  $\alpha$  decides the shape of the yield surface was given by Desphande and Fleck [120] as follow:

$$\alpha = \frac{3k}{\sqrt{(3k_t+k)(3-k)}} \quad (4-12)$$

where  $k$  and  $k_t$  are the shape factors, which can be calculated by the ratios of the initial yield stress in uniaxial compression  $\sigma_c^0$  and in hydrostatic compression  $p_c^0$  (the initial value of  $p_c$ ) divide the yield stress in hydrostatic compression  $p_c^0$ , respectively:

$$k = \frac{\sigma_c^0}{p_c^0} \text{ and } k_t = \frac{p_t}{p_c^0} \quad (4-13)$$

Here, the hydrostatic compressive yield stress,  $p_c$  expressed the evolution of the yield surface is given by:

$$p_c(\varepsilon_{vol}^{pl}) = \frac{\sigma_c(\varepsilon_{axial}^{pl})[\sigma_c(\varepsilon_{axial}^{pl})\left(\frac{1}{\alpha^2} + \frac{1}{9}\right) + \frac{p_t}{3}]}{p_t + \frac{\sigma_c(\varepsilon_{axial}^{pl})}{3}} \quad (4-14)$$

where  $\varepsilon_{axial}^{pl}$  is the compressive plastic strain, which is set equal to the plastic volumetric strain  $\varepsilon_{vol}^{pl}$ . Therefore, the parameter  $p_c$  can be computed from the data obtained from the compression test on the foam. The mechanical properties of the syntactic foam investigated in sandwich beam have been presented in Table 4-5.

Table 4-5 Mechanical properties of the foam investigated

ID	Foam1	Foam2
Density ( $\text{kg/m}^3$ )	57	198
Compressive modulus(MPa)	69	280
Compressive strength(MPa)	0.9	5.2
Compressive fracture strain	0.7	0.7
Tensile modulus(MPa)	45	175
Tensile strength(MPa)	1.3	6
Shear modulus(MPa)	22	75
Shear strength(MPa)	0.8	3.5
Shear fracture strain	0.16	0.3
Work of fracture in tension ( $\text{kJ/m}^2$ )	0.26	1.33
Work of fracture in shear( $\text{kJ/m}^2$ )	6.48	44.2
Poisson's ratio	0.32	0.32

#### 4.2.5 Modelling of cohesive layer

The adhesive layer was used as contact interactions between cohesive elements and other components. In this project, the adhesive layer with 0.1 mm thickness was modelled using cohesive elements available in ABAQUS [121]. The elastic behaviour was defined using a traction-separation law with the damage initiation criterion and damage evolution based on the maximum nominal stress and the effective displacement which is based on the linear softening law. Therefore, the maximum nominal stress of damage initiation can be calculated as follows:

$$\max\left\{\frac{t_n}{t_n^0}, \frac{t_s}{t_s^0}, \frac{t_t}{t_t^0}\right\}=1 \quad (4-15)$$

In the equation above,  $t_n$ ,  $t_s$  and  $t_t$  are the stress components obtained from the elastic traction-separation behaviour for the current strain without damage and  $t_n^0$ ,  $t_s^0$  and  $t_t^0$  are the associated the critical values of the nominal stress.

On the other hand, the damage evolution was set to be determined by the displacement with the linear softening law. Here, the damage variable  $D_{coh}$  is a function related to effective displacement beyond

damage initiation. The expression of damage variable  $D_{coh}$  has been proposed by Camanho and Davila [122] as follows:

$$D_{coh} = \frac{\delta_m^f(\delta_m^{max} - \delta_m^0)}{\delta_m^{max}(\delta_m^f - \delta_m^0)} \quad (4-16)$$

where  $\delta_m^f$  is the parameter of effective displacement when completely failed and  $\delta_m^0$  is associated to the effective displacement at the damage initiation,  $\delta_m^{max}$  is the maximum value of the effective displacement during the loading history.

### 4.3 Individual models for various structures

Finite element models were created to predict the mechanical response of CFRP tubes under low-velocity impact and sandwich beam based on glass fibre skins and syntactic foam core laminates subjected to three-point bending and impact at different energy levels. The details of models including the geometry, boundary and loading conditions are presented.

#### 4.3.1 Mesh generation of the composite tubes and the hybrid systems

The models of composite tubes using the modified 3D Hashin's damage criteria which were described in section 4.2.2 with rate-dependent behaviour were used for modelling an anisotropic composite material. The interfaces between two composite layers were modelled using cohesive elements.

The element type used for meshing CFRP tubes was C3D8R, which is eight-noded and linear hexahedral element with reduced integration and hourglass control. The mesh generation geometric, loading and boundary conditions are given in Fig. 4.1. There are three tubes with outer diameter sizes of 8, 34.8 and 54 mm being modelled, together with a hybrid tube system in which three small tubes are placed in  $120^\circ$  apart between two big CFRP tubes. The interfaces between composite layers were modelled using eight-node 3D cohesive elements (COH3D8). The compressive loading was applied through the top platen and there was only one degree of freedom in the vertical direction, while the bottom platen was fully fixed. The interaction between the two neighbouring composite layers was defined as general contact and surface-based tie constraints were used between the composite layer and the cohesive layer. The material properties for composite tubes used in numerical modelling are listed in Table 4-3.

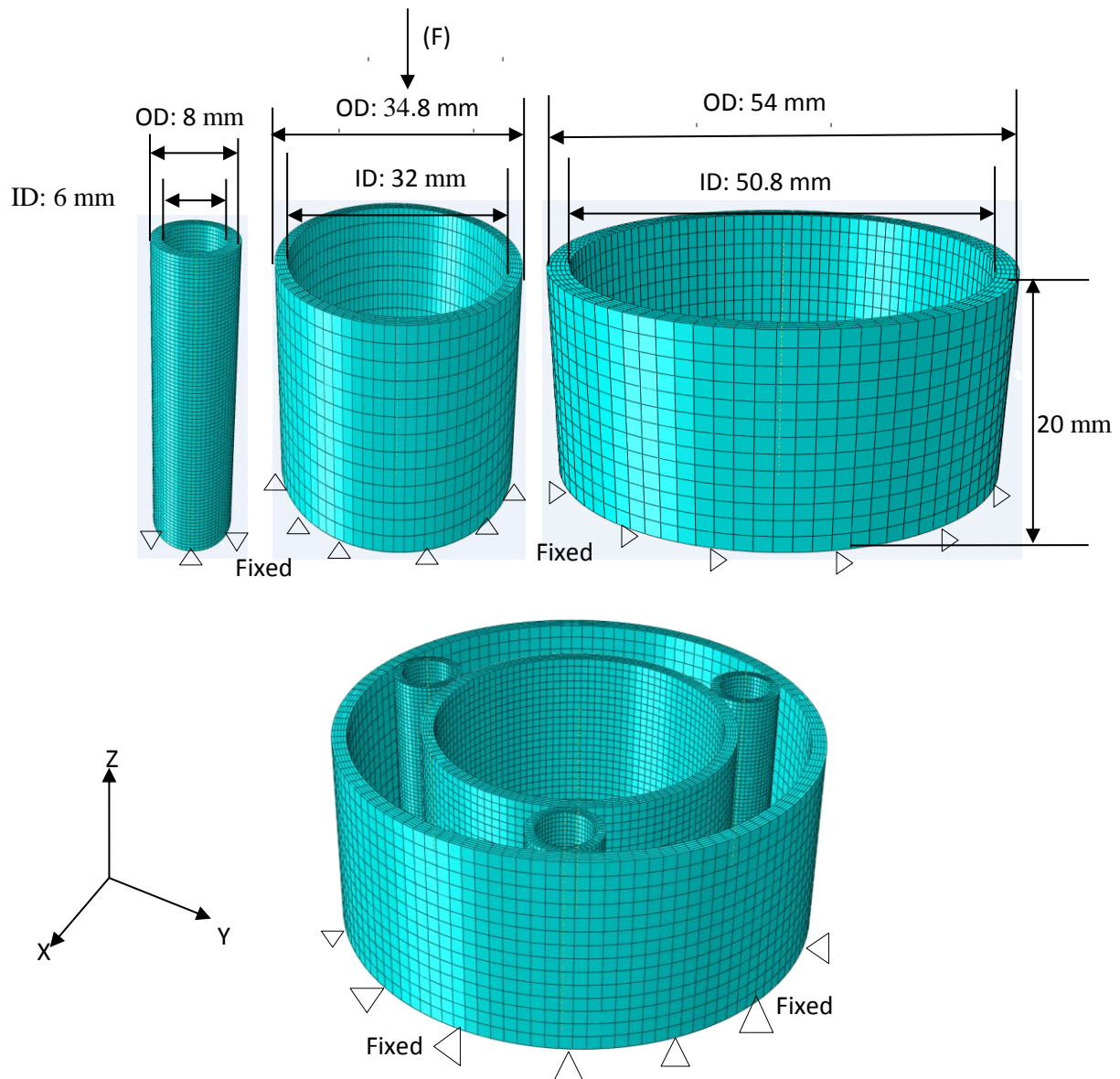
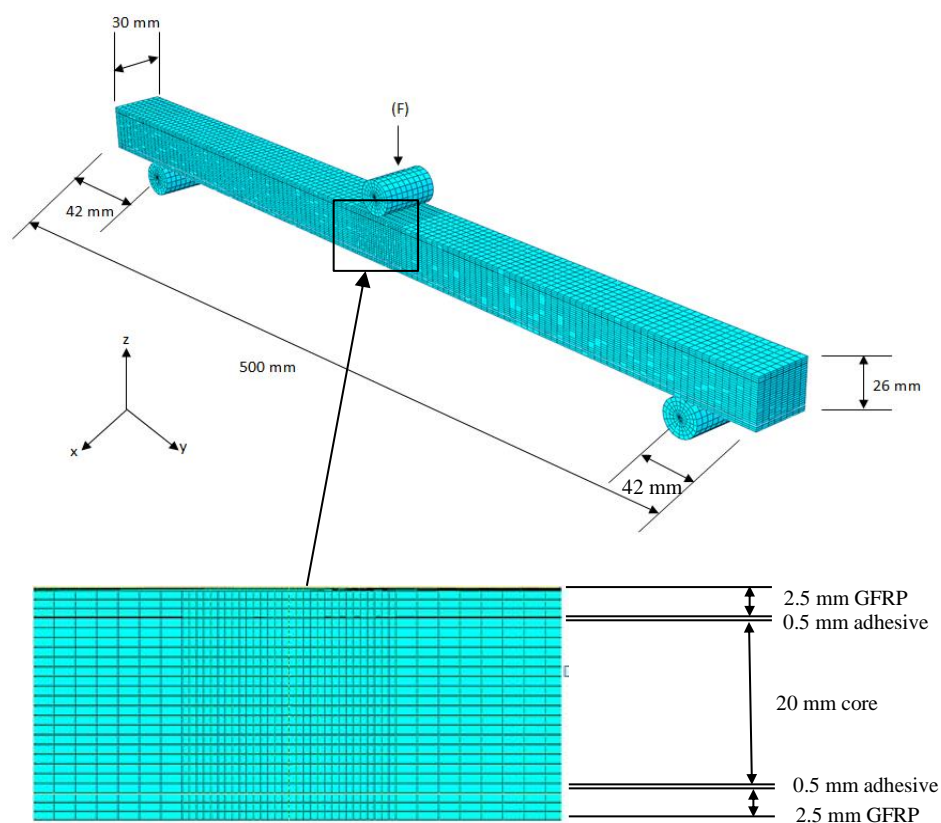


Fig. 4.1 The geometry, mesh and loading conditions for the individual composite tubes and hybrid system 1 subjected to compression loading.

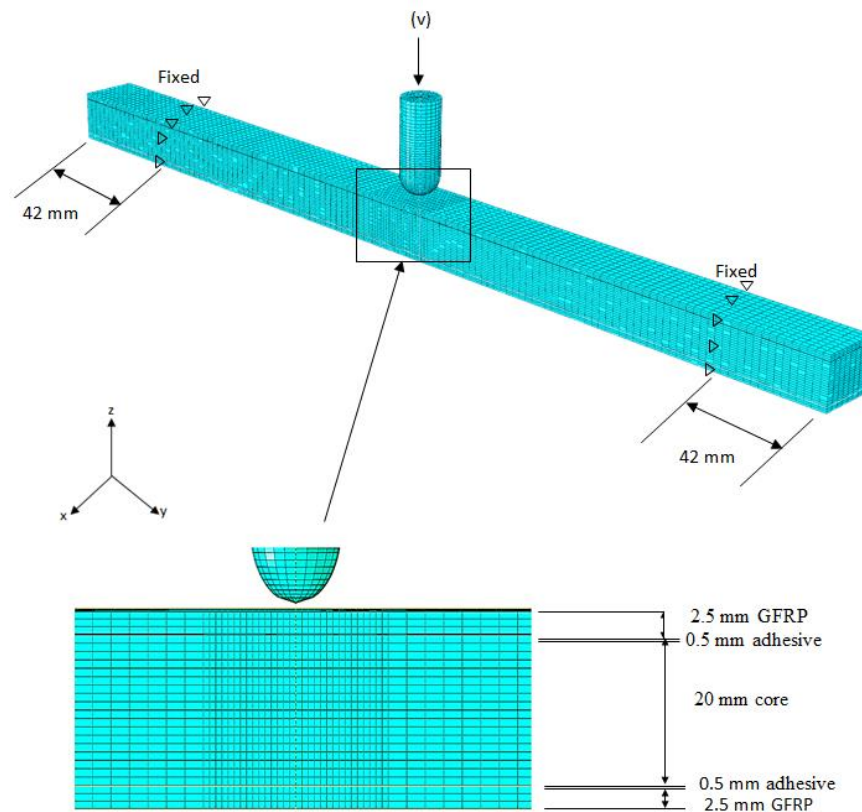
### 4.3.2 Mesh generation of the sandwich beam

The sandwich beam was consisting of two GFRP skins, syntactic based foam core material and adhesive layers between the foam core and skins. The syntactic foam was modelled as crushable foam with rate-dependent hardening, as described in section 4.2.4. The GFRP skins were modelled as an orthotropic based on the 3D Hashin's damage criteria.

A sandwich beam composed of GFRP skins, foam core and adhesive layers was modelled when subjected to three-point bending and low velocity impact loading. The mesh generation geometric, loading and boundary conditions for the sandwich beam subjected to three-point bending and impact loading are shown in Figs. 4.2(a) and 4.2(b), respectively. Both of the GFRP skins and foam core were meshed by eight-node reduced integration elements (C3D8R). The time duration for the modelling of sandwich beam under three-point bending was set to 0.1 s in order to ensure the full damage as in this computation duration has the minimum dynamic effect, while 0.01 s for the sandwich beam under impact. The impact load in Fig. 4.8(a) is obtained from the contact load between the projectile and the sandwich panel. The interaction between the projectile and the face sheet was defined as surface-to-surface contact. A mesh sensitivity analysis has been carried out by changing the mesh density in the plane and through the thickness.



(a) Sandwich beam subjected to three-point bending



(b) Sandwich beam subjected to impact loading

Fig. 4.2 The geometry, mesh and loading conditions of sandwich beam subjected to (a) three-point bending and (b) impact loading

#### 4.4 Mesh sensitivity

As varying mesh density could affect the simulation results apparently, the mesh sensitivity has been conducted to identify the most suitable mesh density. The accuracy of the simulation is increased with increasing mesh density. However, the computation time is increased as well. Thus, it is of great importance to find the balance between mesh density and the computation time. Fig. 4.3 presents the variation of the prediction to test data and CPU time with element size for a special specimen.

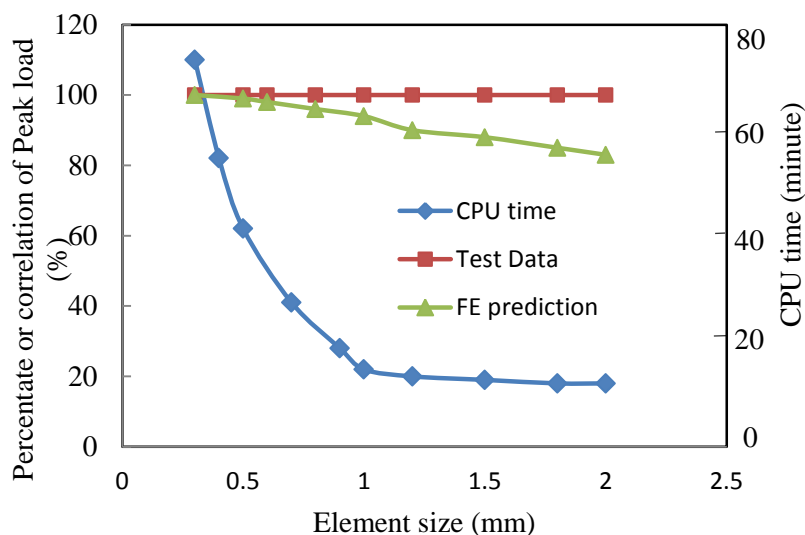


Fig. 4.3 Variation of the prediction to test data and CPU time with element size

#### 4.5 Output of modelling results

History output was defined from the whole model or a specific reference point and the frequency of the data output was dependent on the time interval requested. In the modelling of composite tubes, reaction forces in the longitudinal direction of the tube were defined and the displacement was requested to be a history output from the reference point on the top platen.

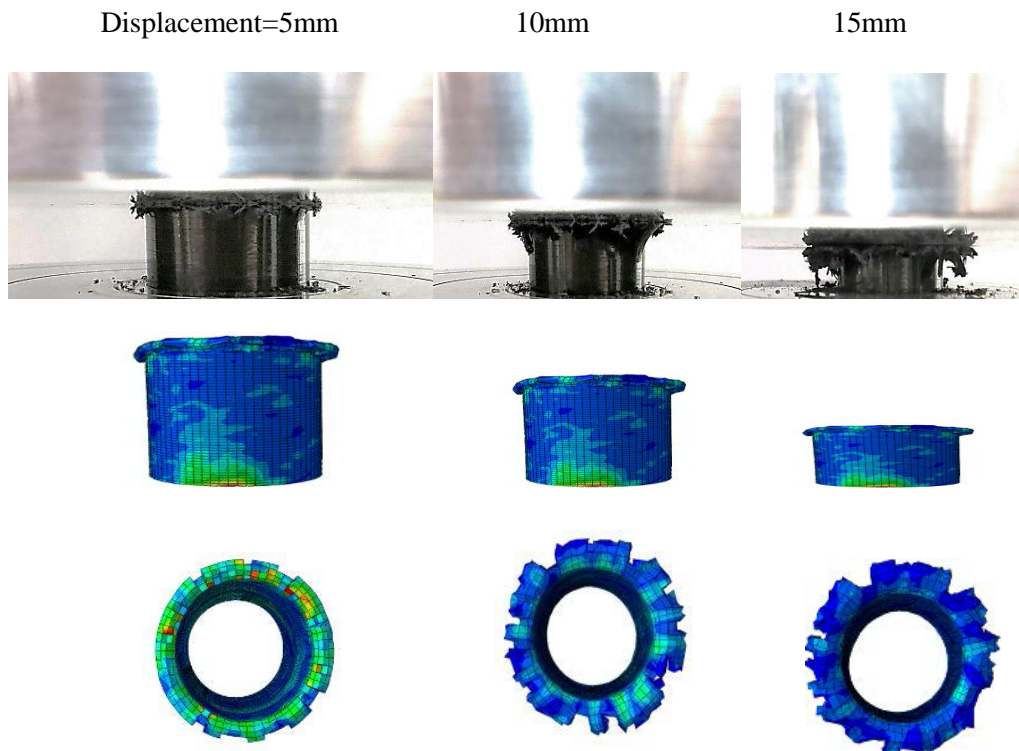
Field output was generated from the data which are spatially distributed from the whole model or a part in the centre of model. In the modelling of the composite tube and sandwich beam, the images of the models in each increment step can be obtained. Moreover, the failure status of the composite tubes and skins were defined as well.

#### 4.6 Simulation results and discussion

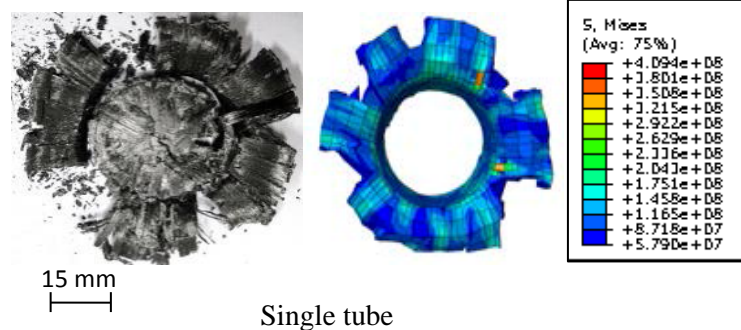
##### 4.6.1 Simulation of CFRP tubes and hybrid systems

Fig. 4.4 shows the comparison of progressive deformations and failure modes of the CFRP tubes with an outer diameter of 34.8 mm and images of crushed tubes obtained from the testing and FE modelling, respectively. The basic features of the extensive splaying, fibre breaking and matrix fracture of the crushed tube were captured. Although, both the testing and FE modelling indicate a progressive collapse of the tube with the output data of von Mises stress, more reasonable results and

failure modes can be achieved by using more accurate material data for the resin and fibre in the hoop direction, which is out of the scope of the current project.

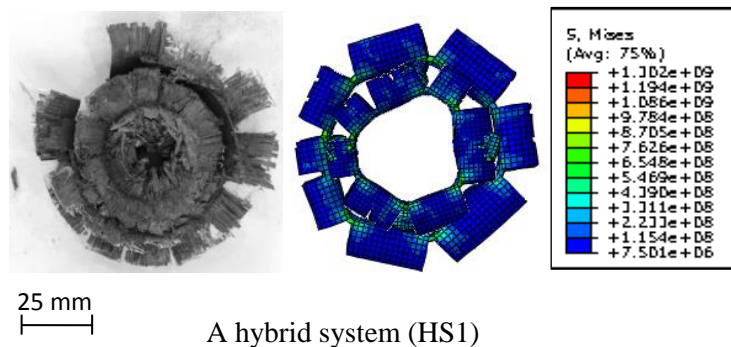


(a) Progress crushing failure of a single tube



15 mm

Single tube



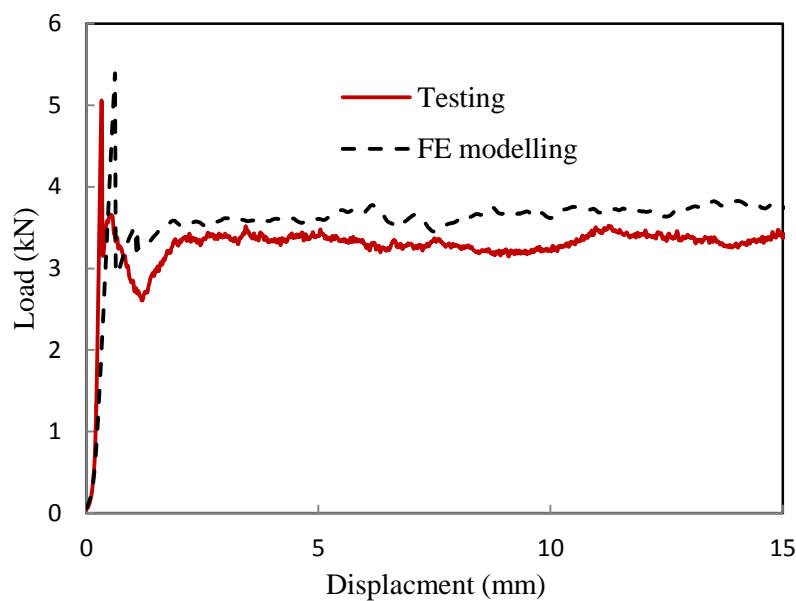
25 mm

A hybrid system (HS1)

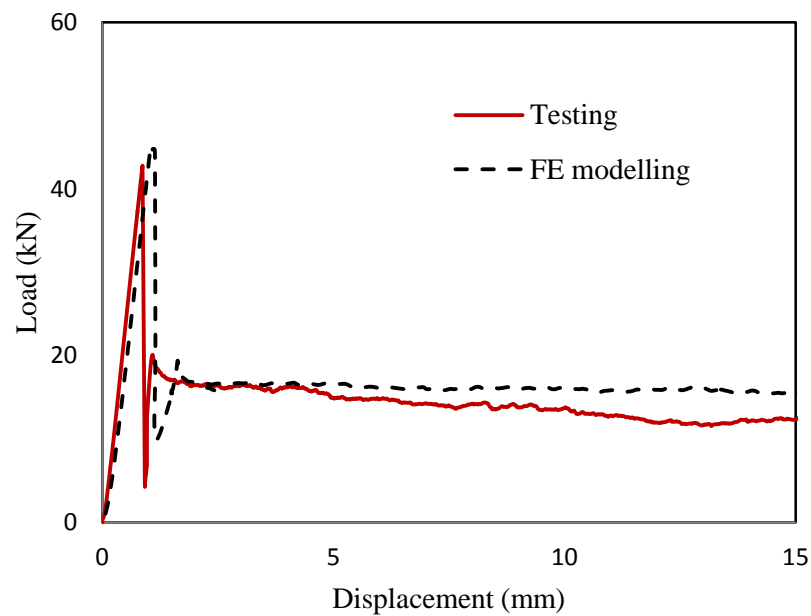
(b) Top view of crushed CFRP tube (OD 34.8 mm) and hybrid system

Fig. 4.4 Comparison of progressive failure of CFRP tube (OD 34.8 mm) and images of crushed CFRP tube and hybrid system between testing and FE modelling.

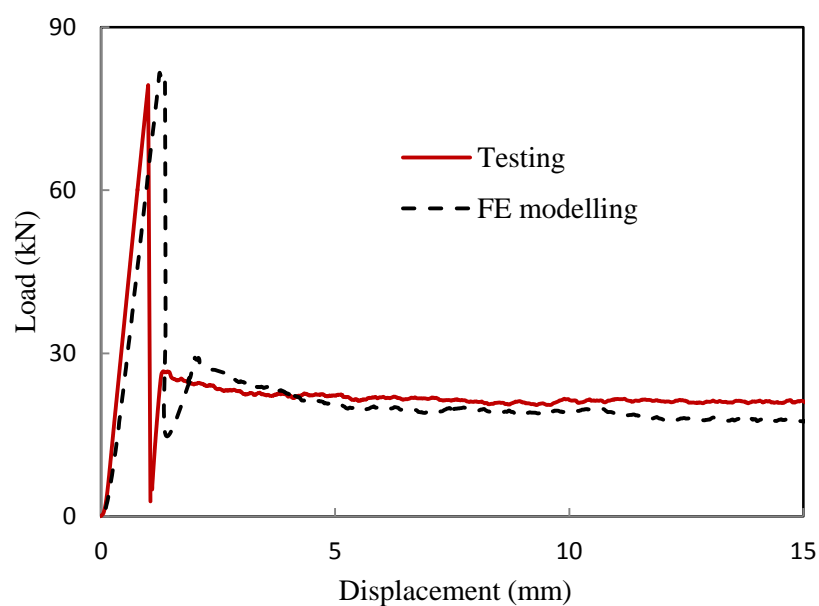
Fig. 4.5 shows the comparison of load-displacement traces obtained from the testing and FE modelling of CFRP tubes. Fig. 4.5(a) presents the load-displacement curves for the CFRP tube with 8 mm outer diameter. Both curves exhibit a similar trend as the load increases rapidly to the maximum value in a linear manner and then decreases sharply to a low resistance level and then go back to the plateau stage. The peak load from the FE modelling is slightly higher than its testing counterpart. Figs. 4.5(b) and 4.5(c) show the load-displacement traces for carbon fibre reinforced plastic tubes in an outer diameter of 34.8 and 54 mm respectively. Both the maximum loads predicted are again slightly larger than those of the measured values. However, the general trend of the experimental load-displacement traces is simulated reasonably well.



(a) CFRP tube with outer diameter 8 mm



(b) CFRP tube with outer diameter 34.8 mm

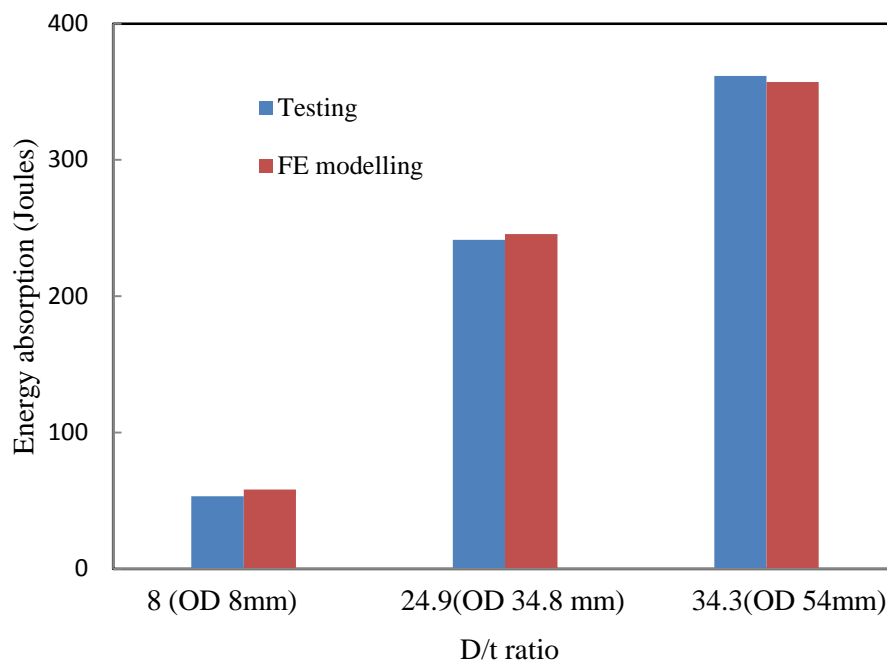


(c) CFRP tube with outer diameter 54 mm

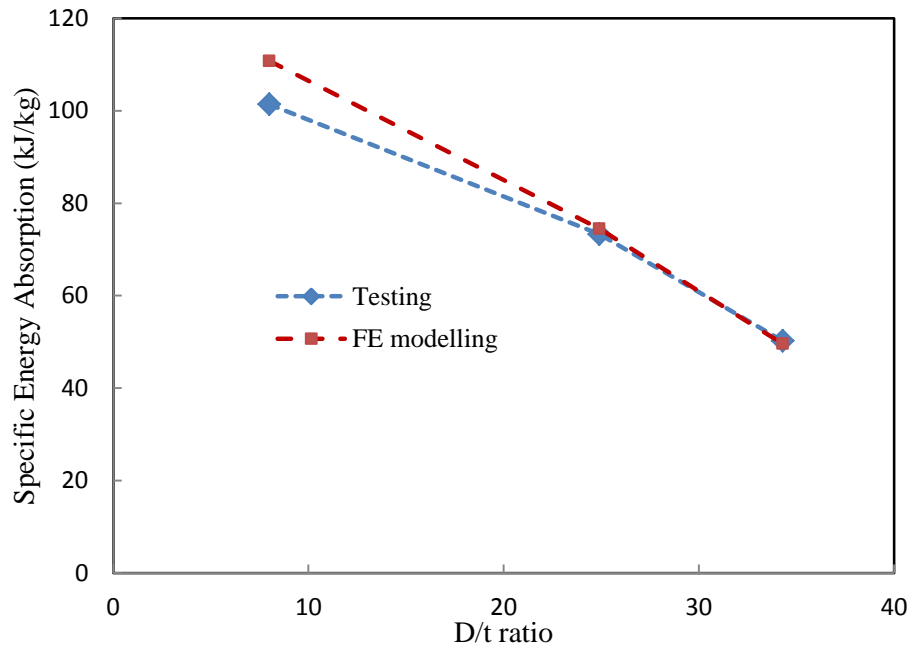
Fig. 4.5 Load-displacement traces of individual CFRP tubes in outer diameter of (a) 8mm (b) 34.8 mm and (c) 54mm.

Fig. 4.6(a) presents a comparison of total energy absorbed from the testing and FE modelling for three CFRP tubes studied. The total energy increases with the increasing of  $D/t$  ratio for both the testing and FE prediction results. The total values of energy absorption of CFRP tubes with outer diameter of 8

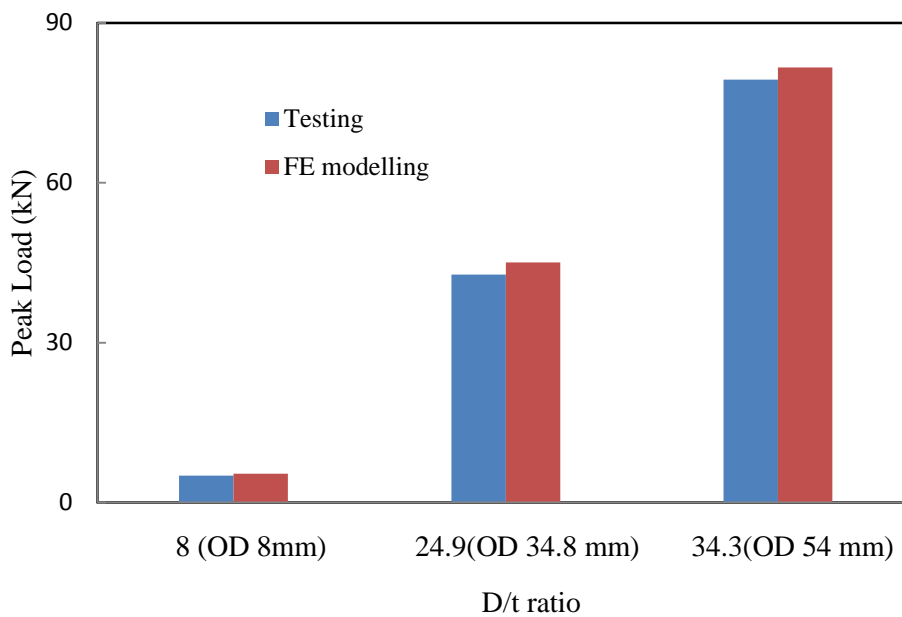
and 34.8 mm are slighter lower than the predicted values, while the situation for CFRP tube with outer diameter of 54.8 mm is on the contrary. Fig. 4.6(b) shows the comparison of specific energy absorption (SEA) values for all the three tubes from testing and prediction. As expected, the SEA decreases with increasing the D/t ratio for both the testing and prediction. Fig. 4.6(c) compares the mean crushing load for CFRP tubes between testing and FE modelling. The peak load increases with the increasing of D/t ratio for both the testing and FE modelling results, as expected, however, they match with each other very well.



(a) Comparison of energy absorption for CFRP tubes between testing and predictions.



(b) Comparison of SEA for CFRP tubes between testing and predictions.



(c) Comparison of mean crushing load for CFRP tubes between testing and predictions.

Fig. 4.6 Comparison of energy absorption, SEA and peak crushing load between testing and predictions

The summary of the peak load, energy absorption and SEA characteristics for the three CFRP tubes from testing and FE modelling is presented in Table 4-6. The values of energy absorption for CFRP

tubes (OD 8, 34.8 mm) obtained from predictions are 58.1 and 245.5 J, which are 9% and 1.7% higher than the measured energy absorptions (53.2, 241.3 J) respectively, while for the CFRP tube (OD 54 mm), the energy absorption in prediction (357.2 J) is only 1% lower than the value in testing (361.6 J). Also, the values of SEA and peak load obtained from the numerical modelling are less than 2% in discrepancy with the experimental counterparts.

Table 4-6 Summaries of energy absorption, mean crushing load and SEA

OD (mm)	Mass (g)	Peak Load (kN)		Energy Absorption (J)		SEA (kJ/kg)	
		Testing	FE modelling	Testing	FE modelling	Testing	FE modelling
8	0.53	5.1	5.4	53.2	58.1	101.4	110.8
34.8	3.29	42.8	45.1	241.3	245.5	73.3	74.5
54	7.20	79.4	81.6	361.6	357.2	50.2	49.6

#### 4.6.2 Simulation of sandwich beams

Fig. 4.7 shows the failure mode of the sandwich beam based on glass fibre woven skins and syntactic foam core subjected to three-point bending loading. The three-point bending and impact tests have been carried out by Pavlopoulou [116]. As shown, a combination of skin fracture, skin delamination and core fracture takes place, which contributes to the final failure, for both the testing and FE modelling. Observed from the FE modelling, the failure mode of skin fracture occurred initially followed by the skin delamination until the skins reach the bending strength before the core fracture happened.

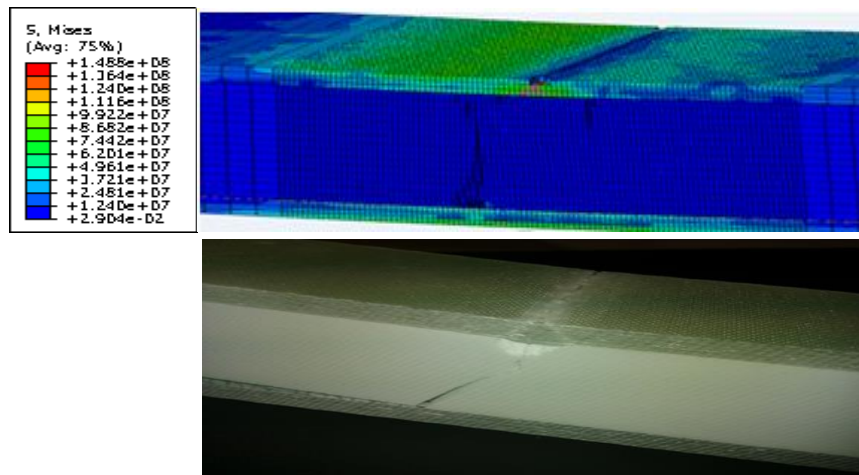
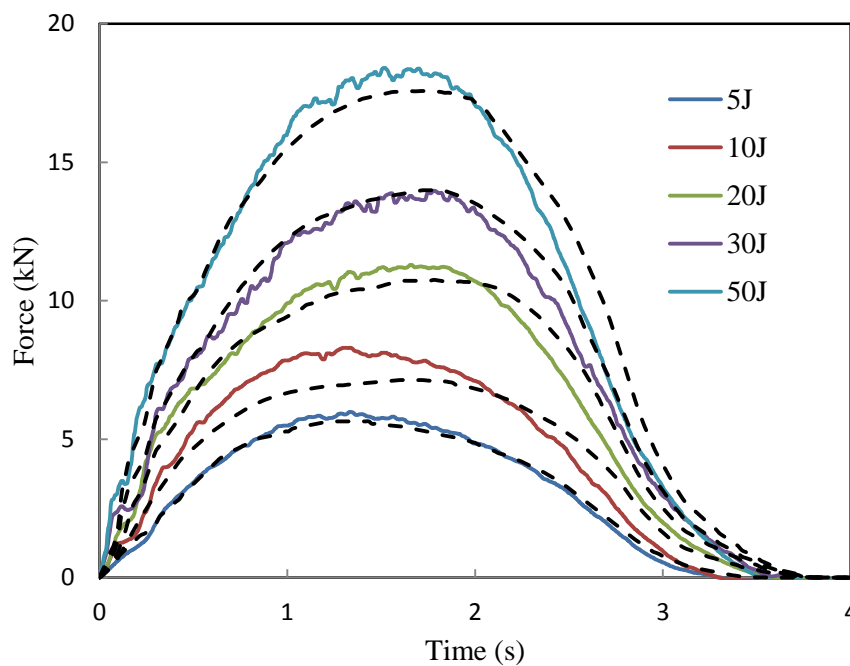
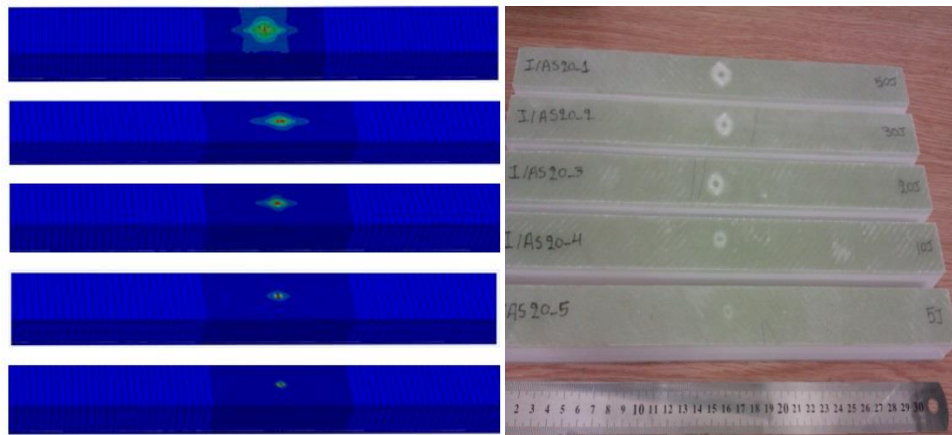


Fig. 4.7 Images of sandwich beam subjected to three-point bending between testing and FE modelling.

Fig. 4.8(a) presents the comparison of impact resistance for sandwich beams subjected to projectile impact with varying impact energy from testing and predictions. All of the five curves exhibit a similar trend as the impact resistance force increases to the maximum value and then dissipates to zero gradually. The values of the peak load from the tests are slightly higher than those obtained from predictions, which indicate the success of the modelling. Fig. 4.8(b) shows the images of sandwich beams after impact with an impact energy from 5 J to 50 J.



(a) Impact resistance



(b) Impacted images

Fig. 4.8 Comparison of (a) Impact resistance and (b) Impacted images for sandwich beam subjected to varying energy impact from testing and FE modelling (The solid lines correspond to test data and dashed lines to predictions)

Fig. 4.9 shows the peak load of impact resistance for sandwich beams subjected to various impact energies from the testing and FE modelling. The values of impact resistance increase with increasing the impact energy. In the test, the maximum impact resistance force is 18.5 kN obtained from an impact energy of 50 J, which is 0.9 kN (5.1%) more than the value (17.6 kN) obtained from the FE modelling, while the minimum value of force is 5.9 kN which is 0.2 kN (3.5%) larger than the value (5.7kN) recorded from predictions related to an impact energy of 5 J. The forces of impact resistance are 8.0, 11.2 and 14.2 kN obtained from testing and 7.1, 10.8 and 13.9kN from FE modelling subjected to an impact energy of 10, 20 and 30 J, respectively. Again, reasonably good correlation is obtained.

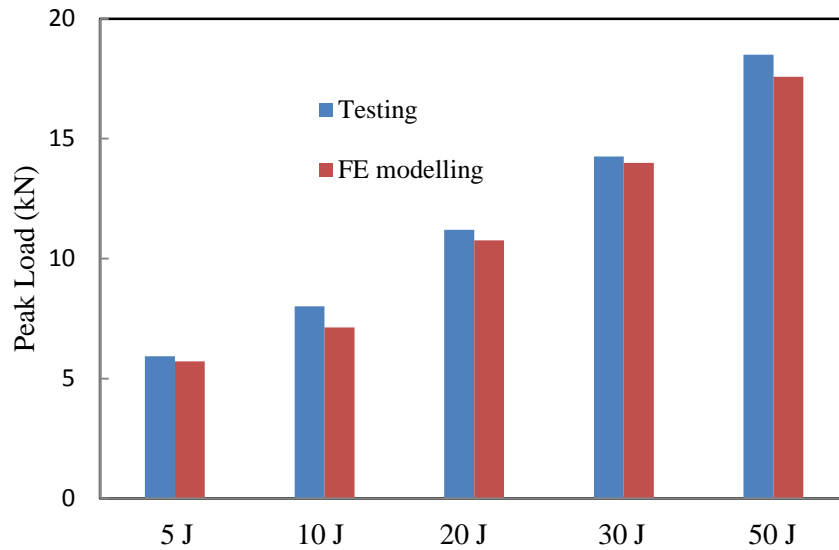


Fig. 4.9 Comparison of peak load of impact resistance for sandwich beam subjected to varying energy impact between testing and FE modelling

#### 4.7 Summary

This chapter summarises the numerical modelling theory and finite element methods employed to simulate the mechanical response of individual composite tubes and a hybrid system under quasi-static compressive and dynamic loading as well as sandwich beams based on glass woven skins and syntactic foam core subjected to three-point bending and impact with varying impact energy.

The modelling of individual CFRP tubes has been developed and good agreements with testing results on the energy absorption, SEA, peak load as well as the failure modes have been obtained. Simulation on hybrid system 1 has been conducted and the failure modes have been captured.

Simulations on sandwich beams subjected to three-point bending and impact have been conducted and the failure modes for three-point bending have been validated by the corresponding results. Furthermore, the predicted impact resistances of the sandwich beam subjected to impact with varying impact energy have been validated by the testing data.

## **CHAPTER 5 THEORETICAL WORK**

### **5.1 Introduction**

This chapter presents theoretical work on predicting the peak load and the corresponding displacement of the PVC foam panels reinforced by carbon fibre and glass fibre rods and bamboo tubes subjected to quasi-static compression. The predicted data are compared with the related experimental results with reasonable good correlation.

## 5.2 Carbon/Glass fibre rod embedded in PVC foam cores

### 5.2.1 The derivation of equations

Fig.5.1 shows a composite rod embedded in PVC foam, subjected to compressive loading. It is assumed that the rod deforms elastically up to the critical buckling load. The equation for the deformation of an elastic rod embedded in elastic medium is given as [123]:

$$\frac{d^2}{dx^2} \left( EI \frac{d^2 y}{dx^2} \right) + \frac{d}{dx} \left( P \frac{dy}{dx} \right) = -q_y \quad (5-1)$$

and

$$q_y = -\mu y \quad (5-2)$$

where  $\mu$  is the stiffness ( $=37 \text{ N/m}^2$ ) of the elastic foundation, i.e. the PVC foam in the present case.

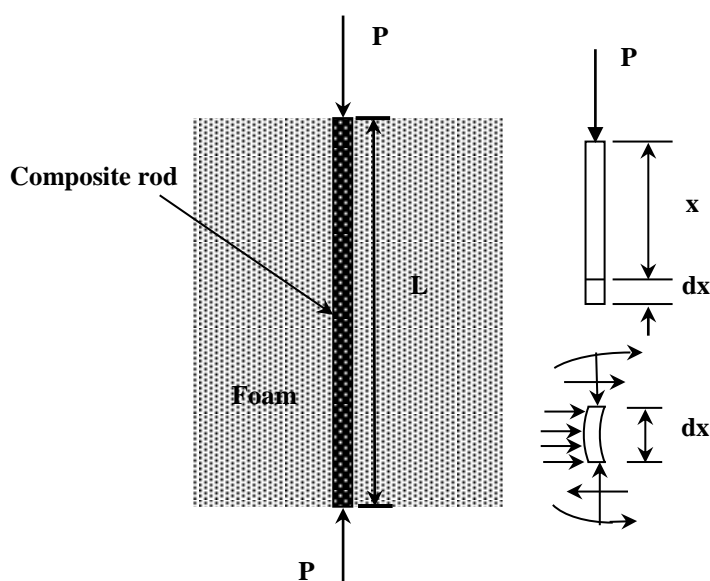


Fig. 5.1 Schematic of a composite rod embedded in PVC foam and subjected to compressive loading.

Equation (5-1) can be rewritten as

$$\frac{d^4 y}{dx^4} + k^2 \frac{d^2 y}{dx^2} + \frac{r^4}{4} y = 0 \quad (5-3)$$

where

$$k = \sqrt{\frac{P}{EI}} \quad \text{and} \quad r = \sqrt[4]{\frac{4\mu}{EI}} \quad (5-4)$$

The boundary conditions associated with the rod shown in Fig. 5.1 are:

$$y(0) = 0; \frac{d^2 y}{dx^2}(0) = 0; y(L) = 0; \frac{d^2 y}{dx^2}(L) = 0 \quad (5-5)$$

Employing the above boundary conditions, the solutions of Eq. (5-3) are classified according to the values of  $r$  and  $k$ , by Chen and Atsuta [124]. Furthermore, the critical buckling load can be shown to be:

$$P_{cr} = \min_{n=1,2,\dots} \left[ \alpha n^2 \frac{\pi^2 EI}{L^2} + \frac{\mu L^2}{n^2 \pi^2} \right] \quad (5-6)$$

where  $\alpha$  is an imperfection factor reflecting the introduction of damage at the two ends of the composite rod. In the absence of the elastic foam foundation, the above equation reduces to the standard Euler buckling equation. Assuming the lowest buckling mode i.e. let  $n = 1$ , the deflection equation of the rod is given as:

$$y(x) = C_2 x \cos \frac{k}{\sqrt{2}} x + C_3 \sin \frac{k}{\sqrt{2}} x \quad (5-7)$$

when  $k = r$ , the relationship between the coefficients  $C_2$  and  $C_3$  can be expressed as:

$$C_2 = -C_3 \frac{1}{L} \tan \left( \frac{k}{\sqrt{2}} L \right) \quad (5-8)$$

Assuming small deformations, the value of  $C_2$  can be obtained by assuming that  $C_3$  lies between 5% and 10% of the rod length, since the larger  $C_3$  is corresponding to the larger deflection. Then, through the iterations in Matlab, the most reasonable predictions of the displacement related to the peak load can be obtained using the following equation [125], which gives good correlation to the experimental data. (the ratio  $C_2/C_3$  can be obtained in terms of specific value  $k$ , therefore, the deflection is decided by the value  $C_3$ . Through the iterations in Matlab, different  $C_3$  can obtain various  $y$  which is the deflection of different point of the rod under compressive load, according to the assumption that the deflection is quite small, so the  $C_3$  can be taken from 5% to

10% of  $\frac{y(x)_{max}}{\frac{C_2}{C_3} \cos \frac{k}{\sqrt{2}} x + \sin \frac{k}{\sqrt{2}} x}$ , where the  $k$  is the value can be used to obtain the  $y(x)_{max}$ .)

$$D = L - \int_0^L \left[ 1 - \left( \frac{dy}{dx} \right)^2 \right]^{\frac{1}{2}} dx \quad (5-9)$$

### 5.2.2 The comparison between the experiment results and calculations

Using the above equilibrium equations, it is possible to calculate the peak load and associated rod displacement for different sizes of reinforcement embedded in foams of varying density. Here, the material properties used in all calculations are given in Table 5-1 and 5-2 [126]. The imperfection factor for glass fibre was taken as  $\alpha = 0.5$  to account for matrix failure, leading to longitudinal splitting at the two ends of the rod. Table 5-3 compares the calculated and experimental values of peak load and end displacement of unsupported (i.e. in the absence of a foam support) 4 mm diameter rods.

Table 5-1 Mechanical properties of the foams used in this study [126]

	C40	C80	C130	C200
Density (kg/m <sup>3</sup> )	40	80	130	200
Tensile modulus (MPa)	28	66	110	175
Tensile strength (MPa)	0.7	2.0	3.8	6.0
Compressive modulus (MPa)	37	97	160	280
Compressive strength (MPa)	0.45	1.3	2.6	4.8
Compressive fracture strain	0.65	0.7	0.7	0.7
Shear modulus (MPa)	13	30	47	75
Shear strength (MPa)	0.5	1.2	2.3	3.5
Shear fracture strain	0.08	0.23	0.30	0.30
Poisson's ratio	0.32	0.32	0.32	0.32
Work of fracture in tension (kJ/m <sup>2</sup> )	0.21	0.44	0.76	1.33
Work of fracture in shear (kJ/m <sup>2</sup> )	4.5	12.6	27.6	44.2

Table 5-2 Mechanical properties of the carbon and glass fibre rods [126]

	Carbon fibre rod	Glass fibre rod
Density (kg/m <sup>3</sup> )	1986	2004
Tensile strength (MPa)	650	500
Compressive modulus (GPa)	8.1	14.3
Compressive strength (MPa)	202	167
Flexural modulus (GPa)	80	43
Flexural strength (MPa)	989	940
Weight fraction of fibre (%)	63.7	78.6

Table 5-3 The predicted peak load and the related displacement of composite rods.

Type of rod	Peak load (kN)		Displacement (mm)		Error (%)		
	Test(without buckling)	Test(with buckling)	Prediction	Test	Prediction	Load	Displacement
Carbon fibre	2.49	2	2.17	0.5	0.49	14.8	2.0
Glass fibre	2.2	0.5	1.30	0.23	0.15	69.2	53.3

The predictions and experimental values of peak load and displacement for the compressively-loaded carbon fibre rods embedded in a range of PVC foams are given in Table 5-4. In general, the level of agreement is reasonably good, particularly in terms of the displacement values. Four values of peak load are over-estimated by more than 20%, probably as a result of damage at the two ends of the rod. This was not taken into account in the calculations for the carbon fibre rods, since observation of the ends did not reveal any apparent splitting.

Table 5-4 The predicted peak load and displacements for the carbon fibre rods embedded in PVC foams.

Diameter of rod (mm)	Foam density(kg/m <sup>3</sup> )	Peak load (kN)		Displacement (mm)		Error (%)	
		Test	Prediction	Test	Prediction	Load	Displacement
2	40	0.67	0.62	2.11	2.4	7.5	12.1
	80	0.94	0.95	1.25	1.3	1.1	3.9
	130	1.39	1.52	1.33	1.5	8.6	11.3
	200	2.18	2.78	1.56	1.7	21.6	8.2
3	40	0.89	1.17	1.1	1.3	24	15.4
	80	1.33	1.5	2.43	2.5	11.3	2.8
	130	1.89	2.07	2.03	2.2	8.7	7.7
	200	2.61	3.32	2.35	2.6	21.4	9.6
4	40	2.06	2.66	1.32	1.5	22.6	12
	80	2.12	2.98	1.18	1.4	28.9	15.7
	130	3.16	3.56	1.4	1.6	11.2	12.5
	200	4.05	4.81	2.43	2.6	15.8	6.5

Table 5-5 compares the predictions and experimental values for the glass fibre rods embedded in a range of foams. Agreements between the predicted and measured values are not as good as for the carbon fibre rod (Table 5-4), particularly for the systems based on low density foams. The stiffness of glass fibre rod is almost doubled of the carbon fibre one, which needs more support from the foam. However, the low density foams seem not providing the necessary support, which

caused the rod fell down to offer a lower resistance to compressive load. This was also observed in the test.

Table 5-5 The calculated peak load and displacement of glass fibre rods embedded in PVC foams.

Diameter of rod (mm)	Foam density (kg/m <sup>3</sup> )	Peak load (kN)		Displacement (mm)		Error (%)	
		Test	Prediction	Test	Prediction	Load	Displacement
2	40	0.22	0.57	1.94	2.0	61.4	3.0
	80	0.74	0.89	2.15	2.3	16.9	6.5
	130	1.2	1.46	1.67	1.8	17.8	7.2
	200	1.94	2.72	1.46	1.5	28.7	2.7
3	40	0.64	0.9	0.81	0.9	28.9	10.0
	80	1.22	1.23	1.25	1.3	0.8	3.9
	130	1.56	1.79	1.77	1.8	12.9	1.7
	200	2.5	3.05	2.13	2.2	18.0	3.2
4	40	1.47	1.78	0.89	1.0	17.4	11.0
	80	1.73	2.11	1.1	1.2	18.0	8.3
	130	2.62	2.67	1.32	1.4	1.9	5.7
	200	3.49	3.93	1.91	2.0	11.2	4.5

The summary of the energy absorption and SEA of plain foam with varying density as well as foam reinforced by carbon or glass fibre rods subjected to both the quasi-static and dynamic impact loadings have been investigated by Jin *et al.* [136] in Table 5-6.

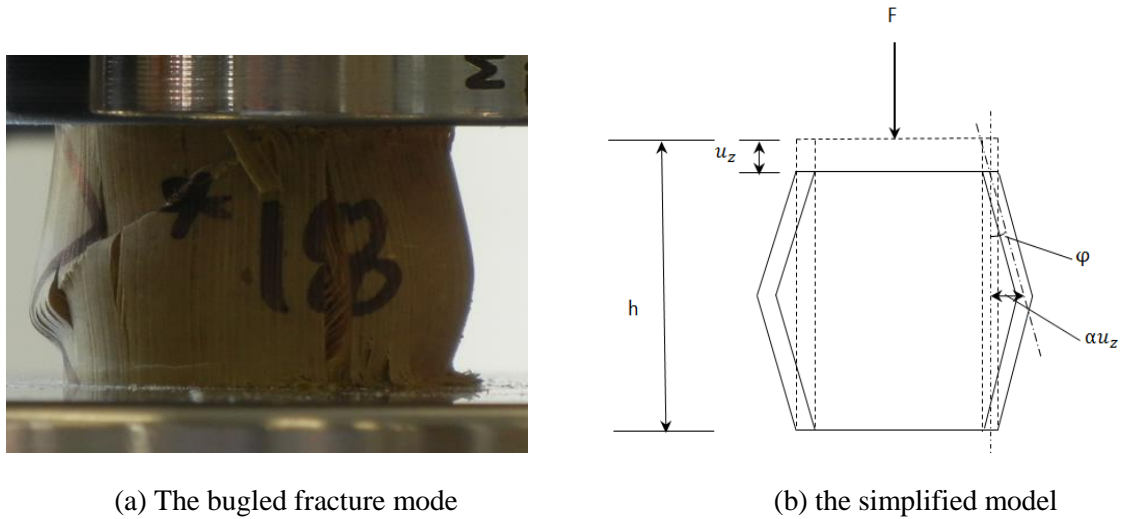
Table 5-6 Summary of the compression strengths and energy absorption properties of the reinforced foams [126]

Specimen ID	Quasi-static		Dynamic		
	Energy (J)	SEA (kJ/kg)	Energy (J)	SEA (kJ/kg)	
Carbon	C80 plain	58.8	13.46	85.8	21.83
	C80C2	87.1	17.4	137.4	27.43
	C80C3	116.1	18.27	204.0	32.08
	C80C4	207.7	28.21	298.2	36.16
	C130 plain	104.4	15.19	161.3	23.47
	C130C2	154.5	19.51	253.0	31.94
	C130C3	206.9	22.34	337.0	36.53
	C130C4	298.5	29.93	476.3	43.08
Glass	C80 plain	58.8	13.46	85.8	21.83
	C80G2	85.2	16.17	104.6	20.85
	C80G3	126.9	19.89	140.4	22.01
	C80G4	210.8	25.45	221.2	26.69
	C130 plain	104.4	15.19	161.3	23.47
	C130G2	149.0	18.79	190.6	24.03
	C130G3	217.8	23.62	238.6	25.8
	C130G4	317.8	28.64	325.5	29.33

### 5.3 Bamboo pipes

#### 5.3.1 Failure mode 1

The simplified mode of the bamboo tube is shown in Fig. 5.2 (b), where the bulged deformation shape is simplified as straight one. Here, it is assumed that the tube is deformed longitudinally by  $u_z$  under the compression load “F” and that there is no deformation along the wall thickness. Due to Poisson’s effect, the tube is expanded by  $u_z$ , where  $\alpha$  is related to Poisson’s ratio.



(a) The bugled fracture mode

(b) the simplified model

Fig. 5.2 Failure mode 1

According to the definition of the strain of materials, there is

$$\varepsilon_z = \frac{u_z}{h} \quad (5-10)$$

where:  $\varepsilon_z$  is axial strain,  $u_z$  is axial displacement,  $h$  is the height of tube.

Based on Fig. 5.2 (b), there is

$$R_m = \frac{R_1 + R_2}{2} \quad (5-11)$$

$$\pi \alpha u_z = \frac{\pi(1 + \varepsilon_\theta) R_m - \pi R_m}{2} \quad (5-12)$$

where:  $R_m$  is average diameter,  $R_1$  is internal diameter,  $R_2$  is external diameter,  $\varepsilon_\theta$  is circumferential strain,  $\alpha$  is related to longitudinal Poisson ratio.

From equation (5-11), there is

$$\varepsilon_\theta = \frac{2\alpha u_z}{R_m} \quad (5-13)$$

According to the general Hook's law, the  $\varepsilon_z$  and  $\varepsilon_\theta$  can be written as

$$\varepsilon_z = \frac{\sigma_z}{E_z} - \frac{\nu_{\theta z}}{E_\theta} \sigma_\theta \quad (5-14)$$

$$\varepsilon_\theta = -\frac{\nu_{z\theta}}{E_z} \sigma_z + \frac{\sigma_\theta}{E_\theta} \quad (5-15)$$

where:  $E_z$ ,  $E_\theta$  are Young's moduli in the cylindrical coordinates system i.e. longitudinal, circumferential respectively,  $\nu_{\theta z}$ ,  $\nu_{z\theta}$  are Poisson's ratios in the cylindrical condition.

From equations (5-10), (5-13), (5-14), (5-15), the relationship between  $\varepsilon_z$  and  $\varepsilon_\theta$  can be derived as

$$\sigma_z = \frac{2\alpha h k_1 + k_3}{2\alpha h k_2 + k_4} \sigma_\theta \quad (5-16)$$

where:  $k_1 = \frac{1}{E_z}$ ,  $k_2 = \frac{\nu_{\theta z}}{E_\theta}$ ,  $k_3 = \frac{1}{E_\theta}$ ,  $k_4 = \frac{\nu_{z\theta}}{E_z}$

It is assumed that the increment in Z direction is uniform, and then we can get the relationship between stress and axial load

$$\sigma_z = \frac{F}{A} \quad (5-17)$$

$$A = \frac{\pi t (R_1 + R_2)}{2} \quad (5-18)$$

where: F is axial load; 'A' is cross-section area of the tube, t is the thickness of the tube.

Take the critical hoop stress  $\sigma_\theta^c$  in equation (5-16), from equations (5-16), (5-17) and (5-18), there is,

$$F_c = \frac{\pi t (R_1 + R_2) (2\alpha h k_1 + k_3)}{4\alpha h k_2 + 2k_4} \sigma_\theta^c \quad (5-19)$$

where:  $F_c$  is critical load,  $\sigma_\theta^c$  is critical hoop stress.

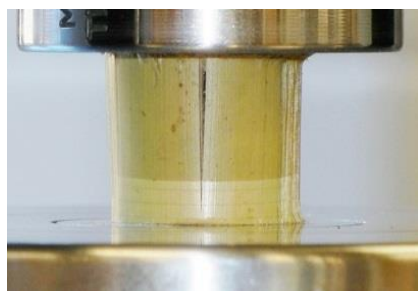
In the (5-19), the value of  $\sigma_\theta^c$  has been taken as 20% of the maximum stress of bamboo tube under compression.

From (5-13), (5-15), (5-17), (5-19), the critical displacement  $u_z$  related to the critical load can be obtained as

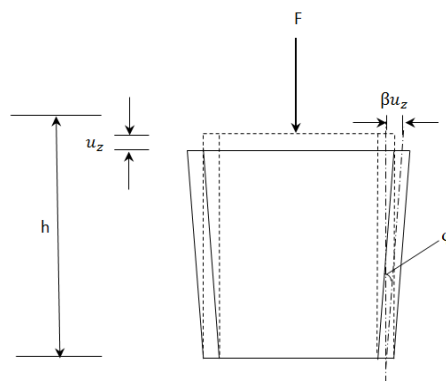
$$u_z = \frac{R_m (-k_4 F_c + k_3 \sigma_\theta^c)}{2\alpha} \quad (5-20)$$

### 5.3.2 Failure mode 2

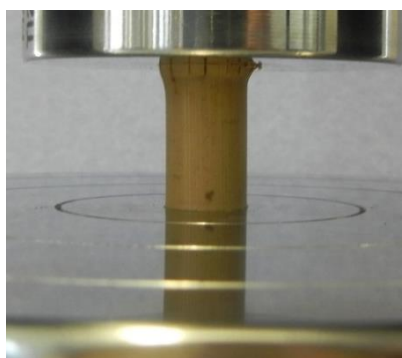
In the failure mode 2, see Fig. 5.3 as shown below.



(a) The top opening mode



(b) The top opening mode



(c) The top local buckling mode for small bamboo tube

Fig.5.3 Failure mode 2

From the failure model 2, see Fig. 5.3 (a) and (b), there is

$$\varepsilon_{\theta} = \frac{2\beta u_z}{R_m} \quad (5-21)$$

where:  $\beta$  is related to longitudinal Poisson ratio.

According to equations (5-10), (5-14), (5-15), (5-21), the final equations for critical load  $F_c$  and related displacement  $u_z$  for failure mode 2 are as below

$$F_c = \frac{\pi t(R_1 + R_2)(2\alpha h k_1 + k_3)}{4\alpha h k_2 + 2k_4} \sigma_{\theta}^c \quad (5-22)$$

$$u_z = \frac{R_m(-k_4 F_c + k_3 \sigma_{\theta}^c)}{2\beta} \quad (5-23)$$

According to the test results, the failure mode of the small tubes is mode 2 with the top local buckling, (Fig. 5.3(c)). Therefore, the constant coefficients  $\gamma_1, \gamma_2$  were introduced when calculating the critical

load and the related displacements for small bamboo tubes as the peak load for bamboo tubes with local buckling is relatively low.

$$F'_c = \gamma_1 F_c = \gamma_1 \left( \frac{\pi t (R_1 + R_2) (2\alpha h k_1 + k_3)}{4\alpha h k_2 + 2k_4} \sigma_\theta^c \right) \quad (5-24)$$

$$u'_z = \gamma_2 u_z = \gamma_2 \frac{R_m (-k_4 F_c + k_3 \sigma_\theta^c)}{2\beta} \quad (5-25)$$

### 5.3.3 Results and Discussion

According to the above equations and the values of the samples tested, the final value of critical load and displacement can be calculated as follows. Besides, the values of the coefficients used in the calculation are listed in the following Table 5-7.

Table 5-7 The values of properties and coefficients used in the calculation.

$E_\theta^{[127]}$	$\nu_{\theta z}, \nu_{z\theta}^{[128]}$	$\mu^{[129]}$	$\alpha$	$\beta$	$\gamma_1$	$\gamma_2$
398 MPa	0.22, 0.055	0.3	0.2	0.35	0.5	1.0

According to the equation (5-19) and (5-20), the final value of prediction of the critical load and related displacement can be calculated in Table 5-8.

Table 5-8 The predicted peak load and the related displacement for large bamboo tubes of mode 1.

Sample	Average diameter (mm)	Peak Load (kN)			Displacement (mm)		
		Test	Prediction	Error (%)	Test	Prediction	Error (%)
1	20.32	25.61	23.16	9.6	1.80	1.57	12.8
3	21.36	25.06	21.36	14.8	1.40	1.48	-5.7
6	21.18	23.00	21.72	5.7	1.54	1.73	-12.3
7	19.80	17.65	15.93	9.8	1.12	1.45	-29.4
9	21.76	22.88	23.87	-4.3	1.52	1.69	-11.2
10	19.80	18.40	17.20	6.5	1.44	1.47	-2.1

The predictions and experimental values of peak load and displacement for the large bamboo tubes of failure model 1 are given in Table 5-8. In general, the level of agreement is reasonably good,

particularly in terms of the displacement values. Just one values of peak load are over-overestimated by more than 20%, probably as a result of damage at the two ends of the rod. This was not taken into account in the calculations large bamboo tube, since observation of the ends did not reveal any apparent splitting.

According to the equations (5-22) and (5-23), the rest samples of large bamboos can be calculated in Table 5-9.

Table 5-9 The predicted peak load and the related displacement for large bamboo tubes of mode 2.

Sample	Average diameter (mm)	Peak Load (kN)			Displacement (mm)		
		Test	Prediction	Error (%)	Test	Prediction	Error (%)
2	21.92	21.68	18.88	12.9	1.10	1.12	-1.9
4	22.07	20.49	18.30	10.7	1.15	1.15	0.0
5	20.20	30.91	27.63	10.6	1.31	1.27	3.1
8	18.7	19.35	15.90	17.8	0.97	1.09	-12.4

As we can see from the Table 5-9 the agreements of the load and displacement between the test and prediction are good for all the 4 samples with the failure mode 2.

According to the equations (5-24) and (5-25), the critical load and displacement for small bamboos can be calculated in Table 5-10.

Table 5-10 The predicted peak load and the related displacement for small bamboo tubes of mode 2.

Sample	Average diameter (mm)	Peak Load (kN)			Displacement (mm)		
		Test	Prediction	Error (%)	Test	Prediction	Error (%)
1	5.90	2.43	1.77	27.2	0.33	0.28	15.2
2	4.58	1.29	1.21	6.2	0.30	0.33	-10.0
3	8.86	4.64	4.79	-3.2	0.47	0.50	-6.4
4	8.94	4.86	4.96	-2.1	0.41	0.49	-19.5
5	9.20	4.80	5.38	-12.1	0.38	0.51	-34.2
6	10.07	7.48	8.53	-14.0	0.50	0.66	-32.0
7	10.67	11.15	11.71	-5.0	0.71	0.83	-16.9
8	11.79	10.65	10.12	5.0	0.60	0.65	-8.3
9	12.01	9.85	8.83	10.4	0.60	0.63	-5.0
10	10.55	8.81	7.63	13.4	0.47	0.55	-17.0

The predictions and experimental values of peak load and displacement for the small bamboo tubes of failure model 2 with local buckling are given in Table 5-10. In general, the level of agreement is reasonably good. Just one value of peak load is over-estimated by more than 20% and two for the displacement, probably as a result of the influence of the local buckling.

#### 5.4 Summary

This chapter has presented two theoretical calculations. Firstly, the calculations are discussed on individual CFRP rod and its reinforced PVC foam subjected to quasi-static compression load. On the other hand, the individual bamboo tube under axial compression load has been computed as well. A good agreement between the predicted and observed results has been obtained for both these two cases. The errors of both the peak loads and corresponding displacements are less than 20% for both the CFRP rods and bamboo tubes.

## CHAPTER 6 CONCLUSIONS AND RECOMMENDATIONS FOR FUTURE WORK

### 6.1 General summary

The objectives of the project are to investigate the energy-absorbing capacity and mechanical response of carbon fibre reinforced plastic tubes and associated hybrid systems subjected to the both quasi-static and dynamic compressive loadings.

The Finite Element Analysis Method has been employed to model the individual CFRP tubes and related hybrid systems subjected to compression loading as well as the response of sandwich beam based on E-glass fibre skins and syntactic foam core under dynamic impact. A vectorised user material subroutine (VUMAT) has been used to define 3D Hashin's failure criteria for composite layers to simulate the associated deformation and failure mechanisms.

#### 6.1.1 Composite tubes

Initially, the quasi-static axial compression tests have been carried out on individual carbon fibre reinforced plastic tubes and the hybrid systems in order to obtain the values of energy absorption and the mean crushing load. There are three dimensions of CFRP tubes with the D/t ratio from 8 to 34.3. The energy-absorbing chart of the CFRP tubes shows that the values of SEA, varying from 49.1 to 99.6 kJ/kg, decrease with the increase of the D/t ratio. In terms of hybrid systems, the energy-absorbing capacity of HS1 and HS2 is about 5% and 3% higher than the sum of the constituent component contributions respectively, while the situations are different in HS3, HS4 and HS5, with 5%, 4% and 6% lower than the values of total energy absorbed by the constituent components. On the other hand, the peak loads of hybrid systems are higher than the sum of individual components but not significant.

Dynamic tests have been conducted on CFRP tubes and hybrid systems subsequently. Both the energy-absorbing capability and the ability to resist the dynamic impact of CFRP tubes as well as the hybrid systems are much higher than those under quasi-static compression. The comparison between

the HS1 and HS4 as well as between HS1 and HS5, the effect of foam on energy-absorbing capacity and compression strength has been summarised, suggesting that the hybrid systems with in-filled foams will not increase the values of energy-absorbing capacity and compression strength compared to the plain hybrid system.

Moreover, the comparisons of energy-absorbing capacity and SEA of individual tubes and hybrid pipe systems subjected to quasi-static and dynamic impact have been summarised. It suggests that the individual CFRP tube with  $D/t$  ratio 34.3 exhibits the greater enhancement on both the energy absorption as well as value of SEA under impact and all of the hybrid systems have a significant improvement on the mean crushing load, energy absorption and SEA.

### **6.1.2 Sandwich beams**

Finite Element simulation has been used to model the sandwich beams based on E-glass fibre skins and syntactic foam core under both the low-velocity impact with impact energy from 5 to 50 J and three point bending.

Initially, the models of plain beam with thickness 6, 10, 13 and 20 mm under impact has been developed and extensive models on sandwich beams with skin thickness varying from 1 to 3 mm. Then the results have been validated by the experimental data suggesting that the optimum skin to core thickness ration is 0.15 in the impact test.

Subsequently, the models of the sandwich beams with different thickness under three-point bending load have been developed. Then the failure modes from the simulation have been validated by the corresponding test results.

## **6.2 Recommendations for future work**

The method on how to enhance the energy absorption and compression strength for hybrid systems needs to be studied further on how a hybrid system is optimised with the corresponding constituent components. Furthermore, it would be interesting to test the hybrid systems with novel structural types with different cross-section.

To carry out high velocity impact tests to the individual CFRP tubes and hybrid systems as well as blasting impact is a possible researching project.

The investigation of the effect of loading-rate on the response of the hybrid tube systems will generate usefull information on the rate-dependent behaviour of the structures proposed. In addition, finite element models to cover all hybrid systems can be developed to assist optimise energy absorbing of various CFRP structures.

More effort can be spared to the investigation on the natural fibre reinforced individual tubes and the associated hybrid systems as the low-cost and environmental friendly materials with high performance on energy absorption will be used in a wide range of structures in the future.

Parametric studies could be undertaken on hybrid systems using the commercial FEA method to model the different characteristics of varying geometry and loading condition.

The theoretical analysis would be another method to predict the response of carbon fibre reinforced plastic tubes and their associated hybrid systems subjected to compressive crushing. To develop an empirical equation based on experimental and numerical data to predict the energy-absorbing capacity and the peak load of the composite tubes with extended configurations.

**REFERENCES**

- [1] Potter, K., "Introduction to Composite Products," First edition, Chapman & Hall, London, UK, 1997.
- [2] Gutowski, T. G., "Advanced Composites Manufacturing," First edition, John Wiley & Sons, New York, USA, 1997.
- [3] Gay, D., Hoa, V., W, S., and W, T., "Composite Materials Design and Applications," CRC Press, 2003.
- [4] Bake, A., Dutton, S., and Ketty, D., "Composite Materials for Aircraft Structures," American Institute of Aeronautics and Astronautics Inc., Reston, Virginia, 2004.
- [5] Hull, D., An introduction to Composite Materials. Cambridge University Press, 1981.
- [6] [http://modernairliners.com/Boeing787\\_files/Specifications.html](http://modernairliners.com/Boeing787_files/Specifications.html)
- [7] <https://aerospace.honeywell.com/news/35-random-facts-about-the-airbus-a350-xwb>
- [8] E, Phil. and Costas, S., Polymer Composites in the Aerospace Industry. Published 2014 Woodhead Publishing. ISBN: 978-0-85709-523-7.
- [9] Spence, B. E., Composites in the Sporting Goods Industry. Handbook of Composite. pp. 1044-1052. 1998.
- [10] Zhu, F., Lu, G., Ruan, D., Plastic Deformation Failure and Energy Absorption of Sandwich Structures with Metallic Cellular Cores, International Journal of Protective Structures, 2011; (4): 507-541.
- [11] Heimbs, S., Computational methods for bird strike simulations: a review, Computers & Structures, 2011; (89): 2093-2112.
- [12] Ramadan, M., Azzam, A., Mohamed, A.E., Hashim, A., Low velocity impact properties of foam sandwich composite: a brief review.
- [13] Anderson, T. and Madenci, E., Experimental investigation of low-velocity impact characteristics of Sandwich composites, Composite Structures, 2000; (50): 239-247.
- [14] Morris, K., The history of PVC: The chemical and industrial production of polyvinyl chloride, MacLaren University of Minnesota, 1969.

- [15] Hassan, M.Z. And Cantwell, W.J., The influence of core properties on the perforation resistance of sandwich structures-An experimental study, *Composite ; Part B: Engineering*, 2012; (43):3231-3238.
- [16] Stanislaw, O. and Pawel, G., Experimental assessment of energy absorption capacity of carbon-epoxy and glass-epoxy composites, *Composite Structures*, 2009; (87): 215-224.
- [17] Xia, F. and Wu, X., Work on low-velocity impact properties of foam sandwich composites with various face sheets, *Journal of Reinforced Plastic and Composites*, 2010; (29)7: 1045-1054.
- [18] Lendze, T., Wojtyra, R., Gvillamat, L., Biateau, C., Imielińska, K., Low velocity impact damage in glass/polyester composite sandwich panels, *Advance in Materials Science*, 2006; (6): 26-34.
- [19] Hosur, Mu., Mohammed, A.A., Jeelanis, processing of nanoclay filled sandwich composites and their response to impact loading, *Journal of Reinforced Plastic and Composite*, 2008;27 (8): 797-818.
- [20] Schubel, P.M., Luom J.J., Daniel, I.M., Low velocity impact behaviour of Composite Sandwich Panels, *Composite Part A: Applied Science and Manufacturing*, 2005; (36)10: 1389-1396.
- [21] Schubel, P.M., Luo, J.J., Daniel, I.M., Impact and post impact behaviour of composite sandwich panels, *Composite Part A: Applied Science and Manufacturing*, 2007; (38)3: 1051-1057.
- [22] Cantwell, W.J., Kiratisaevee, H., Hazizan, M.A., Impact loading of light weight structures, *International Journal of Impact Engineering*, 2008; (35)1: 61-63.
- [23] Hassan, M.Z. and Cantwell, W.J., The influence of core properties on the perforation resistance of sandwich structures-An experimental study, *Composite ; Part B: Engineering*, 2012; (43):3231-3238.
- [24] Xia, F. and Wu, X., Work on low-velocity impact properties of foam sandwich composites with various face sheets, *Journal of Reinforced Plastic and Composites*, 2010; (29)7: 1045-1054.
- [25] Lendze, T., Wojtyra, R., Gvillamat, L., Biateau, C., Imielińska, K., Low velocity impact damage in glass/polyester composite sandwich panels, *Advance in Materials Science*, 2006; (6): 26-34.

- [26] Hosur, Mu., Mohammed, A.A., Jeelanis, processing of nanoclay filled sandwich composites and their response to impact loading, *Journal of Reinforced Plastic and Composite*, 2008;27 (8): 797-818.
- [27] Schubel, P.M., Luo, J.J., Daniel, I.M., Low velocity impact behaviour of Composite Sandwich Panels, *Composite Part A: Applied Science and Manufacturing*, 2005; (36)10: 1389-1396.
- [28] Schubel, P.M., Luo, J.J., Daniel, I.M., Impact and post impact behaviour of composite sandwich panels, *Composite Part A: Applied Science and Manufacturing*, 2007; (38)3: 1051-1057.
- [29] Zhu, F., Lu, G., Ruan, D., Plastic Deformation Failure and Energy Absorption of Sandwich Structures with Metallic Cellular Cores, *International Journal of Protective Structures*, 2011; (4): 507-541.
- [30] Rejab, M.R.M. and Cantwell, W.J., The mechanical behaviour of corrugated-core sandwich panels, *Composite Part B: Engineering*, 2013; (47): 267-277.
- [31] Alia, R.A., Cantwell, W.J., Langdon, G.S., Yuen, S.C.K. and Nurick, G.N., the energy-absorbing characteristics of composite tube-reinforced foam structures, *Composite: Part B*, 61; (2014): 127-135.
- [32] Smith, M., Guan, Z., Cantwell, W.J., Finite element modelling of the compressive response of lattice structures manufactured using the selective laser melting technique, *International Journal of Mechanical Science*, 2013; (67): 28-41.
- [33] Hazizan, M.A and Cantwell, W.J., The low velocity impact response of an aluminium honeycomb sandwich structure, *Composites Part B: Engineering*, 2003; (34)8: 679-687.
- [34] Anderson, T. and Madenci, E., Experimental investigation of low-velocity impact characteristics of Sandwich Composites, *Composite Structures*, 2000; (50): 23-247.
- [35] Lascoup, B., Aboura, Z., Khellil, K., Benzeggagh, M., Impact response of three-dimensional stitched sandwich composite, *Composite Structure*, 2010; (92): 347-353.
- [36] Marasco, A.L., Cartie, D.D.R., Partridge, I.K., Rezai, A., Mechanical properties balance in novel Z-pinned sandwich panels: out-of-plane properties, *Composite Part a*, 2006; (37); 295-302.
- [37] Zhou, J., Guan, Z.W., Cantwell, W.J., Liao, Y., The energy-absorbing behaviour of foam cores reinforced with composite rods, *Composite Structure*, 2014; (114); 346-356.

- [38] Hassan, M.Z. and Cantwell, W.J., Strain rate effects in the mechanical properties of polymer foams, *International Journal of Polymers and Technologies*, 2011; (3): 27-34.
- [39] Alavi, Nia. A. and Parsapour, M., An investigation on the energy absorption characteristics of multi-cell square tubes, *Thin-Walled Struct* 2013; 68:26–34.
- [40] Zhu, F., Lu, G., Ruan, D., Wang, Z., Plastic deformation , failure and energy absorption of sandwich structures with metallic cellular cores, *International Journal of Protective Structures*, 2011; (4): 507-541.
- [41] Mines, R.A.W., Worrall, C.M., Gibson, A.G., Low velocity perforation behaviour of polymer composite sandwich panels, *International Journal of Impact Engineering*, 1998; (21):855-879.
- [42] Nettles, R. and Hodge, A., Impact testing of glass/phenolic honeycomb panels with graphite/epoxy face sheets, *35th International SAMPE Symposium*, Anaheim, CA; 1990.
- [43] Lee, L.J., Huang, K.Y. and Fann, Y.J., Dynamic response of composite sandwich plate impacted by a rigid ball, *Journal of Composite Materials*, 1993; (27): 1238.
- [44] Yang, M. and Qiao, P., Higher-order impact modelling of sandwich structures with flexible core, *International Journal of Solids and Structures*, 2005; (42): 5460-5490.
- [45] Palazotto A.N., Herup EJ and Gummadi LNB, Finite element analysis of low-velocity impact on composite sandwich plates, *Composite Structures*, 2000; (49): 209-227.
- [46] Zhou, J., Hassan, M.Z., Guan, Z.W. and Cantwell, W.J., The low velocity impact response of foam-based sandwich panels, *Composite Science and Technology*, 2012; (72): 1781-1790.
- [47] Pavlopoulou, S. and Potluri, P., Residual flexural strength after impact and hydrostatic cycling in glass/synttactic foam sandwich laminates, *20th International Conference on Composite Materials Copenhagen*, 19-24th July 2015.
- [48] Lin, C. and Hoo Fatt M.S., Perforation of sandwich panels with honeycomb cores by hemispherical nose projectile, *Journal of Sandwich Structures and Materials*, 2005; (7)2: 133-172.
- [49] Buitrago, B.L., Santiuste, C., Sanchez-saez, S., Barbero, E., Navarro, C., Modelling of composite sandwich structures with honeycomb core subjected to high-velocity impact, *Composite Structures*, 2010; (92): 2090-2096.

- [50] Farley, G.L. and Jones, R.M., Crushing characteristics of composite tubes with “Near-Elliptical” cross sections, *Journal of Composite Materials*, 1992; (26): 1741-1751.
- [51] Farley, G., Crushing Characteristics of Continuous Fibre-Reinforced Composite Tubes, *Journal of COMPOSITE MATERIALS*, 1992; (26)1: 37-50.
- [52] Fan, Z., Shen, J., Lu, G. and Ruan, Dong., Dynamic lateral crushing of empty and sandwich tubes, *International Journal of Impact Engineering*, 2013; (53): 3-16.
- [53] DeRuntz, J.A. and Hodge, P.G., Crushing of a tube between rigid plates. *Journal of Applied Mechanics*, ASME 1963; 30:391e5.
- [54] Reid, S.R. and Reddy, T.Y., Effect of strain hardening on the lateral compression of tubes between rigid plates. *International Journal of Solids and Structures*, 1978; 14(3):213e25.
- [55] Gupta, N.K., Sekhon, G.S., Gupta, P.K., Study of lateral compression of round metallic tubes, *Thin-Walled Structures* 2005; 43(6):895e922.
- [56] Leu, D-K., Finite-element simulation of the lateral compression of aluminium tube between rigid plates. *International Journal of Mechanical Sciences* 1999;41(6):621e38.
- [57] Morris, E., Olabi AG, Hashmi MSJ. Lateral crushing of circular and non-circular tube systems under quasi-static conditions. *Journal of Materials Processing Technology* 2007; 191(1e3):132e5.
- [58] Reddy, T.Y. and Reid, S.R., On obtaining material properties from the ring compression test. *Nuclear Engineering and Design* 1979; 52(2):257e63.
- [59] Fan, Z., Shen, J., and Lu, G., Investigation of lateral crushing of sandwich tubes. *Procedia Engineering* 2011; 14:442e9.
- [60] Ashby, M., Evans, A., Fleck, N., Gibson, L., Hutchinson, J., Wadley H. *Metal foams: a design guide*. Oxford: Butterworth-Heinemann; 2000.
- [61] Shen, J., Lu, G., Ruan, D., Compressive behaviour of closed-cell aluminium foams at high strain rates. *Composites Part B: Engineering* 2010; 41(8):678e85.
- [62] Alexander, J.M., An approximate analysis of the collapse of thin cylindrical shells under axial loading. *MechApplMath* 1960; 13(1):5–10.
- [63] Wierzbicki, T., Abramowicz, W., On the crushing mechanics of thin-walled structures. *ApplMech – TransASME* 1983; 50(4):727–34.

- [64] Abramowicz, W., Wierzbicki, T., Axial crushing of multi-corner sheet metal columns. *ApplMech – TransASME*1989; 56(1):113–20.
- [65] Abramowicz, W. and Jones, N., Dynamic axial crushing of square tubes, *International Journal of Impact Engineering*, 1984; 2(2):179–208.
- [66] Abramowicz, W., Jones, N., Dynamic progressive buckling of circular and square tubes, *IntJImpactEng*1986; 4(4):243–70.
- [67] Andrews, K.R.F., England, G.L., Ghani, E., Classification of the axial collapse of cylindrical tubes under quasi-static loading, *IntJMechSci*1983; 25(9–10): 687–96.
- [68] Langseth, M., Hopperstad, O.S., Static and dynamic axial crushing of square thin-walled aluminium extrusions. *IntJImpactEng*1996; 18:949–68.
- [69] Mamalis, A.G., Manolakos DE, Baldoukas AK, Energy dissipation and associated failure modes when axially loading polygonal thin-walled cylinders, *Thin-WalledStruct*1991;12:17–34.
- [70] Zhang, X., Zhang, H., Experimental and numerical investigation on crush resistance of polygonal column sand angle elements, *Thin-Walled Structure* 2012; 57: 25–36.
- [71] Alavi, NiaA., Hamedani, J.H., Comparative analysis of energy absorption and deformations of thin walled tubes with various section geometries extrusions. *Thin-WalledStruct*2010; 48:946–54.
- [72] Hou, S., Li, H., Long, S., Yang, X. and Li, W., Multi objective optimization of multi-cell sections for the crash worthiness design, *IntJImpactEng*2008; 35(4): 1355–67.
- [73] Zhang, X., Zhang, H., Energy absorption limit of plates in thin-walled structures under compression, *IntJImpactEng*2013; 57: 81–98.
- [74] AlaviNia, A. and Parsapour, M., Comparative analysis of energy absorption capacity of simple and multi-cell thin-walled tubes with triangular, square, hexagonal and octagonal sections, *Thin-Walled Structures*, 2014; (74): 155–165.
- [75] Jia, X., Chen, G., Yu, Y., Li, G., Zhu, J, Luo X, et al., Effect of geometric factor, winding angle and pre-crack angle on quasi-static crushing behaviour of filament wound CFRP cylinder, *Composites PartB*2013; 45: 1336–43.

- [76] Yan, L., Chouw, N., Crashworthiness characteristics of flax fibre reinforced epoxy tubes for energy absorption application, *MaterDes*2013; 51: 629–40.
- [77] Mahdi, E., Sahari, B.B., Hamouda, A.M.S., Khalid, Y.A., An experimental investigation into crushing behaviour of filament-wound laminated cone–cone intersection composite shell, *Composite Structure*, 2001;51:211–9.
- [78] Mahdi, E., Hamouda, A.M.S., Sahari, B.B. and Khalid, Y.A., Experimental quasi-static axial crushing of cone tube cone composite system, *Composites PartB*2003; 34: 285–302.
- [79] Mahdi, E., Hamouda, A.M.S., Sahari, B.B., Khalid, Y.A., Effect of hybridisation on crushing behaviour of carbon/glass fibre/epoxy circular cylindrical shells. *J MaterProcessTechnol*2005; 132:49–57.
- [80] Abosbaia, A.S., Mahdi, E., Hamouda, A.M.S., Sahari, B.B., Mokhtar, A.S., Energy absorption capability of laterally loaded segmented composite tubes, *Compos Struct*2005;70:356–73.
- [81] Palanivelu, S., Van, Paepegem.W., Degrieck, J., Kakogiannis, D., Van, Ackeren.J., Van, Hemelrijck.D. et al., Comparative study of the quasi-static energy absorption of small-scale composite tubes with different geometrical shapes for use in sacrificial cladding structures, *Polymer Test*, 2010;(29):381–96.
- [82] Elgalai, A.M., Mahdi, E., Hamouda, A.M.S., Sahari, B.S., Crushing response of composite corrugated tubes to quasi-static axial loading, *Composite Structure*2004; 66:665–71.
- [83] Abdewi, E.F., Sulaiman, S., Hamouda, A.M.S., Mahdi, E., Effect of geometry on the crushing behaviour of laminated corrugated composite tubes, *Journal of Material Process Technol*2006; 172:394–9.
- [84] Abdewi, E.F., Sulaiman, S., Hamouda, A.M.S., Mahdi, E., Quasi-static axial and lateral crushing of radial corrugated composite tubes, *ThinWalledStruct*2008; (46): 320–32.
- [85] Cantwell, W.J., Alia, R.A., Guan, Z., Umer, R. and Balawi, S., The Energy-absorbing Characteristics of Tube-reinforced Foam Structures, *ICCM2014* 28-30th July, Cambridge, England.

- [86] Ramakrishna, S. and Hull, D., Energy Absorption Capacity of Epoxy Composite Tubes with Knitted-Fed Carbon Fibre Fabric Reinforcement, *Composites Science and Technology*, 1993; (49):349-356.
- [87] Ramakrishna, S., Hamada, H. and Maekawa, Z., Energy Absorption Behaviour of Carbon-Fibre-Reinforced Thermoplastic Composite Tubes, *Journal of Thermoplastic Composite Materials*, 1995; (8): 323-344.
- [88] Hull, D., A Unified Approach to Progressive Crushing of, *Composites Science and Technology*, 1991; (40): 377-421.
- [89] Umer, R., Balawi, S., Raja, P. and Cantwell, W.J., The energy-absorbing characteristics of polymer foams reinforced with bamboo tubes, *Journal of Sandwich Structures and Materials*, 2014; 16(1); 108–122.
- [90] Jacob, G.C., Fellers, J.F., Simunovic S, Starbuck JM, Energy absorption in polymer composites for automotive crashworthiness. *Journal of Composite Materials*, 2002; (36); 813-849.
- [91] Ramakrishna and Hull, D., Energy absorption of epoxy composite tubes with knit-fed carbon fibre fabric reinforcement, *Composites Science and Technology*, 1993; (49): 349-356.
- [92] Thornton, P.H. and Edwards, P.J., Energy Absorption in Composite Tubes, *Journal of Composite Materials*, 1982; (16): 521-545.
- [93] Thornton, P.H., Energy Absorption in Composite Structures, *Journal of Composite Materials*, 1979; (26): 247-262.
- [94] Farley, G.L., Effect of specimen geometry on the energy absorption capability of composite materials, *Journal of Composite Materials*, 1986; (20): 390-400.
- [95] Alia, R.A., Cantwell, W.J., Langdon, G.S., Yuen, S.C.K., Nurick, G.N., The energy-absorbing characteristics of composite tube-reinforced foam structures, *Composite: Part B*, 2014; (61): 127-135.
- [96] Zhou, J., Guan, Z.W., Cantwell, W.J. and Liao, Y., The energy-absorbing behaviour of foam cores reinforced with composite rods, *Composite Structure*, 2014; (114): 346-356.

- [97] Schmusser, D.W., Wickliffe, L.E., Impact energy absorption of continuous fibre composite tubes, *Journal Engineering Material Technology*, 1987; (109): 72-77.
- [98] McGregor, C., Vaziri, R. and Xiao, X., Finite element modelling of the progressive crushing of braided composite tubes under axial impact. *International Journal of Impact Engineering*, 2010; (37): 662-672.
- [99] Beard, S.J. and Chang, F.K., Design of braided composite for energy absorption, *Journal of Thermoplastic Composite Materials*, 2002; (15): 3-12.
- [100] Flesher, N.D., Crash energy absorption of braided composite tubes PhD, thesis, Stanford University, 2006.
- [101] Xiao, X., Botkin, M., Johnson, N.L., Axial crush simulation of braided carbon tubes using Mat58 in LS-DYNA, *Thin-Walled Structures*, 2009; (47): 740-749.
- [102] Mamalis, A.G., Manolakos, D.E., Ioannidis, M.B., Papapostolou, D.P., The static and dynamic axial collapse of CFRP square tubes: finite element modelling. *Composite Structures*, 2006; (74): 213-225.
- [103] Silcock, M.D., Giovanola, J.H., Simons, J.W., Erlich D.C., Klopp, R.W. and Skaggs, S.R., Advanced armor technology: application potential for engine fragment barriers for commercial aircraft, Federal Aviation Administration Report No. DOT/FAA.AR-97/53, September 1997.
- [104] Pinho, S.T., Camanho, P.P., Moura, M.F., Numerical simulation of the crushing process of composite materials, *International Journal of Crashworthiness*, 2004; (9): 263-276.
- [105] Alavi, NiaA. and Hamedani, J.H., Comparative analysis of energy absorption and deformations of thin walled tubes with various section geometries extrusions. *Thin-WalledStruct*2010; 48:946–54.
- [106] Zhang, X., Cheng, G., Zhang, H., Theoretical prediction and numerical simulation of multi-cell square thin-walled structures, *Thin-WalledStruct*2006; 44(1): 1185–91.
- [107] Zhang, X. and Zhang, H., Numerical and theoretical studies on energy absorption of three-panel angle elements, *Thin-WalledStruct*2012; 46:23–40.
- [108] Najafi, A., Rais-Rohani, M., Mechanics of axial plastic collapse in multi-cell, multi-corner crush tubes, *Thin-WalledStruct*2011; 49(1):1–12.

- [109] Tang, Z., Liu, S. and Zhang Z., Analysis of energy absorption characteristics of cylindrical multi-cell columns, *Thin-Walled Struct* 2012; 62:75–84.
- [110] <http://www.easycomposites.co.uk/#!/cured-carbon-fibre-products/carbon-fibre-tube>
- [111] Liu, D. and Hyer, M., “Dynamic Effects in Composites”, Published 2012 DEStech Publication, Inc.
- [112] ABAQUS, Theory Manual, Version 6.12 (2012). Pawtucket: Hibbitt, Karlsson & Sorensen, Inc.
- [113] Vo, T.P., Guan, Z.W., Cantwell, W.J., Schleyer GK, “Modelling of the low-impulse blast behaviour of fibre–metal laminates based on different aluminium alloys,” *Composites: Part B*, vol. 44, pp. 141–151, 2013.
- [114] Hashin, Z., “Failure criteria for unidirectional fiber composites,” *Journal of Applied Mechanics*, vol. 47, pp. 329–34.1980.
- [115] Yen, C.F., Ballistic impact modelling of composite materials, In Proceedings of the 7th international LS-DYNA users’ conference, 2002; (6): 15-23.
- [116] Pavlopoulou, S. and Potluri, P., Residual flexural strength after impact and hydrostatic cycling in glass/syntactic foam sandwich laminates, 20th International Conference on Composite Materials Copenhagen, 19-24th July 2015.
- [117] Arezoo, S., et al., “The mechanical response of Rohacell foams at different length scales,” *Journal of Material and Science*, vol. 46(21), pp. 6863-6870, 2011.
- [118] Hooputra, H., et al., “A comprehensive failure model for crashworthiness simulation of aluminium extrusions,” *International Journal of Crashworthiness*, vol. 9(5), pp. 449-463, 1991.
- [119] Deshpande, V.S. and Fleck, N.A., “Multi-axial yield behaviour of polymer foams”, *Acta mater*, vol. 49, pp. 1859–1866, 2001.
- [120] Deshpande, V.S., and N.A. Fleck, “Isotropic constitutive model for metallic foams,” *Journal of the Mechanics and Physics of Solids*, vol. 48, pp. 1253-1276, 2000.
- [121] ABAQUS/Explicit, User’s Manual, Version 6.12 (2012) , Hibbitt, Karlsson & Sorensen, Inc.
- [122] Camanho, P.P and Davila, C.G., Mixed-Mode Decohesion Finite Elements for the Simulation of Delamination in Composite Materials, NASA/TM-2002-211737.

- [123] Teodor, M. Atanackovic., *Stability Theory of Elastic Rods*, World Scientific Publishing Co. Pte, 1996; Ltd.
- [124] Chen, W.F. and Atsuta, T., *Theory of Beam-Columns*, 1976; McGraw Hill, New York.
- [125] Philip, J. Wicks. (1987). Compound Buckling of Elastically Supported Struts. *J.Eng.Mech.* 1987; (113):1861-1879.
- [126] Zhou, J., Guan, Z.W. and Cantwell W.J., The energy-absorbing behaviour of foam cores reinforced with composite rods, *Composite Structures*, 2014; (116): 346–356.
- [127] Torres, L. A., Ghavami, K. and García, J. J., A transversely isotropic law for the determination of the circumferential young's modulus of bamboo with diametric compressive tests, *Lat. Am. appl.res.*, 2007; (37): 4 Bahía Blanca.
- [128] García, J. J., Rangel, C. and Ghavami, K., Experiments with rings to determine the anisotropic elastic constants of bamboo, *Construction and Building Materials*, 2012; (31): 52-57.
- [129] Liang, Z. W., Li, J. Q. and Zhou, X. J., The research on the Friction Properties of Bamboo Fiber Surface, *Journal of Wuhan University Of SCIENCE and Engineering*, 2008;( 8): 16-19.